Part II

Theoretical background

2

Fiber mechanics

X-Q. DAI[1,2] AND Y. LI[1]
[1]The Hong Kong Polytechnic University, China
[2]Soochow University, China

2.1 Introduction

Fibers are the fundamental and the smallest elements constituting textile materials. The biomechanical functional performance of garments and devices are very much dependent on the fiber mechanical and surface properties, which are largely determined by the constituting polymeric molecules, internal structural features and surface morphological characteristics of individual fibers. Scientific understanding and knowledge of the fiber properties and modeling the mechanical behavior of fibers are essential for biomechanical engineering of clothing and textile products. In this chapter, we review the knowledge and processes developed in the area of fiber mechanics in relation to biomechanical engineering.

2.2 Fiber morphology

The morphology of fibers includes macrostructure, microstructure, submiscroscopic structure and fine structure of fibers.

2.2.1 Macrostructure

The features of a textile fiber that are discernible to the human eye constitute its macrostructure; these include width, length, and crimp.

Fiber size Fiber size, often referred to as fineness, is one of the most important properties of fibers. It is usually specified in terms of diameter or linear density. The size of natural fibers is often given as a diameter in micrometer units. It reflects the average width along the fiber's length. The sizes of silk and manufactured fibers are usually given in denier or tex units, which specify the linear density based on weight per unit length. *Denier* is the weight in grams of 9000 m of a fiber; *tex* is the weight in grams of 1000 m of a fiber. *Tex* is one-ninth of 1 *denier*.

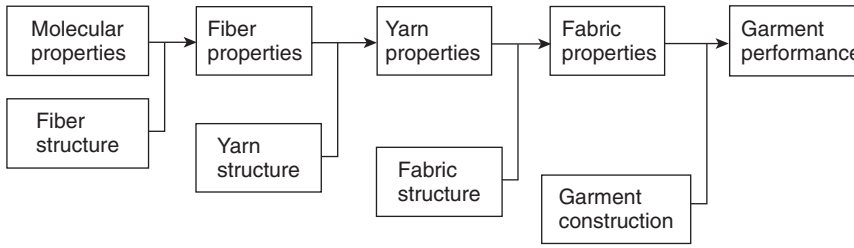

2.1 Hierarchical relationships of fiber, yarn, fabric and garment to the biomechanical function performance of clothing and textile devices.

Fiber size has a very important influence on fiber stiffness, which then affects the stiffness of the fabric made from the fiber and hence the way it drapes and how soft it feels. The fiber stiffness also affects how soft or how prickly the fabric feels when it is worn next to the skin.

Fiber length After size, fiber length is the most important property of a fiber. Fiber length is critical in processing of fibers and yarns and in the translation of fiber strength to yarn strength. In general, a longer fiber length is preferred. Textile fibers are either staple or filament length. Staple fibers range from 2 to 46 cm; filament fibers are of infinite length. All natural fibers except silk are of staple length. Silk and manufactured fibers may be staple or filament fibers.

Fiber crimp Crimp refers to waves, bends, twists or curls along the fiber length. It is expressed as crimps per unit length. Some natural fibers are linear, others form two-dimensional or three-dimensional crimps as shown in Fig. 2.2. Crimped fibers tend to have higher elongation than linear fibers.

2.2.2 Microstructure

Microstructure of fibers includes their surface contour and cross-sectional shape. These features are observable through a light microscope. Surface contour, describing the surface of the fiber along its length, may be smooth, serrated, lobed, striated, pitted, scaly, or convoluted. Surface contour may affect fiber frictional properties and comfort when worn next to the skin.

Cross-sectional shape refers to the shape of a horizontally cut fiber section. It may be round, triangular, dog-bone, kidney-bean, flat, and so on. There is a characteristic shape for each type of natural fiber. The shape of a fiber's cross-section is important in many applications. It has influence on bending stiffness and torsional stiffness of the fiber. Consider the bending

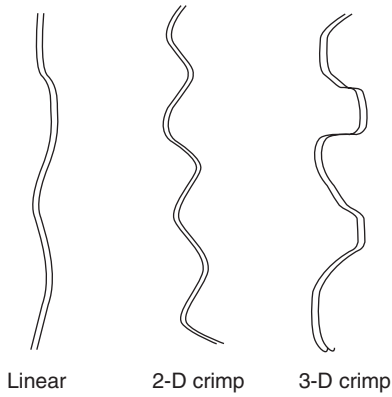

2.2 Fiber crimp.

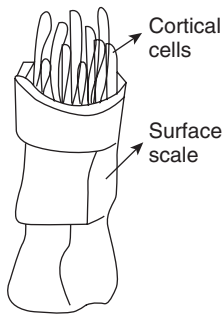

2.3 Fiber submicroscopic structure (wool).

stiffness of the solid fibers, those with round cross-sections offer a high resistance to bending and, hence the fibers are stiff. However, fibers with ribbon-like cross-sections, such as cotton, offer the least resistance to bending.

2.2.3 Submicroscopic structure

Through an electronic microscope, more details of fibers on the surface, as well as in the inner side, are observable. Figure 2.3 shows the schematic microscopic structure of wool fiber.

2.2.4 Fine structure

All fibers are assemblies of macromolecules, called polymers, in the form of hundreds or even thousands of individual chemical units, covalently bonded together one after the other as illustrated in Fig. 2.4. Fine structure

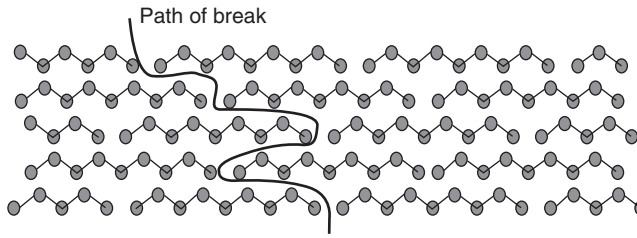

2.4 Fine structure of fiber.

describes the length, width, shape, and chemical composition of these polymers. It largely determines the ability of a fiber to withstand mechanical forces. There are three types of polymers comprising textile fibers: homopolymers, copolymers, and block polymers. In homopolymers, the most common type, one monomer (one chemical compound) repeats itself along the polymer chain. In copolymers, two or more monomers comprise the polymer chain. In block polymers, blocks comprised of homopolymers are repeated along the polymer chain. Polymer length is specified as the number of times the monomer is repeated along the chain, called the degree of polymerization. Polymer length plays a role in fiber tensile properties. If two fibers are alike except for polymer length, the fiber comprised of longer polymers is generally stronger, extends a shorter distance at a given load, and requires more force to cause elongation.

Within fibers, adjacent polymers are found tightly packed together in specially ordered crystalline regions and further apart in amorphous regions. The proportion of crystalline to amorphous regions determines the 'degree of crystallinity'. The thousands of polymers within a fiber lie more or less parallel to the longitudinal axis of the fiber itself. When a relatively high proportion of polymers are aligned with the fiber axis, the fiber is said to be 'highly oriented'. Orientation and crystallinity have a significant impact on various fiber behaviors. If two fibers are alike except for degree of orientation and crystallinity, the fiber that is more crystalline and orientated is stronger and stiffer, and has lower elongation at break.

2.3 Mechanical behavior

The mechanical properties of fibers are their responses to applied forces and to recovery from those forces. They contribute both to the behavior of fibers in processing to yarns and to the properties of the final products so that a knowledge of fiber behavior is essential to an understanding of yarn mechanics and fabrics mechanics.

2.3.1 Tensile properties

Stress–strain curve: Because of the linear shape of a fiber, the tensile properties (the behavior under forces and deformations applied along the fiber axially) are the most important properties and are the most studied. Figure 2.5 illustrates the tensile deformation. In general engineering, the tensile stress = force/area, $\sigma = F/A_0$; the tensile strain = change in length/original length, $\varepsilon = \Delta l/l_0$.

When applying a gradually increasing force along the fiber axis until the fiber breaks, a stress–strain curve is created. It shows many important mechanical characteristics of the fiber. In textile technology, a specific stress is often used instead of the general stress used in engineering area: Specific stress = force/linear density, $\sigma_s = F/d_1$.

Figure 2.6 shows a model stress–strain curve. The curve begins with a straight-line segment that rises as stress is increased (AB) and then suddenly flattens and rises at a slower rate (BC). Close to the failure point, the curve rises steeply (CD). The details of each of the regions is addressed as follows:

- In region AB, the deformation is a result of bond stretching and flexing. It is completely reversible. Hooke's law is obeyed: $\sigma = E\varepsilon$, where E is the slope of the line, called Young's modulus. In this region, the deformation is recoverable, and it is elastic. As the fiber extends along the axial direction, it contracts laterally. Poisson's ratio, defined as the ratio of lateral contraction to axial extension, is another important material characteristic that deals with the behavior in the elastic region.
- After the yield point, deformation becomes nonlinear, and it is usually plastic. The deformation, a result of the polymers slipping by each other, is partially recoverable. In the region BC, the fiber extends more easily.

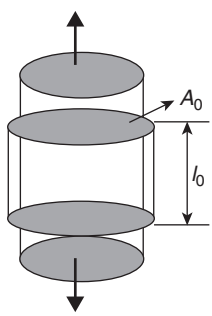

2.5 Schematic tensile deformation of a cylinder.

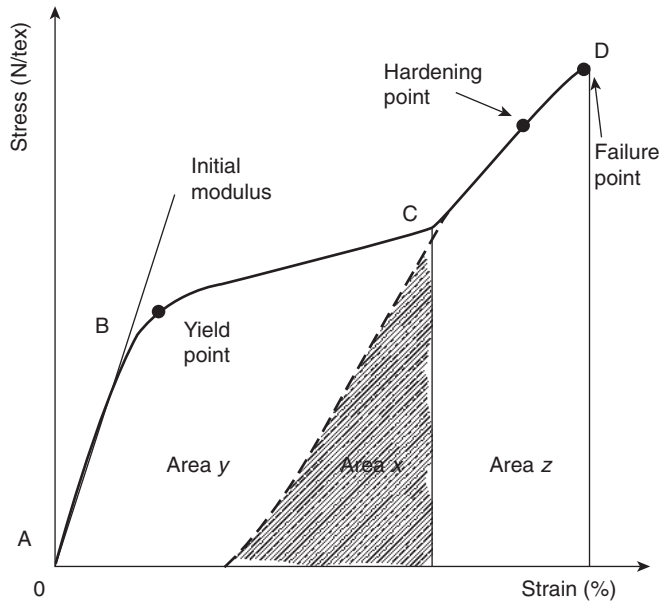

2.6 Schematic stress–strain curve of a fiber.

The slope of the segment BC largely reflects the strength of intrafiber bonding.

- As the polymers become more compact, the fiber reaches a deformation limit, harden point. Following the hardening, the internal structure of the fiber begins to give way and the failure point is reached. The stress and strain at this point give the tenacity and the elongation at break respectively.

Elastic recovery: In the initial segment of the stress–strain curve (AB), the fiber behaves like an elastic spring. Under the applied load, the polymers are being straightened, perhaps becoming more oriented within the fiber. If the load is removed at any point from A to B, the fiber will return to its original length because the polymers can revert to their initial positions. In this case, the elastic recovery is 100%. If the fiber is stretched beyond the yield point but not to its hardening point, and the load is then removed, the fiber will partially recover.

Work of rupture: Work of rupture or toughness is a measure of the ability of a fiber to withstand sudden shocks of energy. The total amount of work required to deform a fiber up to the failure point is indicated by the area under its stress–strain curve, the sum of areas x, y, and z, illustrated in Fig. 2.6.

Resilience: The resilience, also called work of recovery, of a fiber is the ratio of energy returned to energy absorbed when a fiber is deformed and then released. It may be extensional, flexural, compressional, or torsional. In Fig. 2.6, the fiber resilience of extension is the ratio of area x to area $x + y$.

Effects of time, temperature and moisture: The extension caused by a given applied force, or the stress resulting from a given strain in the fiber, depends on how long the force or the strain has been present and on the earlier mechanical history of the fiber; it also depends on the temperature. Time and temperature dependent mechanical behavior is a characteristic of fibers. It is usually called viscoelastic (combined viscous and elastic) and is due to polymers not being ideal elastic solids – they also contain a viscous component. Creep and stress relaxation are the tests developed to probe their time-dependent behavior. In the creep test, the strain increases with time in a sample under constant load. In the stress relaxation test, the stress decays with time after the sample is given an instantaneous strain. Moisture also affects the mechanical behaviors of fibers. Basically, the moisture lodges in the noncrystalline regions and plasticizes them, reducing the modulus.

2.3.2 Forces in various directions

Bending: When a fiber is bent, the polymers must extend and compress to accommodate the bending force. As illustrated in Fig. 2.7, the polymers on the under curvature will compress; those on the upper curvature will extend; and those on the center plane will be unchanged in length.

Flexural rigidity (resistance to bending, stiffness) of a fiber is defined as the couple required to bend the fiber to unit curvature. Thus, in the elastic

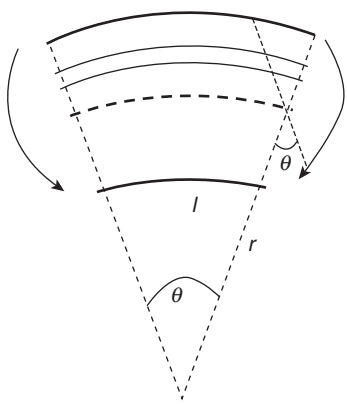

2.7 Bending of a fiber.

region there exists $M_B = BK$, where M_B = force couple, B = flexural rigidity and K = bending curvature. The flexural rigidity can be expressed in terms of the Young's modulus E as: $B = \frac{1}{4\pi}\frac{\eta E T^2}{\rho}$, where, η is a shape factor related to the cross-section of the fiber, and ρ and T are the density and linear density of the fiber respectively.[1] It is convenient to introduce a quantity that is independent of the fineness of the specimen to replace the flexural rigidity. That is the specific flexural rigidity, R_f, equal to the flexura rigidity of a filament of unit tex: $R_f = \frac{1}{4\pi}\frac{\eta E}{\rho}$.

Shear and torsion: Figure 2.8 shows the shear deformation of a solid cube unit. The shear stress τ is expressed as F/A_0 and the shear strain is calculated as $\delta x/y$. Then, in the elastic region, the shear modulus G can be defined as the ratio of shear stress to shear strain: $G = \tau/\gamma$.

Figure 2.9 shows the twisting deformation of a fiber of circular cross-section. If we look at a small region, the fiber is sheared. The torsional rigidity of a fiber, its resistance to twisting, is defined as the couple needed to achieve unit angular deflexion between the ends of a specimen of unit length. Usually the specific torsional rigidity, R_t, the torsional rigidity of a specimen of unit linear density (in tex), independent of the fineness of the particular specimen, is used. Since twisting has the same relation to shearing as bending does to stretching, the torsional rigidity can be obtained in terms of the shear modulus in the same way that the bending rigidity can be obtained in terms of the Young's modulus: $R_t = \eta n/\rho$. Here, ρ and η are the linear density and the shape factor of the fiber respectively. Details can be found in reference 1.

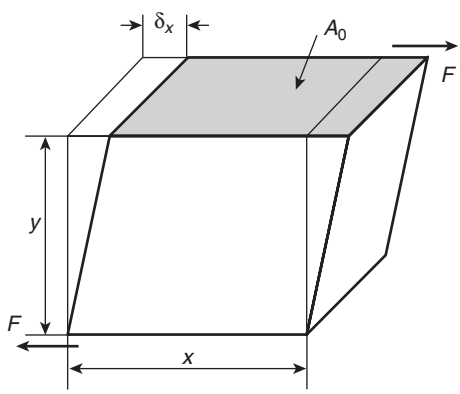

2.8 Shear deformation of a cube.

Compression: Figure 2.10 (a) shows a cylinder under axial compression. A compression stress is simply negative to tensile stress and a compression strain is also a negative one. The initial compressive modulus is generally the same as the initial tensile modulus. However, as the compression force increasing, the fiber will buckle easily. Figure 2.10 (b) shows a cylinder under transverse compression. The transverse modulus is used to reflect the transverse compressive property.

2.3.3 Friction

Fiber friction is the force that holds together the fiber in a spun yarn and the interlacing threads in a fabric. Here, high friction is an advantage to enable a greater proportion of the strength of the individual fibers to be obtained. However, lower friction of a fiber may be desired in other cases,

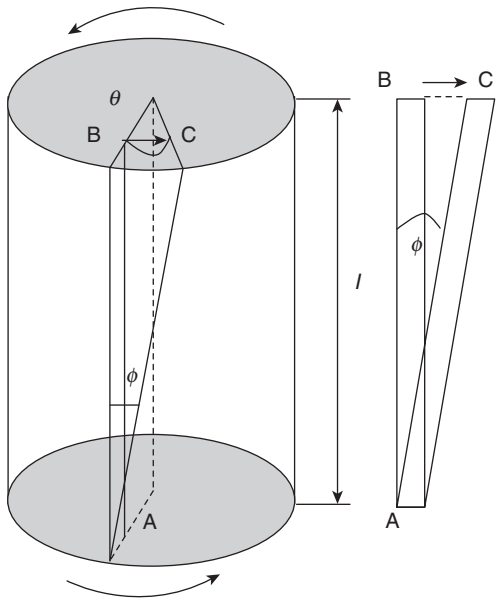

2.9 Shear or torsion on a cylinder.

(a) Axial compression of a cylinder (b) Transverse compression

2.10 Fiber compression.

such as in minimizing wear of fibers and fabrics, providing good fabric drape, and so on. Friction coefficient, μ, is used to denote the friction property of a fiber.

2.4 Modeling of fiber mechanical properties

2.4.1 Structural model

Various models have been proposed to represent the structure of polymers and fibers, and further to calculate fiber mechanical properties on the basis of the properties and arrangement of the components. Fiber scientists often envision a two-phase model, crystalline and non-crystalline, for the structure of polymers and fibers. The three most useful two-phase models for fiber structure are: the isostrain model, the isostress model, and the micellar model, as illustrated in Fig. 2.11. The isostrain model represents a fiber as two continuous phases that are aligned parallel with each other. When the fiber is stretched along the axial direction, the stress will be the appropriate weighted-mean stress contributed by the two components at the same strain, and the modulus of the fiber is a volume-weighted average of the two phases, as the following equation shows: $E_C = E_1V_1 + E_2V_2$. Here, E_C, E_1 and E_2 denote the Young's moduli of the fiber, and the two components respectively.

Figure 2.11(b) show the isostress model, which has the same structure as the isostrain model but is subjected to a stress normal to the fiber direction. In this case, the behavior of the composite system is given by taking the weighted-mean strain with the same stress on each component. The modulus of the composite can be obtained as:

$$1/E_{C\perp} = V_1/E_{1\perp} + V_2/E_{2\perp},$$

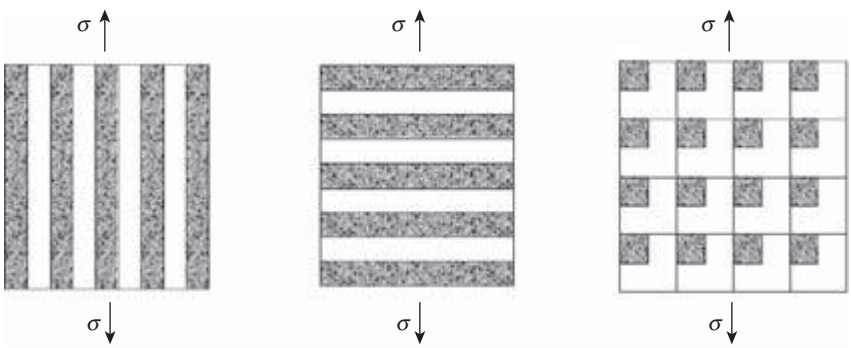

(a) Isostrain model (b) Isostress model (c) Micellar model

2.11 Structural models of fiber.

where $\perp$ indicates that the modulus is measured normal to the axial direction. The micellar model is a little difficult to analyze, and it will give a result between the above two extremes. Details about these models can be found in reference 2.

The two-phase morphology is a reasonable assumption for most fibers. However, there are some problems with these models; for example, the noncrystalline regions are not constant and other phases may be present. Thus, in some cases, three-or-more-phase models may be employed.

Bukosek[3] developed a molecular, supramolecular, and morphological structural model of semicrystalline polymers and the structural factors that influence fiber properties. The contributing effects of wool fiber morphology have been ignored in early mechanical behavioral models, in which the wool fiber has been treated as a two-phase composite with parallel constituents.[4] Liu and Bryson[5] proposed a three-component model of the wool fiber. The stiffness of a wool fiber was derived from the stiffness of the three components: the cuticle, the orthocortex, and the meso/paracortex, and their proportions within the fiber. The developed model may give new insight into the relevance of internal fiber structure to single fiber behavior affecting fiber assemblies in yarns.[5]

2.4.2 Modeling the time-dependent properties

The viscoelasticity of a fiber is often modeled using models composed of ideal springs for the elasticity and ideal dashpots for the viscosity. The springs follow Hooke's law, $\sigma = E\varepsilon$; the dashpots follow Newton's law, $\tau = \eta\dot{\gamma}$. Here, η is a constant, $\dot{\gamma}$ (equaling $d\varepsilon/dt$) is the rate of strain. As shown in Fig. 2.12, if a spring and a dashpot are arranged in series, they make up the Maxwell model; and if they are arranged in parallel, the composed element is called a Voigt–Kelvin model. The Maxwell model can show

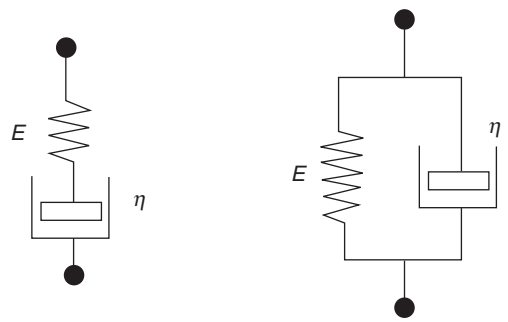

(a) Maxwell model (b) Voigt–Kelvin model

2.12 Spring and dashpot models.

instantaneous extension under the applied load, followed by secondary creep at a constant rate; it can also show stress relaxation at constant length. The Voigt–Kelvin model can show primary creep. The simplest model that can show qualitatively all the features of instantaneous extension, primary and secondary creep and stress relaxation is the four-element model shown in Fig. 2.13(a).

By adding to the number and complexity of arrangements of the springs and dashpots, a complete representation of the mechanical behavior of fibers, exhibiting not only the four effects mentioned above, but also the dynamic properties, which vary with frequency, and nonlinear relations between extension, load, and time, can be obtained. However, there is a limit to such an approach, if all the stress values of a given sequence are doubled, all the strain values will also double. It is often not true for a fiber. Another approach to address this problem is to modify the elements themselves. The three-element system proposed by Eyring *et al.*[9] is the most successful model following this approach. In this model, shown as Fig. 2.13(b), the two springs obey Hooke's law; but the dashpot shows non-Newtonian viscosity, its behavior being represented by a hyperbolic sine law of viscous flow: $d\varepsilon/dt = K \sinh \alpha\sigma$. Here, K and α are constants. Thus, the rate of strain will increase more rapidly with increase of stress than it would do if it were proportional to stress, as in Newton's law. More details about the theories of time-dependence can be found in reference 1.

Applying a three-element model, which has two Hookean springs and a dashpot containing a non-Newtonian power-law liquid, Kumar *et al.*[6] developed equations for creep recovery, stress relaxation and stress–strain behavior of textile fibers. By analyzing the two-element, three-element, four-element and six-element viscoelasticity models, Zhang[7] built up the regression equation of the relaxation curve of Tencel fiber based on the

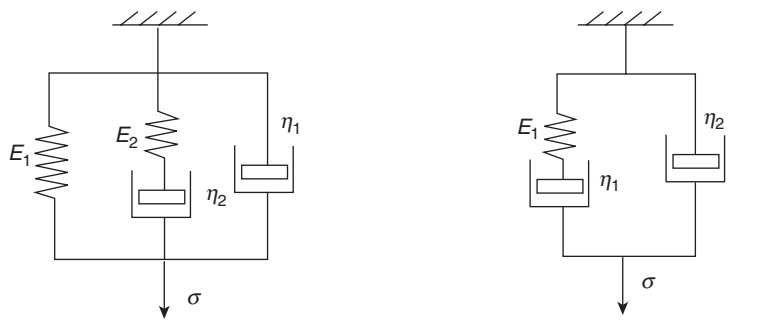

(a) Four-element model (b) Eyring's three-element model

2.13 Viscoelastic models.

six-element model and verified the identity between the six-element model and the test result.

Cai[8] proposed a nonlinear viscoelastic model to describe the time-dependent deformation behavior of fiber assemblies, including braided fiber seals. The models were derived from the standard solid model, but modifications permitted the inclusion of three nonlinear spring and viscous damper elements. For a fiber assembly under a compressive load, the fiber volume fraction characterized the deformation status. The researchers assumed that the elastic spring and viscous damper elements in the proposed model were nonlinear functions of the fiber volume fraction. In the cases of creep and stress relaxation, general deformation solutions were obtained. Baltussen[9] used the Eyring reduced time model to investigate the viscoelastic and yield deformations of polymer fibers, covering the observed tensile behavior of linear polymers in the glassy state, extensions at a constant rate of stress, creep and stress relaxation, and response to complex loading schemes. The experiments showed that the yield deformation and viscoelastic deformation of polymer fibers are strongly related.

2.4.3 Other approaches

The finite element method was also applied to fiber modeling. He *et al.*[10] used a linear elastic finite element model to study the mechanical behavior of irregular fibers. They evaluated the tensile behavior of fibers with simulated dimensional irregularities and determined that variations in fiber diameter affected tensile behavior. They found that greater variation reduced breaking load, Young's modulus, and breaking extension, and increasing the frequency of irregularity reduced breaking load and Young's modulus, but increased breaking elongation.[10]

Komori *et al.*[11] used a curved beam model to investigate the bending behavior of fibers and the micromechanical aspects of fiber compressibility. The analysis was able to reproduce the functional dependence of stress on the strain of a mass by using the structural quantities of assembly density, degree of fiber crimp, and fiber elasticity.

2.5 Conclusion

In this chapter, firstly, the macrostructure, microstructure, sub-miscroscopic structure and fine structure of fibers, which determine the fiber mechanical and surface properties, have been introduced; then the mechanical properties of fibers that contribute both to the behavior of fibers in processing to yarns and to the properties of the final products have been described; finally, several approaches to predict fiber mechanical properties have been briefly reviewed.

2.6 Acknowledgement

We would like to thank Hong Kong Polytechnic University for funding this research through Projects A188 and G-YD31.

2.7 References

1. Morton, W.E. and Hearle, J.W.S., 'Tensile Properties', in *Physical Properties of Textile Fibers.* 1993, The Textile Institute. p. 265–305.
2. Warner, S.B., *Fiber Science.* 1995: Prentice Hall, Inc.
3. Bukosek, V., Importance of Structural Model in Morphology of Fibers. *Tekstilec*, 1998. **41**(5/6): p. 127–133.
4. CSIRO, Models for predicting the mechanical properties of wool fibers, in *CSIRO Annual Report.* 1984: Australia.
5. Liu, H. and Bryson, W.G., A three-component model of the wool fiber – Effects of morphology, elasticity and intermediate filament arrangement on fiber stiffness. *Journal of the Textile Institute*, 2002. **92**(2): p. 121–131.
6. Kumar, S. and Gupta, V.B., Nonlinear viscoelastic model for textile fibers. *Textile Research Journal*, 1978. **48**: p. 429.
7. Zhang, J., The model of viscoplastoelastic behavior of Tencel fiber. *Xibei-Fangzhi-Gongxueyuan-Xuebao*., 1999. **13**(4): p. 399–402.
8. Cai, Z., A Nonlinear Viscoelastic Model for Describing the Deformation Behavior of Braided Fiber Seals. *Textile Research Journal*, 1995. **65**(8): p. 461–470.
9. Baltussen, J.J.M., The Eyring Reduced Time Model for Viscoelastic and Yield Deformation of Polymer Fibers. *Tensile Deformation of Polymer Fibers*, 1996: p. 155–168.
10. He, W., Zhang, S. and Wang, X., Mechanical Behavior of Irregular Fibers – Part I: Modeling the Tensile Behavior of Linear Elastic Fibers. *Textile Research Journal*, 2001. **71**(6): p. 556–560.
11. Komori, T., Itoh, M. and Takaku, A., Model analysis of the compressibility of fiber assemblies. *Textile Research Journal*, 1992. **62**(10): p. 567.

3

Yarn mechanics

K.F. CHOI
The Hong Kong Polytechnic University, China

3.1 Introduction

Yarns are the fundamental elements constituting fabrics. The biomechanical functional performances of garments and devices are very much dependent on the yarn mechanical and surface properties, which are largely determined by the constituent fibers, internal structural features and surface morphological characteristics of individual yarns. Scientific understanding and knowledge of the yarn mechanical properties and modeling their mechanical behavior are essential for biomechanical engineering of clothing and textile products. In this chapter, the knowledge and processes developed in the area of yarn mechanics in relation to biomechanical engineering are reviewed.

There were several reasons for taking a modeling approach to solve yarn mechanical problems. Firstly, yarn models assist the understanding of the structure of yarn and permit exploration of the hidden potential applications of yarns. More importantly, the properties of new yarn structures can be estimated using yarn models, thereby assisting in the mechanical engineering of new textile machines.

3.2 Yarn modeling

The fundamental considerations which were taken into account when deriving the yarn models include the initial yarn structure, material properties, deformed yarn structure, stresses/energy in the yarn, and solution method. In order to study the mechanical response of a yarn, it was necessary to define the initial yarn structure, inclusive of the path and lateral distribution of the constituent fibers.

3.2.1 The fiber path

Most of the researchers in yarn modeling have concentrated on ring spun yarns, although Henshaw[1] presented a model for self twist yarn, Xie *et al.*[2]

published a comprehensive paper on wrap spun yarns and Curiskis, Choi and Shih[3] developed another wrap spun yarn model based on a fiber bundle model.[4] For ring spun yarn, the earliest[5] and also the most popular assumption was that fibers follow a simple helical path. This assumption held that all the helices have the same pitch but have varying helix angles depending on the fiber's radial position in the yarn. According to Morton and Yen,[6] this idealized helical geometry in staple yarns is not practical since fibers on the yarn surface will peel off easily and consequently the yarn will lack cohesion. Morton and Yen performed experiments to determine the yarn structure using a tracer fiber technique. They found that the radial position of a single fiber in the yarn changed along its length. This was termed fiber migration. In contrast, the idealized helical geometry assumed that each of the fibers has a constant radial position.

Morton and Yen[6] explained, 'As the fibers emerge from the front roller of the ring spinning machine at the same rate, those fibers at one instant in the outer layer will follow a longer path, and consequently they will develop a higher tensile stress. The highly tensioned fibers will tend to move towards the yarn axis, displacing the less tensioned fibers already there. When the inner fibers migrate to the outer layer, their tension will build up continuously and they, in turn, will migrate back to an inner position to release tension. As a result, the fiber path is no longer a simple helix, but a helix with a variable helix radius.' Hearle and Bose[7] postulated a geometric mechanism (wrapped ribbon twisting) which explained Riding's[8] experimental findings: the correlation of the migration period in continuous filament yarns with the period of producer's twist. Hearle and Merchant[9] studied the mechanism of filament migration by constructing a seven-ply structure. The first theoretical model relating the migrating frequency with the twist angle, the twisting tension, the free length in the twisting zone, the initial tensile modulus of the filament and the degree of buckling needed to initiate migration was developed. The migration model of the seven-ply yarn was valuable in providing an understanding of what was happening in more complex structures.

Patterns of ideal migration were formulated by Hearle *et al.*[10] and Treloar and Riding,[11] independently, both of them based on the assumption of uniform yarn packing density. The variation of radial position, r, along the yarn length, z, was found to be approximately parabolic, i.e. $z \propto r^2$. Van Luijk *et al.*[12] applied the finite element method to model the long gauge length behavior of staple fiber yarns with the consideration of fiber migration. A V-shaped migration envelope with the fiber ends at the yarn surface was assumed. In addition, the fiber packing density distribution in a yarn cross-section was included in the formulation of the fiber migration path. Treloar and Riding[11] determined the yarn retraction and stress–strain properties based on ideal fiber migration theory. Deviation from the coaxial

helix model was found to be insignificant. Similar work was done by Zurek,[13] and the conclusion did not differ much. As warned by Treloar though, while fiber migration did not have a significant effect on filament yarn retraction and stress–strain properties, for other yarn mechanical properties, fiber migration may have very significant effects.

3.2.2 The fiber distribution

The fiber distribution in the cross-section of an undeformed ring spun yarn depends primarily on the fiber type and the twist level. For an unbulked continuous filament yarn, it was shown[14] that the fibers were virtually close-packed and could be approximated by choosing a uniform packing density. In the case of staple yarns made from crimpy fibers, such as wool worsted yarns, Hickie and Chaikin[15] demonstrated that the packing density varies with the yarn radial position as an inverted parabola with a maximum at a region approximately on a quarter of the yarn radius from the yarn axis. In addition, as might be expected, a high-twist yarn was in general more closely packed than a low-twist yarn.

3.2.3 Material properties

The material properties that mostly affect the yarn's mechanical properties include the fiber stress–strain properties, inter-fiber friction properties and the compressional properties of the fiber mass. The stress–strain properties of fibers have usually been determined by stretching a certain number of the fibers directly using any general-purpose extension machine. The average stress–strain curve can then be obtained.

Staple yarns are the most popular yarn type in the textile and clothing sector. The main difference between staple yarns and continuous filament yarns is that the former are characterized by the discontinuities in fiber length, hence fiber ends will slip relative to the surrounding fibers during yarn extension. The slippage of fibers near their ends hinders the application of energy methods in the yarn mechanical problem because of the energy dissipation against friction involved during fiber slippage. However, it has been pointed out[16] that the build-up of tension from the fiber ends through friction with neighbouring fibers is rapid in most commercially produced yarns, and hence the region of relative slippage of fibers extends only a short distance from the fiber ends. It has been shown that it is possible to make quite successful and accurate models of yarns by treating the fibers as continuous filaments which are arranged in a series of coaxial helices.

Frictional forces oppose relative movement between two contacting bodies. When considering the frictional forces on a fiber in a yarn during yarn extension, the surrounding fibers are moving in different directions

relative to that fiber, so the determination of the resultant frictional force is not straightforward. Hearle[17] introduced a correction factor to take account of the effect of fiber relative movement. Carnaby and Curiskis[4] extended the work further by involving the variation of fiber length. Besides the discontinuity of fiber length, rapid radial migration of fibers also causes fiber slippage. Van Luijk *et al.*[12] worked out the inter-fiber friction differently, and their correction factor for fiber friction was dependent on the type of migration path. The frictional force acting on the fiber surface is a function of the radial position, and its value is constantly changing along a migrating fiber.

Compression properties of fiber strands are highly related to the degree of fiber crimp. Theoretical treatment of fiber mass compression was originated by van Wyk.[18] He first derived the number of the contact points between fibers in a random fiber mass from the probabilistic idea used in the classical kinetic theory of gases. Then he estimated the resistance to compression of the fiber mass from the bending deflection of a fiber segment as supported by two neighbouring contact points. Finally, the fiber mass compression equation was developed. That is: $P = \frac{k \cdot Y \cdot m^3}{36\rho^3}\left(\frac{1}{V^3} - \frac{1}{V_o^3}\right)$, where Y is the Young's modulus of the fiber, m is the mass of the fiber assembly, ρ is the density of the fiber, P and V are the pressure and volume of the fiber mass during compression, and $V = V_o$ at $P = 0$.

In van Wyk's equation, there is an unknown constant k which must be determined experimentally for any particular fiber mass. Experimental studies[19,20] have been carried out to relate fiber properties such as diameter, length, crimp and coefficient of friction to the compressibility of the fiber mass, but no exact relationship has been obtained.

Carnaby[21] modified van Wyk's equation by replacing the bulk volume V by the compressible volume V_c, that is $V_c = V - V_m$, where V_m is the volume of the fiber mass. A better fit to the experimental data could then be obtained.

Stearn[22] modified van Wyk's approach by taking into account the change in fiber orientation during compression of the fiber mass. Komori and Makishima[23] made the fiber mass compression problem more general by introducing the fiber orientation function. Lee and Lee[24] derived the initial compressional behavior of fiber mass in terms of the packing density and a direction density function of the constituent fibers. A large discrepancy between experimental values and theoretical predictions was observed. As explained by the authors, fiber slippage was thought to be one of the main reasons for the big difference. Carnaby and Pan[25,26] described the mechanism of fiber slippage at the microscopic level. The effect of slippage on both the compression and the shear deformation of the fiber mass was expressed analytically, hence the compression and shear hysteresis of the fiber mass was developed.

At present, the micro-mechanics of a fiber mass are still at an early stage of development. Continuous input from research workers is necessary, since a realistic yarn model can only be obtained when the material properties are well defined.

3.2.4 Deformed yarn structure

The lateral strain of yarn can be treated in the following ways:

- unstrained,
- close packed yarn following Hooke's law, mostly with Poisson ratio equal to 0.5 (constant volume),
- compressional pressure inversely proportional to the bulk volume of yarn (van Wyk's equation[18]),
- compression tangent compliance,[27] and
- shortest path principle.[21]

Hearle's initial simple models assumed the yarn lateral strain to be zero, but he realized that this unrealistic assumption should be relaxed. In his later papers, the yarn's lateral strain was determined by the Poisson ratio and the yarn tensile strain. This model worked well only for continuous filament yarn in which close packing of the fibers could be assumed.

For staple yarns, which are more loosely packed, the first two treatments of yarn lateral strain are not appropriate. The lateral strain can be determined by van Wyk's equation,[18] in which the compressional stress is inversely proportional to the cube of the specific volume. The van Wyk equation was derived from the assumption that the fibers in the fiber mass are randomly distributed, and it is valid for small compression strain only. But it has been demonstrated[28,29] that the inverse cubic relationship between the compression stress and bulk volume is quite satisfactory for larger strains and aligned fibers. Even if the orientation function of fibers is taken into consideration,[23,24,30] the result is no better than a modification of the constant factor of the van Wyk's equation.

Compression tangent compliance is a continuum mechanics concept which also enables us to take account of the lateral compression properties of the yarn. At the same time, the compression strain due to axial stress can also be incorporated. This is the continuum approach.

The shortest path analysis was developed by Carnaby.[21] One of the assumptions of this analysis is that fibers will move freely inward to avoid being extended until the fibers are jammed at a particular radial position. This is true if the paths of the fibers in the yarn follow simple coaxial helices. With the shortest-path analysis, quite accurate predictions of load for a semi-worsted wool carpet yarn can be obtained for yarn strain of up to 10%. This is the region of the stress–strain curve where predictions are

dominated by the extent of the lateral movements of the fibers and hence the results provided convincing evidence in support of the shortest-path principle.

3.2.5 Stresses/forces in yarns

In the yarn tensile analysis of Platt,[31] the forces at right angles to the fiber axes were neglected. Hearle[32] pointed out that the transverse forces between fibers played an important part in determining the mechanical properties of yarns. In his model, he assumed that the lateral stress in yarn was hydrostatic and he derived this hydrostatic stress by considering the static equilibrium of a yarn element. The transverse stress distribution in a yarn was expressed in terms of the yarn twist, yarn Poisson's ratio and the yarn strain. The pioneering work of Hearle is the foundation of the continuum approach.

Batra[33] derived the yarn lateral pressure distribution from a different approach, and the contribution of individual helical fibers to the normal force was determined with the consideration of fiber tension, bending and torsional rigidities of the fibers. It was assumed that the yarn is ideally packed in layers and that individual discrete fiber forces can be smoothed out in the layers' surface to give the lateral pressure.

Dogü[34] calculated the transverse pressure distribution in a yarn based on a migrating fiber path and distribution of fiber packing density. The tensions were assumed to be equal along the filaments. Hearle's[35] criticism was that this idealizing assumption could only deal with certain special cases.

Study of the inter-fiber stress is especially important when the recovery route of a textile structure is required. A stress analysis approach is best used to solve yarn mechanical problems which take into consideration inter-fiber friction. Postle *et al.*[36] derived a relationship between the inter-fiber normal force, p, and the external pressure in terms of the mean fiber diameter, the packing fraction of the fiber mass and the coefficient of variation of the fiber diameter. Cox's equation was widely used[2,4,37] by researchers when solving problems of untwisted fiber strand mechanics. In this work, the frictional force, f, between fibers was given as $f = \mu \cdot p + \beta$, where μ and β are related to the surface properties of the contacting pair; β was also related to the self-locking nature of the fiber mass.[37]

3.2.6 Solution method

The solution methods used for yarn mechanical problems can be classified into two approaches: The continuum approach and the discrete fiber approach.

Continuum approach: The continuum concept regards matter as infinitely divisible; thus an infinitesimal volume of material can be referred to as a particle within the continuum. For general engineering purposes, it is convenient to ignore the molecular nature of matter and hence the discontinuity and variation at the microscopic level. The continuum approach makes it possible to formulate the fundamental equations of mechanics with the use of differential and integral calculus. It provides useful results for various practical problems which agree with experience.

This approach has been used by various textile researchers. Under the continuum hypothesis, a yarn is analyzed mechanically as if the contribution of an individual fiber is, in effect, smoothed over a neighbouring region in space. This allows the concepts of stress and strain to be developed. If one is concerned only with effects over distances appreciably greater than the distance between fibers, such an assembly of fibers can be treated as a continuum, in the same way that an ordinary solid is treated as a continuum provided that molecular dimensions are not approached. If this is the case, the well-documented treatment of anisotropic elasticity[38] is directly applicable and apart from the lack of continuity which complicates the constitutive relation, the situation is formally similar to that applying to fiber-reinforced composite materials.

Carnaby and Postle[39] stated that the treatment of yarns as a continuum is divided into two phases: the first phase is to establish the geometrical relationships which connect the external deformation of the yarn to the strain of the continuum in the local co-ordinates of the yarn element, and the second phase is to translate the local strains into stresses. These stresses must combine to match the external loading. The first yarn continuum model was formulated by Hearle *et al.*[32,40] The fibers were assumed to be perfectly elastic and to follow Hooke's Law; the stress at any point was assumed to be constant in all directions at right angles to the fiber axis; further the shear forces acting on the faces of the yarn element were neglected. A more general representation of the stress characteristics of yarns was completed by White *et al.*,[41] and Huang and Funk.[42] The assumptions of no shear forces and hydrostatic pressure acting on the faces of the yarn element were relaxed. Relaxing these two assumptions is not difficult in the formulation part, but one may doubt how this information could be obtained in practice.

Thwaites[43] developed a continuum model to study the tensile and torsional properties of high-twist filament yarn. He concluded that the continuum approach could be used for high-twist filament yarn, since the filaments were very much constrained and the energy loss due to filament slippage was only a small proportion of the strain energy.

Van Luijk *et al.*[44] solved the yarn continuum problem using the finite element method. The yarn was sub-divided into concentric axisymmetric

cylindrical elements, and the longitudinal cross-section of the elements was rectangular. A realistic fiber radial distribution was used in the initial yarn geometry. The problem-solving technique they used can be considered as an informal application of the finite element method. The shear forces between elements were neglected and the lateral stress–strain relationship was determined by a generalized van Wyk's equation. During yarn deformation, they allowed transport of fiber material from one element to another; this was due to the slipping of the fibers. The yarn force was determined using the virtual work principle with numerically calculated derivatives of the work done against slippage.

Djaja *et al.*[27] introduced the tangent compliance matrix for the fiber unit cell into a three-dimensional finite element analysis, so that the fiber strand under combined tensile and torsion load could be estimated. The analysis was confined to small strains only.

The advantage of using the continuum approach is that any complex deformation modes of the yarn can be tackled by applying the well-established theory of continuum mechanics. This approach is successful only if the numerous tangent compliance matrices in different load cases are available. This is generally not the case except for various unrealistically simplified situations.

The relative fiber movement due to fiber end slippage and fiber migration makes the representation of the displacement field in a continuous function impossible. Strictly speaking, the continuum approach cannot be directly used to take account of the fiber slippage and fiber migration effects.

Five independent material parameters are needed for the continuum analysis. An attempt[16] to measure these parameters revealed the considerable difficulties in achieving comprehensive mechanical characterization of the material. As the cohesion of unstrained fiber assemblies is relatively poor, this leads to difficulties both in applying the uniaxial load and in recording the various Poisson ratio parameters.

Since the mechanical responses of a fibrous assembly are highly nonlinear, and the tangent compliance matrix must be updated frequently with the changing yarn configuration, a very large data base containing the values of the compliances corresponding to different load cases is required. This cannot be justified, especially when exploring the mechanical properties of new yarn structures. An alternative route is to derive the compliances theoretically based on the individual fiber's contribution, but here the accuracy of the current models is poor.

Discrete fiber approach: An alternative route used to solve the yarn mechanics problem is the discrete fiber approach. In this approach, each fiber is treated as a discrete component of the structure and the aggregate response

of the assembly is obtained simply by adding the separate contributions of the individual fibers.

The merits of the discrete fiber approach are as follows:

- Phenomena of mass transfer, such as fiber slippage and fiber migration, can be taken into consideration.
- Simple yarn structures can easily be extended to complex geometries and deformations, such as the torsional properties of plied yarns.
- The computational effort is relatively lower than the continuum approach.

Limitations of the discrete fiber approach:

- It is very tedious to take into account every fiber in the yarn.
- A discrete fiber model is mostly for a specific loading situation; for each new load case, a new analysis must be created or an old analysis must be modified.

As for the first limitation, it is not actually necessary to consider the effect of all individual fibers. The fibers can be grouped in a yarn according to their similarities and the effect of each group of fibers determined as a whole. For example, fibers at the same radial position may have roughly the same helix angle and hence the same amount of fiber extension when the yarn is extended. This, in effect, reduces the complexity of the yarn model. In the case of a fiber migration model, not all fibers in the same radial position have the same behavior. This problem may be solved by subdividing the fibers into outwardly migrating and inwardly migrating fibers and treating them separately. However, it is essentially unacceptable to use the continuum approach to solve this aspect of the problem, since the displacement function of the mixed fibers is not a continuous one for the types of yarns found in practice with about 50 fibers in the yarn cross-section.

As for the second limitation, it is the case that in the past, no discrete fiber models were developed for the analysis of combined loading situations. In this chapter, the yarn mechanical model was developed for combined load cases, such as the combined tensile–torsional model for a single ring-spun yarn. The model will be described in a later section, but this is still the most serious limitation of the method.

3.3 Theoretical modeling of a single yarn

A refined singles yarn torsional model was built based on a previously developed singles yarn model.[45] The initial yarn density distribution was found to be a very important yarn parameter governing the torsional property of singles yarns. Detailed study of the differential volumetric changes within the yarn has shown that jamming of the structure is the key factor

initiating longitudinal tensile and compressive strains in the fibers. The yarn model was summarized in the form of a system of non-linear equations.

Huang[46] studied the finite extension of a strand with a central core surrounded by a single layer of helical wires based on the theory of slender curved rods. In his analysis, the distributed moments and distributed forces due to inter-wire contact were included together with the external axial force and twisting moment. Huang's fundamental work is very useful in the analysis of multi-ply structures. However, although it has been applied to mechanical models of helically armoured cables,[47,48] it has not similarly been directly applied to single staple yarns. There are several main reasons. Firstly, in a staple yarn the fibers are not closely packed and the yarn density (especially a staple woollen or worsted yarn) varies with its radial position. Yarn density distribution is a very important yarn parameter; it governs the initial non-linear deformation of the yarn as well as the pattern of fiber strain distribution during yarn deformation. Secondly, many staple fibers are not straight. Wool fibers, for example, are crimpy in nature; this contributes to the handle and warmth of woollen garments. Fiber crimp imposes further complications in the yarn model. Thirdly, the radial position of the helical wires in a cable is constant, so their geometry can be described quite easily. But as revealed by the tracer fiber technique,[6] a staple fiber in a spun yarn does not follow a simple helical path; instead its radial position varies along the yarn axis (fiber migration). This makes a mathematical description of the path of a fiber more complex, and hence the extent of the fiber deformation is harder to calculate. Lastly, the length of fibers in the staple yarn is finite; this implies that the yarn is held together by frictional forces between the fibers. From zero at each end of a fiber, the tensile force builds up with distance along the fiber axis up to a certain value which is large enough to make the fiber extend the same amount as the surrounding fibers.

3.3.1 A tensile torsional model of the single yarn

A singles yarn model developed by Choi *et al.*[49] is described in this section. In brief, the yarn model can be described as follows: A singles yarn is composed of concentric simple helices with equal pitch. The fiber helices are perfectly elastic thin rods and the yarn is assumed to be a conservative system. The fibers are in one of two states; a jammed state or a freely moving state. When a fiber is in the jammed state, its radial movement is restricted. When a fiber is in the freely moving state, its neighboring fibers do not have any interaction with it. It finds its equilibrium state subject to the rule that it remains helical at a prescribed pitch and zero tensile strain.

Only the fibers in the jammed state have tensile strain because the fibers in the freely moving state can readily move inward or outward to avoid

being strained. As the fibers move, the yarn density distribution will change accordingly. If the yarn density of a yarn region reaches a prescribed maximum value, fibers in that yarn region will be in a jammed state.

Notation:

r_A – Initial radial position of outer boundary of jammed region I
r_B, r_C – Initial radial position of inner and outer boundary of jammed region O
r_h – Radius of hollowed yarn region.
r_{yo} – Initial radius of yarn
ϕ_{jam} – Maximum yarn density
e_y – Applied yarn tensile strain
e_θ – Applied yarn rotational strain
L – Length of fiber helix
H_o – Initial helical pitch of fiber in singles yarn
ϕ – Yarn density function
ρ_f – Fiber density
r – Helix radius of fiber
e_f – Fiber extension
θ – Rotation of the fiber helix

The single yarn tensile torsional model can be expressed in terms of a system of equations.

Independent variables : e_y, e_θ, r_A, r_B, r_C, r_h
Given constants/function : H_o, E_f, ρ_f, ϕ_{jam}, $\phi(r)$
Generalized external forces : T_y, T_{or}

Let $\psi(r) = \int_0^r s \cdot \phi(s) \cdot \mathrm{d}s$ and $x_1 = 1 + e_y$, $x_2 = 1 + e_\theta$, $x_3 = r_A$, $x_4 = r_B$, $x_5 = r_C$,

$x_6 = r_h$. The equilibrium configuration $[e_y{*}, e_\theta{*}, r_A{*}, r_B{*}, r_C{*}, r_h{*}]$ of the modeled single yarn under prescribed generalized external forces $[T_y, T_{or}]$ can be determined by solving the following system of non-linear equations:

$\tilde{f}(\tilde{x}) = 0$ where $\tilde{f}: D \subset \Re^6 \rightarrow \Re^6$ and $\Re^6$ denotes the real six-dimensional Euclidean space, with

$$\tilde{f} = [f_1, f_2, f_3, f_4, f_5, f_6]^t \quad \tilde{x} = [x_1, x_2, x_3, x_4, x_5, x_6]^t$$

and

$$f_1(x_1, x_2, x_3, x_6) = \frac{2{x_2}^2 \cdot \psi(x_3)}{x_1 \cdot \phi_{jam}} + (x_2 x_6)^2 + \left(\frac{H_o}{2\pi}\right)^2 ({x_1}^2 - 1) - {x_3}^2$$

$$f_2(x_1, x_2, x_3, x_6) = \int_0^{x_3} g(r) \cdot \mathrm{d}r$$

$$f_3(x_1,x_2,x_4,x_5) = \psi(x_5) - \psi(x_4) - \frac{({x_5}^2 - {x_4}^2)x_1 \cdot \phi_{jam}}{2{x_2}^2}$$

$$f_4(x_1,x_2,x_4,x_5) = \int_{x_4}^{x_5} g(r) \cdot \mathrm{d}r$$

$$f_5(\tilde{x}) = \frac{x_1 \cdot \rho_f \cdot T_y}{\pi \cdot E_f} - \int_0^{x_3} g(r) \cdot [3{H_0}^2{x_1}^2 - {L_f}^2(r)] \cdot \mathrm{d}r + \int_{x_4}^{x_5} g(r) \cdot [{L_f}^2(r) - {L_{fo}}^2(x_4)] \cdot \mathrm{d}r$$

$$f_6(\tilde{x}) = \frac{x_2 \cdot \rho_f \cdot T_{or}}{H_o E_f} - \int_0^{x_3} g(r) \cdot [{L_f}^2(r) - {H_o}^2{x_1}^2] \cdot \mathrm{d}r - \int_{x_4}^{x_5} g(r) \cdot [{L_f}^2(r) - {L_{fo}}^2(x_4)] \cdot \mathrm{d}r$$

where

$$L_{fo}(r) = \sqrt{(2\pi \cdot r)^2 + {H_o}^2}$$

$$L_f(r) = \sqrt{{H_o}^2{x_1}^2 + \frac{8\pi^2{x_2}^2}{x_1 \cdot \phi_{jam}} \cdot \psi(r) + (2\pi \cdot x_6)^2} \quad \text{when} \quad 0 \le r \le r_A$$

$$L_f(r) = \sqrt{H_o^2 + (2\pi \cdot x_4)^2 + \frac{8\pi^2{x_2}^2}{x_1 \cdot \phi_{jam}} \cdot [\psi(r) - \psi(x_4)]} \quad \text{when} \quad r_B \le r$$

$$e_f(r) = \frac{L_f(r) - L_{fo}(r)}{L_{fo}(r)}$$

$$g(r) = \frac{r \cdot \phi(r) \cdot [L_f(r) - L_{fo}(r)]}{{L_{fo}}^2(r) \cdot L_f(r)}$$

The system of non-linear equations was solved numerically using Newton–Raphson's Method. A special loading case, yarn torque–rotation property under constant yarn tension, is considered. The model prediction and experimental results are compared in the next section.

3.3.2 Experimental verification

In order to verify the yarn models' applicability of predicting the torsional properties of the yarns which involve a large amount of lateral fiber movement during yarn deformation, a sample of medium-twist woollen spun carpet yarn was chosen for the torsional test. The yarn torque rotation relationship was determined experimentally and the results were compared with the theoretical results based on the model. The inputs of the model include the parameters of fiber properties and yarn structure. As some of these properties are difficult to measure, simplifying assumptions are made.

For example, the fiber axial compressional modulus is very difficult to measure and it is generally assumed that the axial compression modulus of a fiber is equal to its tensile modulus.

The most direct way to determine the torsional properties of a yarn is to measure the torque rotation relationship of the yarn in a torsion meter. The torsion meter, KES-YN1, used in this experiment was manufactured by the Kato Tech Co. Ltd, Japan. The load range is from –500 mgf.cm to +500 mgf.cm. During testing, the yarn specimen is subject to a constant tension and its length is allowed to change freely. The torsion meter is based on the torsion balance principle: a standard metal wire of known torsional stiffness is connected to the yarn at the upper end and the rotational displacement of the wire is measured by a very sensitive displacement transducer. The amplified signals of the transducer output are sent to the plotter and a torsion rotation curve can be obtained.

Specification of yarn:

Yarn type	: Woollen spun carpet yarn
Yarn linear density	: 246 tex
Yarn twist level	: 191 turns per meter (Z-direction)
Yarn state	: Boil-set (almost zero residual torque)
Yarn test length	: 3 cm
Fiber type	: New Zealand Romney Wools
Mean fiber radius, r_f	: 1.805×10^{-3} cm
Density of fiber, ρ_f	: 1.31 g/cm^3
Initial tensile modulus of fiber, E_f	: 3.97×10^7 gf.cm
Shear modulus of fiber, G_f	: 1.391×10^7 gf.cm

The woollen yarns (see Fig. 3.1) and the yarn specifications were supplied by the Wool Research Organisation of New Zealand (Now Canesis Ltd).

A random sample of ten yarn specimens were taken for the torsional test. Each yarn specimen was twisted in a cyclic manner under a constant tension of 20 gf. The mid-points of yarn torque of the upper and lower hysteresis curves at different levels of yarn torsional strain were compared with the output of the yarn torsion model. The singles yarn model gave reasonably accurate predictions of the yarn torque rotation relationship, even though the yarn structure was not fully measured and incorporated into the yarn models. Properties such as the fiber crimp and fiber migration were ignored.

3.4 Conclusion

Research works on yarn mechanics in the past years have been briefly described in this chapter. The discrete fiber approach was considered to be more favorable when compared with the continuum approach. A

3.1 Woollen yarns – longitudinal view.

tensile–torsional singles yarn model developed by Choi *et al.*[49] was described in this chapter. The internal strain energy arising from fiber longitudinal strains has been used to calculate the torque/rotation behavior of the yarn. Bennett and Postle[50] were first to recognize that fiber tensile energy could swamp helical torsion and bending energy effects when yarns are twisted. However, in their work the tensile strain was generated by an unrealistic geometry. This new treatment allows much more realistic freedom of fiber movement in the radial direction, as dictated by the new jamming criterion.

Because this new model allows the initial geometry to have nearly zero twist, there is for the first time a theoretical means of calculating the internal strain distribution in a freshly twisted yarn. This has been cited by Postle, Carnaby and De Jong[16] as one of the great limitations in earlier yarn models since they nearly all assume the fibers to be perfectly set at zero strain in their initial helical geometry. Admittedly the case modeled applies strictly

only to static twisting,[39] since under dynamic twisting, migration effects occurring in the twist triangle below the front roller will drastically alter the developed fiber tensions. However, no previous analysis known to the authors enables this distribution to be realistically modeled for a yarn with an arbitrary initial yarn density.

3.5 References

1. Henshaw, D.E., 'A Model for Self-twist Yarn', *JTI* **62** 1970 p97–107.
2. Xie, Y., Oxenham, W. and Grosberg, P., 'A Study of the Strength of Wrapped Yarns', *JTI* 77 1986 p295–326.
3. Curiskis, J.I., Choi, K.F. and Shih, T.M., 'Mechanics of Wrapped Yarns Using Fibre-bundle Model', *The Proceedings of the 8th International Wool Textile Research Conference*, Christchurch, New Zealand, February 1990.
4. Carnaby, G.A. and Curiskis, J.I., 'The Tangent Compliance of Staple-fibre Bundles in Tension', *JTI* **78** 1987 p293–305.
5. Gegauff, C., 'Force et Elasticite des Files Sur Cotton', *Bull. Soc. Ind. Mulhouse* **77** 1907 p153–212.
6. Morton, W.E. and Yen, K.C., 'The Arrangement of Fibres in Fibro Yarns', *JTI* **43** 1952 T60–66.
7. Hearle, J.W.S. and Bose, O.N., 'Migration of Fibers in Yarns, Part II: A Geometrical Explanation of Migration' *TRJ* **30** 1965 p693–699.
8. Riding, G., 'An Experimental Study of the Geometrical Structure of Single Yarns', *JTI* **50** 1959 T425–442.
9. Hearle, J.W.S. and Merchant, V.B., 'Interchange of Position among the Components of a Seven-ply Structure : Mechanism of Migration', *JTI* **53** 1962 T537–552.
10. Hearle, J.W.S., Gupta, B.S. and Merchant, V.B., 'Migration of Fibers in Yarns, Part I: Characterization and Idealization of Migration Behaviour', *TRJ* **30** 1965 p329–334.
11. Treloar, L.R.G. and Riding, G., 'Migrating Filament Theory : Apparent Variation of Twist with Radial Position', *JTI* **56** 1965 T381–383.
12. Van Luijk, C.J., Carr, A.J. and Carnaby, G.A., 'The Mechanics of Staple-fibre Yarn, Part I: Modelling Assumptions and Part II Analysis and Results', *JTI* **76** 1985 p11–29.
13. Zurek, W., 'Some Properties of Continuous Filament Yarn', *TRJ* **31** 1961 p504–514.
14. Hearle, J.W.S. and Bose, O.N., 'The Form of Yarn Twisting, Part I: Ideal Cylindrical and Ribbon-twisted Forms, Part II: Experimental Studies', *JTI* **57** 1966 T294–320.
15. Hickie, T.S. and Chaikin, M., 'Some Aspects of Worsted Yarn Structure, Part III: The Fibre Packing Density in the Cross-section of some Worsted Yarns', *JTI* **65** 1974 p433–437.
16. Postle, R., Carnaby, G.A. and De Jong, S., *The Mechanics of Wool Structure*, Ellis Horwood Limited 1983.
17. Hearle, J.W.S., 'Theoretical Analysis of the Mechanics of Twisted Staple Fiber Yarns', *TRJ* **35** 1965 p1060–1071.

18. van Wyk, C.M., 'Note on the Compressibility of Wool', *JTI* **37** 1946 T285–292.
19. Chaudri, M.A. and Whiteley, K.J., 'The Influence of Natural Variations in Fiber Properties on the Bulk compression of Wool', *TRJ* **38** 1968 p897–906.
20. Sebestyen, E. and Hickie, T.S., 'The Effect of Certain Fibre Parameters on the Compressibility of Wool', *JTI* **62** 1971 p545–560.
21. Carnaby, G.A., *The Structure and Mechanical Properties of Wool Carpet Yarns*, PhD Thesis (University of Leeds) 1976.
22. Stearn, A.E., 'The Effect of Anisotropy in the Randomness of Fibre Orientation on Fibre-to-fibre Contacts', *JTI* **62** 1971 p353–360.
23. Komori, T. and Makishima, K., 'Numbers of Fiber-to-fiber Contacts in General Fiber Assemblies', *TRJ* **47** 1977 p13–17.
24. Lee, D.H. and Lee, J.K., 'Initial Compressional Behaviour of Fibre Assembly', in *Objective Measurement: Applications to Product Design and Process Control*, Edited by Kawabata, S., Postle, R., Niwa, M., The Textile Machinery Society of Japan, Osaka 1985 p613–622.
25. Carnaby, G.A. and Pan, N., 'Theory of the Compression Hysteresis of Fibrous Assemblies', *TRJ* **59** 1989 p275–284.
26. Pan, N. and Carnaby, G.A., 'Theory of the Shear Deformation of Fibrous Assemblies', *TRJ* **59** 1989 p285–292.
27. Djaja, R.G., Carnaby, G.A., Moss, P.J., Carr, A.J. and Lee, D.H., 'Finite Element Modelling of an Oriented Assembly of Continuous Fibers', *TRJ* **62** 1992 p445–457.
28. Dunlop, J.L., 'The Determination of the Compressive Bulk Modulus from Acoustic-impedance Measurements: The Development of the Technique', *JTI* **65** 1974 p344–346.
29. Dunlop, J.L., 'Characterizing the Compression Properties of Fibre Masses', *JTI* **65** 1974 p532–536.
30. Carnaby, G.A., 'The Compression of Fibrous Assemblies with Application to Yarn Mechanics', *Proceedings of the NATO Advanced Study Institute on Mechanics of Flexible Fibre Assemblies*, Kilini, Greece, August 19–September 2, 1979.
31. Platt, M.M., 'Mechanics of Elastic Performance of Textile Materials, Part III: Some Aspects of Stress Analysis of Textile Structure – Continuous Filament Yarns', *TRJ* **20** 1950 p519–533.
32. Hearle, J.W.S., 'The Mechanics of Twisted Yarns: The Influence of Transverse Forces on Tensile Behaviour', *JTI* **49** 1958 T389–403.
33. Batra, S.K., 'The Normal Force between Twisted Filament, Part I: The Fibre-wound-on-cylinder Model – Analytical Treatment', *JTI* **63** 1972 p209–222.
34. Dogü, I., 'The Distribution of Transverse Pressure in a Twisted Yarn Allowing for the Fiber Migration and Variation of Fiber Packing Density', *TRJ* **42** 1972 p726–733.
35. Hearle, J.W.S., Communications to the Editor, *TRJ* **65** 1974 p394.
36. Postle, L.J., Ingham, J. and Cox, D.R., 'The Measurement of Inter-fibre Friction in Slivers', *JTI* **43** 1952 T77–90.
37. Grosberg, P., 'Strength of Twistless Sliver', *JTI* **54** 1963 T223–233.
38. Lekhnitskii, S.G., *Theory of Elasticity of an Anisotropic Elastic Body*, Holdenday, San Francisco, California, 1963.

39. Carnaby, G.A. and Postle, R., 'Discrete Fibre Versus Continuum Models in the Mechanics of Staple Yarns', *Journal of Applied Polymer Science: Applied Polymer Symposium* **47** 1991 p341–354.
40. Hearle, J.W.S., El-Behery, H. and Thabur, V.M., 'The Mechanics of Twisted Yarns: Theoretical Development', *JTI* **52** 1961 T197–220.
41. White, J.L., Cheng, C.C. and Duckett, K.E., 'An Approach to Friction Effects in Twisted Yarns', *TRJ* **46** 1976 p496–501.
42. Huang, N.C. and Funk, G.E., 'Theory of Extension of Elastic Continuous Filament Yarns', *TRJ* **45** 1975 p14–24.
43. Thwaites, J.J., 'A Continuum Model for Yarn Mechanics', *Proceedings of the NATO Advanced Study Institute of Mechanics of Flexible Fibre Assemblies*, Kilini, Greece, August 19–September 2, 1979.
44. Van Luijk, C.J., Carr, A.J. and Carnaby, G.A., 'The Finite Element Analysis of Yarns, Part I: Yarn Model and Energy Formulation, Part II: Stress Analysis', *JTI* **74** 1983 p343–363.
45. Tandon, S.K., Carnaby, G.A., Kim, S.J. and Choi, K.F., 'The Mechanics of the Torsional Behaviour of Singles Yarns – Part I: Theory', *JTI* 1995 p187–193.
46. Huang, N.C., 'Finite Extension of an Elastic Strand with a Central Core', *Journal of Applied Mechanics* 1978 p852–853.
47. Costello, G.A. and Phillips, J.W., 'A More Exact Theory for Twisted Wire Cables', *Journal of the Engineering Mechanics Division*, *ASCE*, **100** 1974 p1096–1099.
48. Lanteigne, J., 'Theoretical Estimation of the Response of Helically Armoured Cables to Tension, Torsion and Bending', *JAM* 1985 p423–432.
49. Choi, K.F., Carnaby, G.A., Shih, T.M. and Lo, M.T., 'A Theoretical Torsional Model of Singles Yarn', *Research Journal of Textile and Apparel*, **2**, No. 1, Oct. 1998, pp. 1–12.
50. Bennett, J.M. and Postle, R., 'A Study of Yarn Torque and its Dependence on the Distribution of Fibre Tensile Stress in the Yarn, Part I: Theoretical Analysis, Part II: Experimental', *JTI* **70** 1979 p121–141.

4

Fabric mechanics

X-Q. DAI[1,2], K.F. CHOI[1], Y. LI[1]
[1]The Hong Kong Polytechnic University, China
[2]Soochow University, China

4.1 Introduction

Fabrics are the fundamental materials constituting garments and textile devices. The biomechanical functional performance of garments and devices is very much dependent on their fabrics' mechanical and surface properties, which are largely determined by the constituting fibers and yarns, internal structural features and surface morphological characteristics of the individual fabrics. Scientific understanding and knowledge of the fabric mechanical properties and modeling their mechanical behavior are essential for biomechanical engineering of clothing and textile products. In this chapter, the knowledge and processes developed in the area of fabric mechanics in relation to biomechanical engineering are reviewed.

Textile fabrics are manufactured assemblies of fibers and/or yarns that have substantial surface area in relation to thickness and sufficient mechanical strength to give the assembly inherent cohesion. Based on the nature of the yarn or fiber arrangements, fabrics are classified as woven, knitted, twisted and knotted, non-woven, or compound fabric. Among them, woven fabric and knit fabric are the major materials for apparel use. Thus, these two types of fabrics will be focused on.

4.2 Woven fabrics

4.2.1 Structure

Woven fabric consists of two or more sets of yarns that are interlaced at right angles to each other. Figure 4.1 illustrates a small section of a woven fabric; a surface view is presented along with two cross-sectional views, one lengthwise and one crosswise. The yarns in the lengthwise direction are warp yarns, and those transverse crosswise are weft yarns. The bias direction is any direction other than lengthwise and crosswise and a 'true bias' indicates that it runs at a 45° angle to the lengthwise direction.

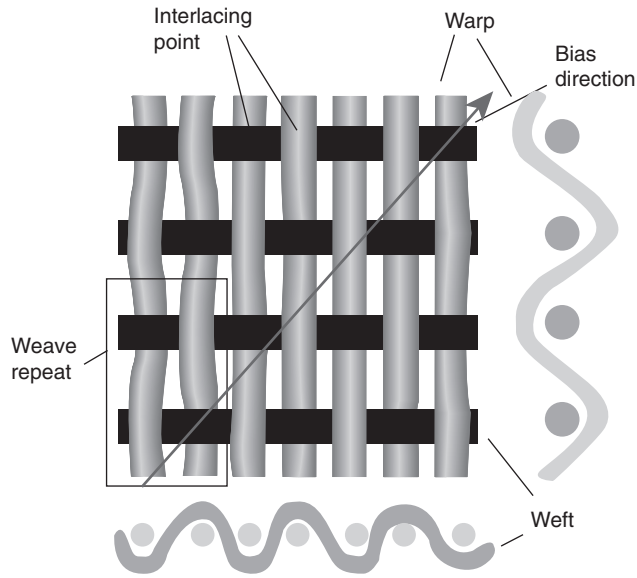

4.1 Woven fabric.

Woven fabrics have a face and back. The face usually has the more attractive appearance and is the side viewed during wear or use. An interlacing pattern is used to describe the movement of the warp or the weft yarns from the surface to the back of the fabric and *vice versa*, and of the manner in which adjacent yarns complete the movement relative to one another. The weave repeat marked in Fig. 4.1 is sufficient to show one pattern. The smallest number of warp and weft yarns can be represented: In this case, two warp and two weft yarns are just sufficient. Besides the description of fabric weave, there are several other parameters to describe fabric geometry:

Fabric count is the number of warp and weft (or filling) yarns per inch (25 mm) of a fabric. It is often written as $W \times F$. Fabric count is an important determinant of the quality of fabric and affects various mechanical properties of the fabric.

Balance is the ratio of warp yarns to weft yarns in a fabric. A balanced fabric has approximately one warp yarn for every filling yarn, thus the ratio is 1:1. Balance is helpful in determining the warp direction of fabrics, which usually have more warp yarns than filling yarns.

Fabric thickness is one of the basic properties of a fabric giving information on its warmth, heaviness, and stiffness in use.

Fabric weight is fabric mass per unit area. It is often used commercially as an indicator of thickness instead of fabric thickness itself.

Fabric width depends on the loom on which the fabric is manufactured.

4.2.2 Mechanical behavior

Basic deformation of fabric

Fabrics are complex assemblages of interwoven threads, which are themselves assemblages of twisted fibers. The frictional forces between the fibers and the threads give the fabric a stable structure. Fabrics are therefore anisotropic, inhomogeneous, discontinuous materials. In practical use, fabrics are subject to a wide range of complex deformations. Among them are included such effects as drape, wrinkling, creasing and other aesthetic characteristics. In order to understand fabric mechanics well, it is necessary to split such deformations up into a collection of simpler deformations such as tensile, shearing, bending, and twisting.

Tensile: When a fabric is subjected to a load applied to the warp or weft direction at a constant rate of elongation, it is stretched. Due to the fabric discontinuity, the fabric shows different extension response during the lower and higher extension regions. Figure 4.2 shows a typical load–extension curve, which can be divided into three sections. In the first part, the load increases rapidly along with the elongation; the slope of the curve in this region is taken as Young's modulus to denote this tensile property of the fabric. This initial high modulus is probably due to the frictional resistance to the bending of the thread. Once this resistance is overcome, the extension during the second part is due mainly to crimp redistribution; a

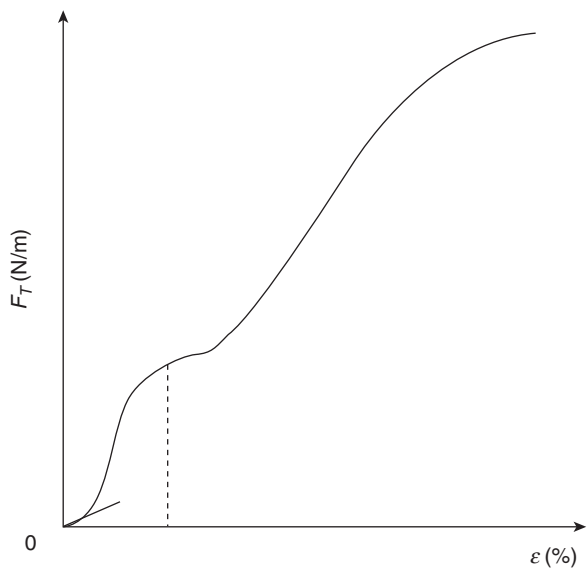

4.2 Modeled load–elongation curve.

relatively low modulus is obtained, which is mainly governed by the force needed to de-crimp the threads in the direction in which the load is being applied (illustrated in Fig. 4.3), and simultaneously the need to increase the curvature in the interlaced threads. As the crimp is decreased, the load rises very steeply and, as a result, the threads in the loaded direction begin to be extended. In this final region, the load–elongation properties of the fabric are almost entirely governed by the load–elongation properties of the yarns themselves. Because a fabric usually has a different construction of warp and weft yarns, the tensile moduli in the warp and the weft directions may differ largely; thus the fabric shows obvious anisotropy of tensile properties.

Shear: The shear deformation of woven fabrics is very different from that of continuous materials such as paper or plastic film. Because there may be slippage between threads at crossover contact regions (Fig. 4.4a), the

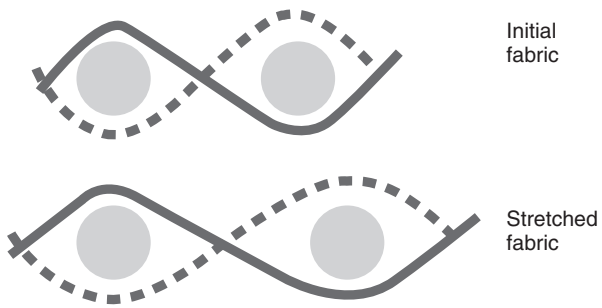

4.3 Stretch deformation.

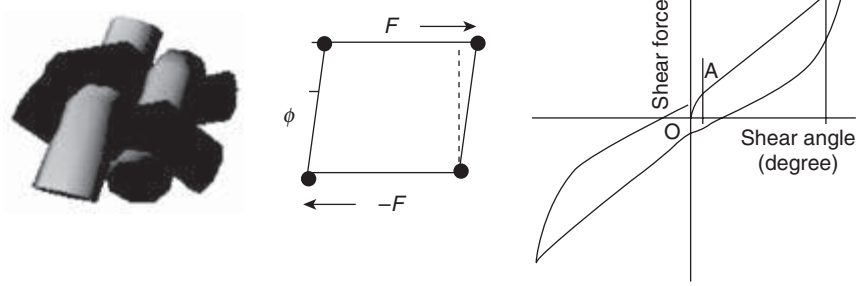

(a) Shear deformation (b) Common representation of shear (c) Schematic shear stress/shear-strain curve

4.4 Fabric shear.

resistance to shear deformation is very low compared with tensile deformation. A common representation of shear is illustrated in Fig. 4.4b: a rectangular element of sheet material is subjected to pairs of equal and opposite stresses F, which are acting parallel to the side of the element; in the case of simple shear, it is assumed that the element deforms in such a way that its area remains constant.[1] The shear strain is defined as the tangent of the change in angle between the sides of the element ϕ. Then, for elastic material, there exists: $F = G\tan\phi$, where G denotes the shear modulus.

However, fabric is not an elastic material, so its shear property also shows nonlinearity. The shear response is often reflected as the shear stress–strain curve (Fig. 4.4c). The curve can be divided into three regions: the initial, nonlinear region, where the shear is governed by the frictional forces resisting the relative rotation of the yarns, coupled with the elastic bending deformation of the yarns; the second, linear region, after the slippage between threads has taken place, where, therefore, the shear is due progressively to this slippage and the intersection of the bent yarns in the crimp requires further bending of the yarns; and the third, nonlinear region, where the shear resistance rapidly increases because of the increasing contact area between the two threads and the jamming of the structure. The slope of the second part of the shear-force/shear-angle curve (the shear rigidity) is often taken to represent the shear property. The curve shows obvious hysteresis.

Bending: Fabrics undergo large deformations for small applied forces. What distinguishes fabrics from other sheet materials is their ability to buckle gracefully in rounded folds and form draped shapes. A complete understanding of the mechanism of the bending of a woven fabric requires knowledge of the relationship between fabric bending rigidity, the structural features of the fabric and the tensile/bending properties of the constituent yarns. Former studies have made it clear that the resistance in the simple warp-wise or weft-wise bending is made up of three components: the bending resistance of the threads, some interaction between the threads, and a frictional restraint.[2] Figure 4.5a illustrates the yarn deformation during fabric bending.

The bending property is represented usually by the relationship of bending moment (M) and bending curvature (K), which is measured in pure bending as illustrated in Fig. 4.5b. If the material is elastic, then $M = BK$, where B denotes the bending rigidity. Figure 4.5c shows a schematic bending curve. The initial bending is governed by the frictional restraint to bending. The frictional force is produced mainly by an inter-yarn pressure acting at the cross-over regions in a woven fabric. The behavior is nonlinear. After the frictional force is overcome, completely free bending begins and it is of

an elastic nature. This final bending rigidity is of the same order of magnitude as (often greater than) the sum of the bending resistances of the crimped yarns in the fabric. The excess bending resistance arises from the increased inter-yarn penetration of the two crossed yarns during bending. The slope taken from the linear part of the bending curve illustrates bending rigidity. The bending curve also shows hysteresis.

Twisting: When a fabric is bent along a bias direction, the deformation is complicated by consisting of warp-wise and weft-wise bending, and twist.[3] As illustrated in Fig. 4.6, twist is a 3D deformation. The twist property is usually represented by the relationship of torsional torque (T) and twist deformation (K_W). If the relationship is linear, then $T = \tau K_W$, where τ denotes the twist rigidity.

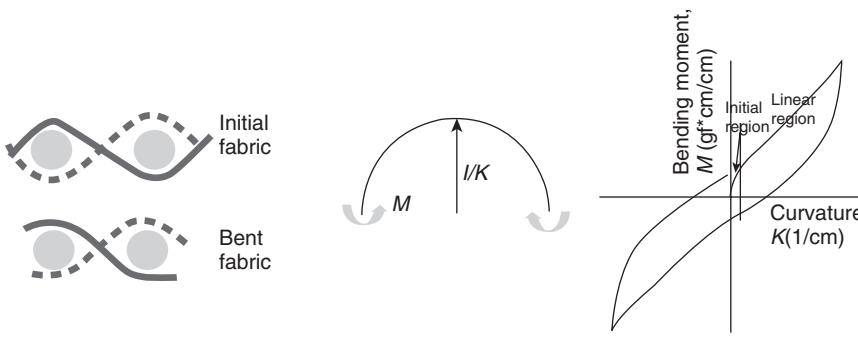

(a) Bending deformation (b) Bending moment and curvature (c) Schematic bending curve

4.5 Bending.

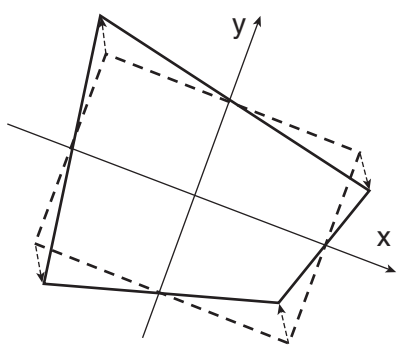

4.6 Twist.

Complex deformation

Buckling: When a fabric is under axial compression, it buckles easily rather than being compressed. The load at which buckling occurs is called the buckling load. Before buckling occurs, the fabric may be compressed a certain distance. This compression at buckling load is called buckling compression. It will be of special importance in determining the formability of a fabric. When a plate fabric buckles, it often takes up a sinusoidal shape. This is called plate buckling. The buckling of a cylindrical fabric will be of a more complex nature. It involves buckling not only in the length direction but also produces a form of wave at the cross-sectional direction. Such deformation is usually called shell buckling.

Rheological behavior: As a fabric is worn, it is subjected to stretching, bending, shearing, twisting, compression, and other distorting forces. These forces will cause wrinkles and creases; consequently, the fabric will bag or sag. Bagging is a typical behavior resulting from fabric rheological properties. It is a type of 3D residual deformation of fabric after prolonged use. Garment bagging often occurs at positions such as the knees, the elbows, the seat and the shoulders, where repeated or prolonged deformations are exerted by moving body parts. Several test methods have been developed to investigate fabric rheological behavior. In the bagging test developed by Zhang,[4] a fabric specimen is clamped in a circle and is deformed repeatedly from the center by a steel ball, and then the bagging height along with the load is recorded. Bagging deformation may involve a number of structural changes: (i) yarn rotation and slippage at the interlacing points during shearing; (ii) yarn bending and compression at interlacing points during tensile and shearing; (iii) yarn extension between interlacing points; (iv) fibre slippage and extension in the yarns at interlacing points and between interlacing points. All of these changes interact with each other to meet the requirements of 3D deformation of the fabric at different bagging stages. Although bagging involves so many sophisticated structural changes and various mechanical deformation processes in fibers, between fibers and between yarns, the deformation during bagging can be classified into three categories: elastic deformation, viscoelastic deformation and frictional deformation.

4.2.3 Model simple mechanical behaviors

There are two major approaches to model woven fabric mechanical behavior: one is to consider a structural weave unit of the fabric (low level) and the other one is to consider fabric deformation of a large-scale shape and neglect the micro-structure (high level). The low-level models are used to

investigate the tensile, shearing and bending properties separately, while the high-level models are often used to predict the whole aesthetic appearance of fabrics such as folding, wrinkling and draping. Here, the focus is on the low-level modeling. High-level modeling will be addressed in the next chapter.

Geometric–mechanical models

Peirce[5] was the first pioneer in cloth modeling research. In the mid-1930s he developed and analyzed a basic modeling cell of fabric geometry, detailing the geometric relationships among yarns at a yarn crossing. He shows that if it is assumed that the bending resistance of the yarns is negligible and that the yarn is circular in cross-section, a purely geometrical model, which involves no consideration of internal forces, can be set up for the determination of the various parameters that are required. This model becomes a basic description of woven fabrics. Peirce derived a set of equations for these parameters. The three equations involve seven parameters; and given four of them, the other three can be obtained.

The basic difficulty in such a calculation when using the Peirce approach arises from the fact that the yarn cross-section is often far from circular. Many attempts have been made to modify Peirce's original relationships by assuming various shapes for the yarn cross-sections. The ellipse and racetrack are the two proposed cross-sections.[6,7] The geometry model of fabric can be used to calculate the weave angles, radii of curvature and crimp height for a plain weave fabric in which the thread spacing and crimps are known, and to estimate the degree of flattening of the yarns. It can also be used to find the minimum value of p_2 for a plain weave fabric made from the same yarn, whose diameter is given, and the value of p_1 is also fixed. Details can be found in reference 6.

Besides the pure geometrical model of a fabric, Peirce also proposed an elastic thread model to take account of the yarn bending resistance. An elastica is used to represent the crimped thread. The physics of elasticas was explored by Euler in 1744 and has been concisely summarized by Konopasek.[8] An elastica is a slender rod, and it is assumed that the bending moment at any point along the central axis of the rod is linearly proportional to the increment of the curvature caused by that moment. The warp and weft threads only touch at the crossing point, and U and V denote the external force components in horizontal (x) and vertical (y) directions. Thus, there is:

$$EI\frac{\mathrm{d}\varphi}{\mathrm{d}s} = -Vx + Uy.$$

Here, EI is the bending rigidity of the thread, $\mathrm{d}\varphi/\mathrm{d}s$ denotes the curvature of the yarn. Only one solution for the equation when U is zero is obtained,

and the yarn crimp for various values of weave angles is calculated. The case where the yarns are in line contact with the cross yarns is also analyzed.

In 1964, Olofsson[9] proposed a model that is structurally similar to Peirce's elastic thread model. He considered that the geometry of yarns in a weave is a function of external forces and reaction forces in the fabric, and assumed that the forces produced by continuous contact between yarns may be approximated with point forces. He studied the general case of bi-axially loaded fabric, wherein both vertical and horizontal forces are present at the yarn crossover points. In addition, he introduced the idea of the permanent deformation of yarns due to bending, leading to 'setting' of the yarn in crimped form. A new parameter, the form factor, φ, is used as a measure of setting. He then assumed a relationship between the curvature of the yarn in the fabric and in the released state:

$$\frac{\mathrm{d}\varphi_0}{\mathrm{d}s_0} = (1+\psi)\frac{\mathrm{d}\varphi}{\mathrm{d}s}.$$

Then the bending moment is modified as

$$M = -E_b I\left(\frac{\mathrm{d}\varphi}{\mathrm{d}s} - \frac{\mathrm{d}\varphi_0}{\mathrm{d}s_0}\right).$$

A bending energy is also derived, based on the mechanics of elastic structures. He also introduced the thread diameters as secondary parameters and suggested that the flattening of the thread should be considered. Through his analysis, he presented equations for the equilibrium conditions and stress–strain relationships within the yarn-crossing structure under low stress. However, no evidence was provided to support the validity of his results.

Grosberg and Kedia[10] also presented a model similar to Olofsson's. The assumptions made are: the length of yarn between two intersecting points remains constant during extension, and its shape is determined by the forces acting at the intersections and can be obtained by assuming the yarn to be an infinitely thin beam. Therefore, the tensile and bending properties are considered, and the effect of compression is ignored. The bending moment equation is solved arithmetically by means of a Taylor series method. The load–extension relationship is obtained by a graphical method. By using this model to investigate the initial load extension modulus of several fabrics, they showed that the theoretical deductions were in accord with experimental findings.

Konopasek,[8,11] in his treatment of the elastica-based model, considered two planar bending curves as the axes of the warp and weft threads. He obtained the equilibrium fabric structure by solving two sets of equations of planar bending curves for warp and weft threads with properly formulated boundary constraints.

In 1985, Leaf and Anandjiwala[12] enhanced Peirce's model by assuming that the yarn in this model can be considered as an elastica with Huang's bilinear bending-moment model. Huang[13] proposed that the moment–curvature relationship of bending fabric can be modeled by two linear segments: the first one has a steep slope in the low-curvature region while the second one has a much lower slope in the high-curvature region. They developed equations that defined the relationship between the geometric parameters of their modeling structure. Their paper provides some data that confirm the ability of their model to predict these geometric relationships. Furthermore, Anandjiwala and Leaf[14,15] use the model to analyze the large-scale load–extension behavior of a plain weave fabric subjected to biaxial forces over repeated cycles of loading and unloading. The yarn bending, extension and inter-yarn compression are considered. They point out that the stress behavior is predominantly influenced by yarn bending parameters. Their theoretical analysis is also confirmed by experiments.

Ghosh, Batra and Barker[2,16,17] proposed a further extension and revision of Peirce's model that is similar to the work of Olofsson, and Leaf and Anandjiwala. Both linear and bilinear bending-moment models were used to study the bending behavior of plain-woven fabrics. The extension they made was to model a line contact between crossing yarns. They produced a set of calculations to predict a range of fabric bending rigidities that reasonably matched the corresponding experimental results. However, the samples were limited to fabrics made of monofilament yarns that closely behave as elasticas.

Lomov *et al.*[18] also proposed a model to predict the fabric-to-yarn bending stiffness ratio of plain-woven set fabric. The model was structurally similar to Peirce's model. A polynomial approximation for the elastica was constructed, and both point contact and line contact were modeled. The fabric deformation was considered as a coordinate transformation. Their model was validated by comparison with published experimental data.

Most of the above-mentioned models try to describe the 2D curve of the loaded thread axis; the cross-threads are often considered by adding various constraints at crossing point or contact line. In 1973, Kawabata, Niwa and Kawai[19–21] proposed a model to describe a 3D yarn crossing structure of woven fabric. The warp and weft yarns can be represented by straight lines that bend at two points on the axis perpendicular to the fabric plane. The equilibrium formula is

$$F_c = 2F_{T1}\cos\theta_1 = 2F_{T2}\cos\theta_2.$$

Here, F_c is the compression force between the warp and weft yarns at the contact point, F_{T1} and F_{T2} denote the tensile forces in the warp and weft yarns respectively, and θ_1 *and* θ_2 denote the bending angles of the two yarns. Additional to the yarn tensile property, the yarn compressibility

under the action of a lateral compressive force is also introduced into the model. Graphic methods are used to solve the equation under different conditions. Their model includes several 'black boxes', which contain mechanical data experimentally obtained from real fabrics. They predicted the biaxial and uniaxial tensile properties and the shearing properties of several fabrics. Comparison of the theoretical and experimental results shows that the compressive properties of yarns have a great influence on the tensile properties. In the uniaxial-deformation simulation, the bending rigidity of the transverse yarn is also considered. The complete load–extension curve from the initial to the ultimate extension is predicted. Neglection of the bending effect of the yarn along the load direction seems to account for the small error for low-extensions. It is stated that the uniaxial-deformation theory is limited to the relatively large-deformation range.

More recently, Realff, Boyce and Backer[22] took an approach similar to Kawabata's, modeling the entire uniaxial tensile stress–strain behavior of the fabric. By applying the beam theory model to the cross-yarn, the yarn curvature is taken into account. The model includes a more complete representation of yarn behavior. The yarn properties used, such as tensile response, flattening, bending and consolidation, are measured out of the fabric; no properties are back-calculated based on the fabric behavior. The tensile behavior of several fabrics of differing weave and yarn construction is investigated. In most cases, there is good agreement between the theoretical and experimental results reported, while they suggested some modification for the tightly woven fabric.

Strain energy methods

In the late 1970s, De Jong and Postle[23–26] presented an energy method to model the shape of deformed yarns, based on the assumption that yarns have simple elastic deformation properties and any fabric structures consisting of such yarns reach equilibrium in a minimum strain energy configuration. In a quarter-wave of the yarn crimp in plain-woven fabric under tension, let P denotes the cloth extension and Q represents half the reaction force of the crossing yarn. Since fabric shear is not taken into account, the 3D problem is reduced to 2D form. The total strain energy stored in the quarter-wave subjected to forces P and Q, includes bending and longitudinal tension, based on the curvature and extension of the yarn geometry: $U = \int_0^1 \frac{1}{2}\left\{(m_1 - m_1^0)^2 + \frac{Y}{B}(m_h - 1)^2\right\}\mathrm{d}s$. Here, Y, and B are the extension and bending rigidities of the yarn; m_1, m_1^0 are the yarn curvature inside the fabric and that released from the fabric respectively; and m_h is the local length of the yarn element (its value is 1 for un-extended yarn). The energy function is minimized by applying methods from optimal control theory. With this model, De Jong and Postle predicted tensile and bending

properties of several materials, producing reasonable results when compared to actual fabrics.

Knoll[27,28] modified the work of De Jong and Postle by including the effects of jamming and contact constraints between cross-yarns. He showed that many of the yarn configurations modeled by Peirce could be reproduced with the same results by using De Jong and Postle's method.

Sinoimeri and Drean[29] applied De Jong and Postle's energy approach to the study of the pure shearing of a plain-woven fabric. One extension was that a rheological model was introduced in the analysis to account for the possible slippage between threads at crossover contact regions. In this model, the slippage threshold and the slippage angle were assumed to be linearly related to the sum of the compression forces between the threads. The predicted shear stress–strain curves agreed well with the corresponding experimental ones.

Hearle and Shanahan[3,30] also developed an energy-based modeling approach very similar to De Jong and Postle's. Their technique employed a somewhat awkward explicit formulation of yarn geometry, as compared to De Jong and Postle's parametric yarn geometry description. Therefore, it is less general than De Jong and Postle's method. They derived equations for the Peirce and Kemp yarn structures, and their own 'lenticular' geometry, which is constructed to avoid the difficulties encountered with Kemp's racetrack geometry. An interactive system called QAS (Question Answering Systems on algebraic equations) was used to solve the sets of non-linear simultaneous equations representing the combination of the three cases: (i) crimp interchange mechanism with or without (ii) yarn stretching and/or (iii) yarn bending rigidity effects. They calculated the load–extension and bending–curvature plots for various yarn structures.

Leaf and Kandil[31] used a model structurally the same as Kawabata's model to analyze the initial load–extension behavior of plain weave fabric. The energy stored in the unit, consisting of bending, extension and compression strain energies, is calculated. Castigliano's theorem is used to solve the fabric extension. Many fabrics of various materials and constructions were investigated, and most of the predicted initial Young's moduli showed good agreement with the experimental results.

Finite element method

Both the geometrical–mechanical approach and energy approach describe the geometry of parts of a weave structural unit, and try to obtain the centerline shape of the thread. The yarn is modeled as a one-dimensional line, not a solid with volume. It is difficult for these models to discuss the deformation of the cross-section and the contact detail among threads. And it is also impossible for them to describe fabrics of other weaves of non-symmetric and complex geometrical structures. To solve these problems,

Tarfaoui[32] tried to apply the Finite Element Method (FEM) to woven fabric modeling. The cross-section of the yarn is meshed by quadrangles with four nodes; the mesh of the yarn is obtained from the basic section, to which is applied adequate translations of well-defined vectors. Basic cells of a plain weave and a twill weave fabric were constructed and their mechanical behavior when subjected to several kinds of stress (uniaxial tensile, biaxial tensile and shear) was investigated. An overload phenomenon was observed.

FEM enables the simulation of complex fabrics subjected to various loads. However, since a single yarn piece between cross-points is represented by a large number of elements, the computational cost becomes a critical issue and thus limits the application of FEM to micro-mechanics of fabrics. FEM is also used in modeling woven composites.[33]

Computational micro-particle model

In the above-mentioned models, only a structural weave unit is considered, and various boundary conditions are added denoting the stress to which the fabrics are subjected. The yarns in fabrics are often assumed to remain in the same plane during extension and bending, and the 3D problem is reduced to a 2D one. This is quite different from the actual state for a piece of fabric under a load. Li and Dai[34] developed an approach to dynamically simulate a piece of fabric subjected to various tensile loads. Similarly to Kawabata's model, the yarn centerline is simplified as straight-line segments and the yarn cross-sections are assumed as circles. Various springs of separation, bending, compression, wrapping and torsion are imaged acting among particles to simulate various yarn behaviors. The model was used to investigate the tensile response under low extension of plain weave fabrics of various fabric counts. The simulated load–elongation curves were compared with the experimental results. A good summary of low-level fabric modeling can be found in reference 35.

4.2.4 Buckling model

When a fabric buckles, it often takes up a sinusoidal shape. By taking a cross-sectional view of a simply buckled fabric, it may be represented by a planar curve. An elastica is often used to simulate this curve. The differential equation for the elastica is $B\frac{\mathrm{d}s}{\mathrm{d}\phi} = -Py$, where B is the fabric bending rigidity, P is the compressive load, and s is the distance measured along the curve. By integrating ds along the length of the curve when the value of s becomes equal to l, the gauge length, the following equation can be obtained:

$$Pl^2/B = 4\{F(k)\}^2,$$

where $F(k)$ is the complete elliptic integral of the second kind of modulus k (= $\sin\alpha/2$). The standard solutions for the curve are usually expressed as the variation of $Pl^2/4B$ with the percentage compression of the fabric. For elastic buckling, the plot is a straight line. However, it has been found that cloth, when buckled, behaves in a different way. Grosberg *et al.*[10,36] have shown that before a cloth bends in a linear fashion, the frictional couple M_0 is needed to overcome the initial friction between the fibers in the interaction. It can be written as:

$$\begin{cases} 1/\rho = 0 & M < M_0 \\ B/\rho = M - M_0 & M > M_0. \end{cases}$$

Here, ρ corresponds to the radius of bending curvature. By assuming this relationship, they derived a series of theoretical buckling curves that were in accord with the actual buckling of cloth. They also found that nearly all the hysteresis seen during buckling and the amount of strain left after one cycle are almost wholly determined by the frictional restraint that arises in the fabric due to inter-yarn pressures.

More recently, Clapp and Peng published a series of papers that attempted to refine the classical models for describing the buckling of woven fabrics.[37–39] Using Timoshenko's elastica theory, they established a differential equation of fabric in which fabric weight is taken into account. The fabric elastica was modeled as a curved beam of constant cross-section; numerical solutions for the differential equation were obtained under two types of boundary conditions at the beam's two ends of (i) symmetrical, free–free ends and fixed–fixed ends, and (ii) unsymmetrical, free–fixed ends. They found that both frictional couple and fabric weight may jointly contribute to determine the buckling state if their values are not negligible.

Shinohara *et al.*[40,41] developed a mathematical model to describe the buckling deformation of a tubular fabric in axial compression. Two groups of contour hyperbolas, which can be determined by boundary conditions for any lobe ratio, can be used to represent the deformed surface on a lobe. They declared that the mathematical model can be used to predict the buckling pattern with any specified lobe ratio and many characteristics of the buckling pattern can be understood with the use of three-dimensional graphics.

4.2.5 Rheological model

Grosberg[42] pointed out that the energy loss during cyclic deformation of a fabric is due to two separate reasons: fiber viscoelastic properties; and the frictional restraint to inter-fiber and inter-yarn movements in fabric during deformation. Theory of fabric rheology was introduced by Olofsson[43–45] and by Grosberg.[42,46,47] They considered the role of inter-fiber and inter-yarn

friction in order to predict fabric hysteresis and recovery from the deformation. In 1969, Olofsson[45] reported an extensive study on fabric rheological behavior. He proposed a series of fabric models that contained elastic, viscous and frictional elements to describe features of bending and shear deformation. In 1977, Grosberg[42] made a detailed analysis on the role of friction in the tension, shearing, and bending deformations of woven fabric at the initial deformation stage. Fabric rheology was further studied by Chapman in the seventies, with the inclusion of fiber viscoelasticity as well as inter-fiber and inter-yarn friction in the models of fabric deformation and recovery.[48–50] He presented a model that took into account the linear viscoelasticity and the frictional moment of fabric, to predict the bending and bending recovery of fabric strip.[50] By measuring the fiber viscoelastic processes of stress relaxation and creep, the deformation of a viscoelastic textile material could be predicted using this model.

More recently, Zhang *et al.* did a systematic study about the rheological mechanism in fabric bagging, and developed a series of models to describe bagging deformation of fabric.[51–56] Their models[4,53] were based on the standard solid model[57] and Olofsson's rheological model of fabric.[45] The stress–strain relations for elastic elements and viscoelastic elements in the models were assumed to be linear. By specifying the fundamental properties of fibers, the measurable parameters of the yarn and fabric structural features, and the geometrical relation between strain and bagging height, their models were able to predict fabric bagging behavior.

4.3 Knitted fabrics

4.3.1 Structure

Knit fabrics are composed of intermeshing loops of yarns. There are two major types of knits: weft knits and warp knits, as illustrated in Fig. 4.7. In weft knits, each weft yarn lies more or less at right angles to the direction in which the fabric is produced, and the intermeshing yarn traverses the fabric crosswise. In warp knits, each warp yarn is more or less in line with the direction in which the fabric is produced, and the intermeshing yarn traverses the fabric lengthwise. Similar to the way that woven fabrics have warps and wefts, knit fabrics have courses and wales, which lie in the crosswise and lengthwise direction, respectively. However, unlike woven fabrics, courses and wales are not composed of different sets of yarns; rather are formed by a single yarn.

'Loop' is the basic unit of knit fabric. As illustrated in Fig, 4.7a, in weft knits, a loop, called a needle loop, consists of a head and two legs, and the section of yarn connecting two adjacent needle loops is called the sinker. In warp knits, the needle loop is divided into overlap and underlap, as

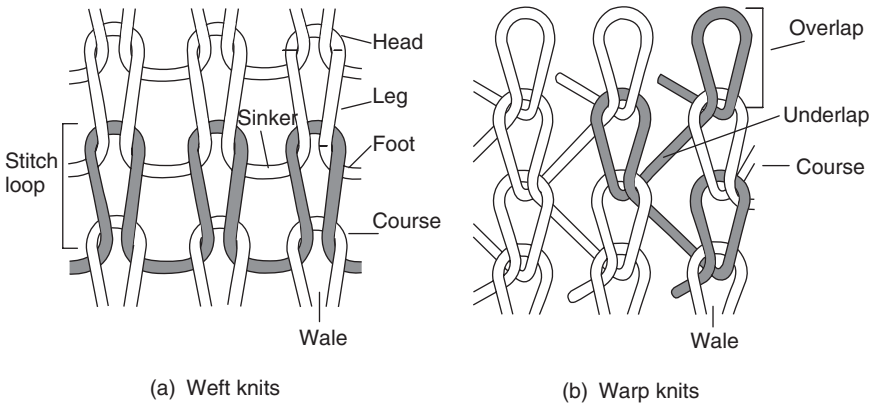

(a) Weft knits (b) Warp knits

4.7 Knit fabric.

illustrated in Fig. 4.7b. Each loop in a knit fabric is a stitch. Alternative to fabric count for woven fabrics, cut (or gauge) and stitch density are used to represent the closeness of the intermeshing loops. Cut or gauge indicates the number of knitting needles per unit length along the crosswise or lengthwise direction. The greater the number, the closer together the loops are to each other. Stitch density is the number of stitches per unit area, obtained by multiplying the number of courses per inch (25 mm) by the number of wales per inch (25 mm). Like woven fabrics, a knit fabric also has a technical face and a technical back and can differ in appearance on each side. The technical face is the side where the loops are pulled toward the viewer. Knit fabric also has an effect side, which is intended to be used outermost on a garment or other textile product. In some cases, the technical face and the effect side are the same; but in others, they are opposite.

4.3.2 Mechanical behavior

The basic factors that govern the mechanical properties of knit fabrics are the same as those that govern the mechanical properties of woven fabrics. In most cases, knitted fabrics are treated as merely variants of woven fabrics; for example, the bending and buckling of knit fabrics has never been treated separately. However, the load–extension behavior of knit fabrics, while similar in kind to the behavior of woven fabrics, shows a large difference of degree in the relative size of the initial extension as well as in the initial modulus. Generally, the resistance of the cloth to extension is mainly due to the resistance of parts of the structure to bending and torsion; therefore it is relatively small. As a result, the relative size of the frictional restraint to the extension is high. Research concerning the warp-wise load–

extension of warp knit fabrics shows that the extension modulus is dependent entirely on the resistance of the yarn to the changes in curvature that take place in the loop during extension. However, the extension of this analysis to plain weft knit seems not to be successful.

Knitted fabrics are usually subject to biaxial stresses under relatively high loads. In such cases, the knitted structure becomes only a tension transmitting body and the internal bending and shear energy changes can be neglected; thus an analysis is available. An analysis of the weft-wise stretching of rib fabrics shows that the mechanical behavior is probably determined almost entirely by the resistance of the link connecting the face and back loop in the fabric, to being twisted or sheared. Furthermore, some analysis leads to a generalization of the mechanical behavior of knitted fabrics: the load to give a fixed extension is proportional to m/l^3 when the resistance is due to bending energy changes, and to G/l^3 when it is mainly due to shear energy changes. Here, l is the loop length, and m and G denote the bending rigidity and the torsional rigidity of the yarn, respectively. More details about the mechanical behavior of knit fabrics can be found in reference 1.

4.3.3 Modeling

Geometrical model

In attempts to understand the dimensional behavior of knitted fabrics, the key element is on the geometry of the knitted loop. Peirce,[58] Leaf,[59,60] Doyle,[61] Munden,[62] Postle,[63,64] and recently Demiroz and Diaz,[65] all have significant contributions to the geometrical analysis of plain knitted fabric.

Peirce[58] extended his geometric model for plain woven fabric to plain knitted fabric. Based on the same assumptions, he deduced that the basic structure of a knitted fabric is one in which the loops consist of parts of circles joined by straight lines and in which the maximum packing of the yarns had taken place. He also assumed that the loops lie on a cylinder, to allow for the 3D properties of the needle loop. From these assumptions, he deduced an equation to describe the relationship between the stitch length l, the course spacing c, the wale spacing w, and the yarn diameter d.

Doyle[61] then suggested that, by using certain dimensionless ratios of the lengths, the properties of knit fabrics could be adequately described in a simple way. He showed that the product of c and w is proportional to l^2. Later work by Munden[62] showed that the relationship can be more universal; the slope of the graph of stitch density against $1/l^2$ is independent of the value of d/l.

Leaf,[59] and Leaf and Glaskin[66] pointed out that there was some intrinsic problem in Peirce's original geometry. They proposed an alternative – that

the loop consists merely of a set of circular arcs. Their model was further improved by assuming that the loop consists of two elasticas joined as mirror images.[59] The success of the model was due to its simplicity and a good description of the actual fabric. Recent innovative work[65] on loop geometry is the application of spline curves to represent the loop. It is especially useful in the visual display of knitted fabric in a CAD system.

Geometric–mechanical model

The dimensional properties of knitted fabric were studied by some researchers alternatively using a force method. In the theoretical models of Postle,[63] Shanahan and Postle[67] and Hepworth and Leaf,[68] yarn was treated as an elastica[69] which is naturally straight. Attempts have been made by MacRory *et al.*[70] and Hepworth and Leaf[71] to tackle the biaxial load–extension problem of knitted fabric. MacRory's model emphasized the slippage between loops and the biaxial load case with the loop elements being straightened, while Hepworth's model concentrated on the effect of yarn jamming.

Energy model

Choi and Lo[72] proposed an energy model with sufficient degrees of freedom for loop deformation, including changes in loop height and width. The yarn forming the loops is perfectly elastic and incompressible, with zero friction. It is naturally curved and its paths in the deformed states are the elements of a prescribed family of space curves. The yarns can be axially compressed or extended at the low-load region. Conditions of loop jamming are taken as the geometric constraints of loop deformation. The total mechanical energy is calculated based on the difference in bending strain and torsional strain of the yarn with respect to the natural curvature and torsion. This model can be applied to determine the biaxial tensile behavior of plain knitted fabric.

Micro-particle model

Eberhardt *et al.* proposed a model to represent knit fabrics based on the assumption that threads bond and interact with each other only at bonding points (BPs).[73] By regarding each BP as a particle, and evaluating the forces exerted by the springs that represent the stretch, compression and bending of the yarns at the bonding points, the dynamics of the particle system corresponding to the micro-structure of the knitting pattern can be simulated. Some simulations taking an initial knit configuration and 'relaxing' it to a minimal energy state were presented in reference 73.

4.4 Conclusion

As the main materials constituting garments and textile devices, woven fabrics and knitted fabrics have been addressed from various aspects, including structure, mechanical behavior and modeling. Tension, shearing, bending and twisting are the basic mechanical behaviors in garment wear. The complex deformation of fabrics includes buckling and rheological behavior. Since the fabric mechanical properties are largely determined by the constituting fibers and yarns, internal structural features and surface morphological characteristics, fabrics' micro-structures and micro-mechanics were focused on here, and the work developed in the area of lower-level fabric modeling was reviewed.

4.5 Acknowledgement

We would like to thank Hong Kong Polytechnic University for funding this research through Projects A188 and G-YD31.

4.6 References

1. Grosberg, P., *The Mechanics of Knitted Fabrics, in Structural Mechanics of Fibers, Yarns and Fabrics*, S. Backer (Editor). 1969, Wiley-Interscience: New York. p. 439–450.
2. Ghosh, T.K., Batra, S.K. and Barker, R.L., The Bending Behavior of Plain-woven Fabric, Part I: A Critical Review, *Journal of the Textile Institute.* 1990. p. 245–254.
3. Shanahan, W.J. and Hearle, J.W.S., Energy Method for Calculations in Fabric Mechanics, Part Two: Examples of Application of the Method to Woven Fabrics, *Journal of the Textile Institute.* 1978. p. 92–100.
4. Zhang, X., (ed.) *Mechanism of Woven Fabric Bagging.* Institute of Textile and Clothing. 1999, The Hong Kong Polytechnic University: Hong Kong.
5. Peirce, F.T., The Geometry of Cloth Structure, *Journal of the Textile Institute.* 1937. p. T45–T97.
6. Hearle, J.W.S., Grosberg, P. and Backer, S., *Structural Mechanics of Fibers, Yarns and Fabrics.* 1969, Wiley-Interscience: New York.
7. Kemp, A., An Extension of Peirce's Cloth Geometry to the Treatment of Non-circular Threads, *Journal of the Textile Institute.* 1958. p. T44–48.
8. Konopasek, M., Classical Elastica Theory and its Generalizations, *Mechanics of Flexible Fiber Assemblies*, J. Amirbayat (Editor) 1980, Sijthoff & Noordhoff, Alphen aan den Rijn. p. 255–274.
9. Olofsson, B., A General Model of a Fabric as a Geometric–Mechanical Structure. *Journal of the Textile Institute.* **55** 1964. T541–T557.
10. Grosberg, P. and Kedia, S., The Mechanical Properties of Woven Fabrics, Part I: The Initial Load Extension Modulus of Woven Fabrics, *Textile Research Journal*, **36** No. 1, 1966, p. 71–79. Part II: The Bending of Woven Fabrics, *Textile Research Journal.* 1966. p. 205–211.

11. Konopasek, M., Textile Applications of Slender Body Mechanics, *Mechanics of Flexible Fiber Assemblies*, J. Amirbayat, Editor. 1980, Sijthoff & Noordhoff, Alphen aan den Rijn. p. 293–310.
12. Leaf, G.A.V. and Anandjiwala, R.D., A Generalized Model of Plain Woven Fabric, *Textile Research Journal.* 1985. p. 92–99.
13. Huang, N.C., Finite Biaxial Extension of Completely Set Plain Woven Fabrics, *Journal of Applied Mechanics.* 1979. p. 651–655.
14. Anandjiwala, R.D. and Leaf, G.A.V., Large-scale Extension and Recovery of Plain Woven Fabrics, Part One: Theoretical, *Textile Research Journal.* 1991. p. 619–634.
15. Anandjiwala, R.D. and Leaf, G.A.V., Large-scale Extension and Recovery of Plain Woven fabrics, Part Two: Experimental and Discussion, *Textile Research Journal.* 1991. p. 743–755.
16. Ghosh, T.K., Batra, S.K. and Barker, R.L., The Bending Behavior of Plain-woven Fabric, Part II: The Case of Linear Thread-bending Behavior, *Journal of the Textile Institute.* 1990. p. 255–271.
17. Ghosh, T.K., Batra, S.K. and Barker, R.L., The Bending Behavior of Plain-woven Fabric, Part III: Thread-bending Behavior and the Effect of Fabric Set, *Journal of the Textile Institute.* 1990. p. 272–287.
18. Lomov, S.V., Truevtzev, A.V. and Cassidy, C., A Predictive Model for the Fabric-to-Yarn Bending Stiffness Ratio of a Plain-woven Set Fabric, *Textile Research Journal.* 2000. p. 1088–1096.
19. Kawabata, S., Niwa, S. and Kawai, H., The Finite Deformation Theory of Plain-weave Fabrics, Part One: the Biaxial-deformation Theory, *Journal of the Textile Institute.* 1973. p. 21–46.
20. Kawabata, S., Niwa, S. and Kawai, H., The Finite Deformation Theory of Plain-weave Fabrics, Part Two: the Uniaxial-deformation Theory, *Journal of the Textile Institute.* 1973. p. 47–61.
21. Kawabata, S., Niwa, S. and Kawai, H., The Finite Deformation Theory of Plain-weave Fabrics, Part Three: the Shear-deformation Theory, *Journal of the Textile Institute.* 1973.
22. Realff, M.L., Boyce, M.C. and Backer, S., A Micromechanical Model of the Behavior of Woven Fabric, *Textile Research Journal.* 1997. p. 445–459.
23. De Jong, S. and Postle, R., An Energy Analysis of Woven-fabric Mechanics by Means of Optimal-control Theory, Part Two: Pure-bending Properties, *Journal of the Textile Institute.* 1977. p. 362–369.
24. De Jong, S. and Postle, R., An Energy Analysis of Woven-fabric Mechanics by Means of Optimal-control Theory, Part One: Tensile Properties, *Journal of the Textile Institute.* 1977. p. 350–361.
25. De Jong, S. and Postle, R., A General Energy Analysis of Woven-fabric Mechanics Using Optimal-control Theory, *Textile Research Journal.* 1978. p. 127–135.
26. De Jong, S. and Postle, R., Modified Equations for the Energy Analysis of the Plain Weave, Including Theory, *Journal of the Textile Institute.* 1979. p. 359–364.
27. Knoll, A.L., The Geometry and Mechanics of the Plain-weave Structure: A Comparison pf the General Energy Method of Analysis and Previous Models, *Journal of the Textile Institute.* 1979. p. 163–171.
28. Knoll, A.L., Modified Equations for the Energy Analysis of the Plain Weave, Including Yarn Extension, *Journal of the Textile Institute.* 1979. p. 355–358.

29. Sinoimeri, A. and Drean, J.Y., A Study of the Mechanical Behaviour of the Plain-weave Structure by Using Energy Methods: Fabric Shear, *Journal of the Textile Institute.* 1996. p. 120–128.
30. Hearle, J.W.S. and Shanahan, W.J., Energy Method for Calculations in Fabric Mechanics, Part I: Principles of the Method, *Journal of the Textile Institute.* 1978. p. 81–91.
31. Leaf, G.A.V. and Kandil, K.H., The Initial Load–extension Behaviour of Plain-woven Fabrics, *Journal of the Textile Institute.* 1980. p. 1–7.
32. Tarfaoui, M. and Drean, J.Y., Predicting the Stress–strain Behavior of Woven Fabrics Using the Finite Element Methods, *Textile Research Journal.* 2001. p. 790–795.
33. Haan, S.I., Charalambides, P.G. and Suri, M., A Specialized Finite Element for the Study of Woven Composites, *Computational Mechanics.* 2001. p. 445–462.
34. Li, Y. and Dai, X.Q., Simulate Woven Fabric Behavior during Low Extension with a Computational Micro-mechanical Model, submitted to *Textile Research Journal.* 2005.
35. House, D.H. and Breen, D.E., *Cloth Modeling and Animation.* 2000, A. K. Paters Ltd: Natick, Massachusetts. p. 55–77.
36. Grosberg, P. and Swani, N.M., The Mechanical Properties of Woven Fabrics, Part III: The Buckling of Woven Fabrics, *Textile Research Journal.* 1966. p. 332–338.
37. Clapp, T.G. and Peng, H., Buckling of Woven Fabrics, Part III: Experimental Validation of Theoretical Models, *Textile Research Journal.* 1990. p. 641–645.
38. Clapp, T.G. and Peng, H., Buckling of Woven Fabrics, Part II: Effect of Weight and Frictional Couple, *Textile Research Journal.* 1990. p. 285–292.
39. Clapp, T.G. and Peng, H., Buckling of Woven Fabrics, Part I: Effect of Fabric Weight, *Textile Research Journal.* 1990. p. 228–234.
40. Shinohara, A., Ni, Q.Q. and Takatera, M., Geometry and Mechanics of the Buckling Wrinkle in Fabric, Part II: Buckling Model of A Woven Fabric Cylinder in Axial Compression, *Textile Research Journal.* 1991. p. 100–105.
41. Shinohara, A., Ni, Q.Q. and Takatera, M., Geometry and Mechanics of the Buckling Wrinkle in Fabric, Part I: Characteristics of the Buckling Wrinkle, *Textile Research Journal.* 1991. p. 94–100.
42. Grosberg, P., The Role of Friction in the Mechanical Behaviour of Fabrics, *Surface Characteristics of Fibres and Textiles, Part II*, M.J. Schick (Editor) 1977, Marcel Dekker Inc: New York and Basel. p. 563–575.
43. Olofsson, B., A Study of Inelastic Deformation of Textile Fabrics, *Journal of Textile Institute.* 1967. p. 221–241.
44. Olofsson, B., The Mechanics of Creasing and Crease Recovery. *Textile Research Journal.* 1968.
45. Olofsson, B., Rheology of Textile Fabrics, in *Rheology – Theory and Application*, B. Olofsson (Editor) 1969, Academeic Press: New York. p. 492–545.
46. Grosberg, P., The Mechanical Properties of Woven Fabrics, Part V: The Initial Modulus and the Frictional Restraint in Shearing of Plain Weave, *Textile Research Journal.* 1966. p. 420–431.
47. Grosberg, P., The Mechanical Properties of Woven Fabrics, Part IV: The Determination of the Bending Rigidity and Frictional Restraint in Woven Fabrics, *Textile Research Journal.* 1966. p. 338–345.

48. Chapman, B.M. and Hearle, J.W.S., The Bending and Creasing of Multicomponent Viscoelastic Fiber Assemblies Part I: General Consideration of the Problem, *Textile Research Journal.* 1973. p. 385–403.
49. Chapman, B.M., The Bending and Creasing of Multicomponent Viscoelastic Fiber Assemblies Part III: The Mechanics of a Two-dimensional Assemblies of Generalized Viscoelastic Fibers of Different Types, *Textile Research Journal.* 1974. p. 306–309.
50. Chapman, B.M., The Bending and Recovery of Fabrics under Conditions of Changing Temperature and Relative Humidity, *Textile Research Journal.* 1976. p. 113–122.
51. Zhang, X. *et al.*, Fabric Bagging, Part I: Subjective Perception and Psychophysical Mechanism, *Textile Research Journal.* 1999. p. 511–518.
52. Zhang, X. *et al.*, Fabric Bagging, Part II: Objective Evaluation and Physical Mechanism, *Textile Research Journal.* 1999. p. 598–606.
53. Zhang, X., Li, Y. and Yeung, K.W., Mathematical Simulation of Fabric Bagging, *Textile Research Journal.* 2000. p. 18–28.
54. Zhang, D. and Yuen, M., Collision Detection for Clothed Human Animation, *Pacific Graphics Conference*, Hong Kong. 2000. p. 328–337.
55. Zhang, X. *et al.*, Relative Contributions of Elasticity and Viscoelasticity of Fibers and Inter-fiber Friction in Bagging of Woven Wool Fabrics, *Journal of Textile Institute.* 2000. p. 577–589.
56. Zhang, X. *et al.*, Fabric-bagging: Stress Distribution in Isotropic and Anisotropic Fabrics, *Journal of Textile Institute.* 2000. p. 563–576.
57. Frindley, W.N., Lai, J.S. and Onaran, K., *Creep and Relaxation of Nonlinear Viscoelastic Materials.* 1976, North-Holland Publications. p. 50–105.
58. Peirce, F.T., Geometrical Principles Applicable to the Design of Functional Fabrics, *Textile Research Journal.* 1947. p. 123–147.
59. Leaf, G.A.V., Models of the Plain Knitted Loop, *Journal of the Textile Institute.* 1960. p. T49–58.
60. Leaf, G.A.V., The Stresses in the Plain Knitted Loop, *Journal of the Textile Institute.* 1961. p. T351–365.
61. Doyle, P.J., Some Fundamental Properties of Hosiery Yarns and Their Relation to the Mechanical Characteristics of Knitted Fabrics, *Journal of the Textile Institute.* 1952. p. 19–35.
62. Munden, D.L., The Geometry and Dimensional Properties of Plain-knit Fabric, *Journal of the Textile Institute.* 1959. p. T448–471.
63. Postle, R., Analysis of the Dry Relaxed Knitted Loop Configuration, *Journal of the Textile Institute.* 1967. p. 329–365.
64. Postle, R., Dimensional Stability of Plain Knitted Fabrics, *Journal of the Textile Institute.* 1968. p. 65–77.
65. Demiroz, A. and Dias, T., A Study of the Graphical Representation of Plain-knitted Structure, Part I: Stitch Model for the Graphical Representation of Plain-knitted Structures, *Journal of the Textile Institute.* 2000. p. 463–480.
66. Leaf, G.A.V. and Glaskin, A., The Geometry of the Plain Knitted Loop, *Journal of the Textile Institute.* 1955. p. T587–605.
67. Shanahan, W.J. and Postle, R., A Theoretical Analysis of Plain Knitted Structure, *Textile Research Journal.* 1970. p. 656–665.
68. Hepworth, B. and Leaf, G.A.V., The Mechanics of an Idealised Weft-knitted Structure, *Journal of the Textile Institute.* 1976. p. 241–248.

69. Szeliski, R. and Teonnesen, D., Surface Modeling with Oriented article Systems, *SIGGRAPH'92*, 1992: Chicago. p. 185–194.
70. MacRory, B.M., McCraith, J.R. and McNamara, A.B., Biaxial Load–Extension Properties of Plain Weft-knitted Fabrics: A Theoretical Analysis, *Textile Research Journal.* 1975. p. 746–760.
71. Hepworth, B. and Leaf, G.A.V., The Biaxial Load-extension Behaviour of a Model of Plain Weft-knitting, *Journal of the Textile Institute.* 1978. p. 101–107.
72. Choi, K.F. and Lo, T.Y., An Energy Model of Plain Knitted Fabric, *Textile Research Journal.* 2003. p. 739–748.
73. Eberhardt, B., Meissner, M. and Strasser, W., Knit Fabrics, *Cloth Modeling and Animation*, D.E. Breen (Editor) 2000, A K Paters: Natick, Massachusetts. p. 123–144.

5

Clothing mechanics

X-Q. DAI[1,2], Y. LI[1]
[1]The Hong Kong Polytechnic University, China
[2]Soochow University, China

5.1 Introduction

Garments and textile devices are the final products that provide biomechanical functions to human bodies. The biomechanical functional performance of garments and devices is very much dependent on the fabric mechanical and surface properties. However, garments and devices are made from pieces of fabrics by sewing them together. Scientific understanding and knowledge of the cloth mechanical properties and modeling their mechanical behavior and their sewing process are essential for biomechanical engineering of clothing and textile products. In this chapter, the knowledge and processes developed in the area of clothing mechanics in relation to biomechanical engineering are reviewed.

5.2 Characteristics of clothing deformation

Garments are made from flat fabrics. By sewing 2D patterns of certain geometric topology, various apparel items can be constructed, and they show variable aesthetic appearances when worn on the human body. According to the degree of space allowance between the body and the garment during the body movement, F, garments can be classified as three types: (i) foundation garments ($F < 0$), as the garment area is less than the body area (e.g. girdles and compression garments); (ii) perfect fitting garments ($F \geq 0$) as the garment area is equal to or slightly larger than the body area (e.g. suits and socks); (iii) loose garments ($F >> 0$) as the garment area is far larger than the body area (e.g. dresses and flared skirts). Postle and Norton[1] pointed out that the mechanical problems in clothing can be roughly divided into two classes. The first is free-form problems, e.g. fabric drape, buckling, wrinkling, in which fabric stresses are essentially limited to those supported by fabric curvature, and where gravitational forces are frequently important. The second is form-fitting problems, often involving prescribed curvatures and larger stresses. Then, type (i) and (ii) garments

belong to form-fitting problems and type (iii) to free-form problems. Different from other sheet materials, such as paper and plastic film, cloth deformation often shows a complex nature of mixed tension, shear and bending, and may form 3D shapes of double curvature. It is this ability that enables fabric to form beautiful draping shapes and to be fitted to a body shape of complicated geometry.

5.2.1 Free-form

Buckling has been discussed in the previous chapter. Here the focus is on drape. Drape is when a fabric deforms under its own weight. It is an important factor that influences aesthetic appearance and has an outstanding effect on the formal beauty of the fabric. Drapability is related to fabric weight, stiffness (flexural rigidity), and shearing rigidity. The greater the fabric weight, the more likely it is to drape. The greater the fabric stiffness, the less likely it is to drape. The greater the fabric shear rigidity, the less the folds formed by fabric drape. However, the draping qualities required from a fabric will differ completely depending on its end use, therefore a given value for drape cannot be classified as good or bad.

5.2.2 Form-fitting

As a subject for garments, the human body surface has very complex geometry. To construct a garment of a certain style, it is often necessary to sew cloth patterns of a certain topology together to build 3D shapes of prescribed curvatures, especially for the perfect-fit garment. Two-dimensional pattern design is a very important procedure in garment manufacture. However, it is out of the scope of this book. Here, the focus is on the deforming ability of fabric. People must be able to move around in the garments they wear, especially sportswear. Discomfort may result if a fabric restrains movement, creates a burden or exerts pressure on the body. Therefore, the form-fitting ability includes not only the ability of a fabric to be perfect-fitted or tight-fitted to a static body, but also its ability to deform dynamically to fit along with the body movement.

When people move, their skin stretches; it elongates and recovers. Skin is a highly elastic material. Fabric placed close to the skin needs to be elastic too. It must elongate to accommodate body movement and then recover. Fortunately, fabric is a flexible material. It can not only form a shape of complicated curvature, but also stretch to a certain extent in two principle directions (warp and weft), even simultaneously. Stretch is the ability of a fabric to stretch when a pulling force is applied and then recover relatively quickly and fully to its original dimensions when the force is removed. Fabric of high stretch will have good form-fit ability. Various stretch fabrics

differing in extensibility are expected to meet the requirement for different special end use.

5.2.3 Sewing

A garment is often made from several pieces of cloth pattern by sewing them together along pairs of prescribed seam lines. This process is realized in a sewing machine by using the sewing thread to stitch pairs of cloth pattern borders together. Failure at a seam makes a garment unusable even though the fabric may still be in good condition. There are many possible causes for seam failure. For example, the sewing thread wears out or fails before the fabric does, or the yarns making up the fabric are broken or damaged by the needle during sewing. These problems are specific to the making-up process and depend on the sewing machine used, the sewing thread, the sewing speed and so on. A typical seam failure that is related to fabric property is seam slippage. It is a condition where a seam sewn in the fabric opens under load. Some of this gap may close on removal of the load but some of it may be a permanent deformation. The resistance to such yarn slippage in fabric is called seam strength. It is an important property for fabric in garment construction and its test will be detailed in a later chapter.

5.3 Clothing modeling

Since fitting formability problems involve contact with the human body, they will be dealt with later, in Chapter 8. Here the focus is on cloth modeling. Many techniques have been developed to model overall fabric shape. Among them, there are two major approaches: to consider fabric as a continuum whole (continuum model) and to discretize fabric into mass points (discrete model).

5.3.1 Continuum models

Even though a fabric is made up of two groups of threads, the discontinuity in the fabric can be neglected when a large piece is considered. Therefore a fabric can be treated as a continuum without its discrete microstructure, and by means of elasticity theory, continuum solid mechanics are used to model it. In 1963, Kilby[2] first applied elasticity theory to fabric modeling. He developed planar stress–strain relationships for a fabric model of a simple trellis, using a conventional elasticity-based analysis. Through his analysis, he predicted that the Young's modulus is a function of angle across a woven fabric surface.

Shanahan, Lloyd and Hearle[3] used the engineering theory of sheets, shell and plates to characterize the elastic behavior of fabrics in complex deformations. The simplest form of the plate and shell theory assumes that the material is homogeneous, that strains and displacements are small, and that the material behavior is linearly elastic. In spite of their concerns with the applicability of this theory to modeling fabric, they derived equations for the generalized tensile, shearing bending, and twisting rigidities of fabric.

$$\begin{pmatrix} F_1 \\ F_2 \\ F_{12} \end{pmatrix} = \begin{Bmatrix} \frac{E_1}{1-\nu_1\nu_2} & \frac{\nu_2 E_1}{1-\nu_1\nu_2} & 0 \\ \frac{\nu_1 E_2}{1-\nu_1\nu_2} & \frac{E_2}{1-\nu_1\nu_2} & 0 \\ 0 & 0 & G \end{Bmatrix} \begin{pmatrix} \varepsilon_1 \\ \varepsilon_2 \\ \varepsilon_{12} \end{pmatrix} \quad \text{(based on Eq. 8 in reference 3)}$$

$$\begin{pmatrix} M_1 \\ M_2 \\ M_{12} \end{pmatrix} = \begin{Bmatrix} B_1 & \sigma_2 B_1 & 0 \\ \sigma_1 B_2 & B_2 & 0 \\ 0 & 0 & \tau \end{Bmatrix} \begin{pmatrix} K_1 \\ K_2 \\ K_{12} \end{pmatrix} \quad \text{(based on Eq. 9 in reference 3)}$$

Lloyd[4] further introduced non-linear extensions into these equations. He applied the finite element method to simulate a series of experiments on fabric structures, and the results compared favorably with actual fabric samples. Their characterization is only valid for the special case of small strains due to the assumption of small strains and deformations; however, it provides a framework for further study.

Accompanying the rapid advance of computer techniques, the finite difference, finite volume and finite element methods are widely used in many engineering fields and computer aided design areas. To aid fabric and apparel design, and to generate clothed character animation, various fabric simulations have been carried out by many research groups from textile areas, as well as by the computer graphics community.

Draping simulation

Draping, where a fabric deforms under its own weight, is an important aesthetic property in garment end-use and has been widely simulated. During draping, fabrics bend through large displacements but are not easily stretched; this leads to classification of draping behavior as a small-strain/large-displacement problem in finite element analysis. When large deformations occur in a finite element solution, the non-linearity due to a change in the geometry of the body has to be considered to obtain the correct load-response. The general approach to handling the geometric non-linearity is the increment method based on the total Lagrangian formulation. Instead

of the one-step solution found in linear problems, the loads are applied incrementally to the system and at each step the equilibrium equation is

$$[K]\{\Delta q\} = \{\Delta f\}$$

Non-linearity is handled by calculating the stiffness matrix $[K]$ in each step as a function of the displacement vector $\{q\}$. In the total Lagrangian formulation, the Green–Lagrange strain and the Piola–Kiechhoff stress refer to the shape and position of the body at the initial time.

$${}^{t}_{0}\varepsilon_{ij} = ({}^{t}_{0}u_{i,j} + {}^{t}_{0}u_{j,i} + {}^{t}_{0}u_{k,i}{}^{t}_{0}u_{k,j})/2$$

$${}^{t}_{o}S_{ji} = \frac{{}^{o}\rho}{{}^{t}\rho}\,{}^{o}_{t}x_{i,\alpha}{}^{t}_{0}x_{j,\beta}\,{}^{t}\tau_{\alpha\beta}$$

In 1988–89, Imaoka *et al.*[5,6] developed a continuum mechanics model of a fabric for their 3D apparel CAD system. Triangular finite elements were employed to investigate the drape of fabrics. To solve the large deformation problem, the total Lagrangian formulation was employed. The tensile, bending, shearing and twisting rigidities of fabrics were used in deriving the strain energy equations for tensile, bending and shear deformations. The energies were then minimized, using a form of Newton's method, to place a 3D cloth structure in a final configuration over a human body. The simulations of a skirt and several blouses were presented.

In 1991 Collier *et al.*[7] used a geometric non-linear finite-element method based on a simple shell theory to predict fabric drape behavior in which fabric deformation is characterized as a non-linear small-strain/large-displacement problem. The fabric is treated as an orthotropic shell membrane. The flat-shell is a four-node quadrilateral bending/membrane element with five degrees of freedom at each node. The generalized displacement is defined in terms of the nodal displacement with an appropriate interpolation function, which is a twelve-term fourth-order polynomial. Three parameters, which are the measured tensile modulus in the two planar principal directions and literature values of Poisson's ratio, are used for material properties. A Newton–Raphson solution procedure is used in the draping analysis, and a non-linear load/deflexion relation is assumed. A traditional drape test on a cotton plain weave fabric is simulated. The result obtained is the projection of the deformed area on the *x-y* plane and from it, the drape coefficient was calculated as 71.0% compared with the experimental value of 68.4%.

Kang *et al.*[8] assumed a fabric to be an elastic material with orthotropic anisotropy and considered it as a thin flexible plate under the plane stress condition. The geometric non-linear phenomenon is dealt with by a total Lagrangian approach. The quadrilateral elements with four nodes and five degrees of freedom for each node are used. A transverse-shear-strain

interpolation method is adopted to avoid the shear-locking phenomenon that is commonly observed in thin-plate analysis. The mechanical parameters used in the simulation are tensile, shear, bending and torsional rigidities. Predicted 2D and 3D draping shapes show reasonably good agreement with those obtained experimentally. The authors also pointed out that the bending properties are more important than the tensile ones in draping simulation.

Chen and Govindaraj[9,10] used a shear flexible shell theory to predict fabric drape. The fabric is considered as a continuous, orthotropic medium. The geometry of the shell is represented by the coordinates and normal vectors at nodes situated on the middle surface. A nine-node, doubly curved shell element with five degrees of freedom per node is used. The kinematics of the shell theory consists of measuring membrane strain on the reference surface from the derivatives of a point position with respect to position on the surface, and bending strain from the derivatives of the unit normal to the reference surface at the point. The strain measures that are used for this purpose are approximations to Koiter–Sanders theory strains. The transverse shear strains are measured as the change in the projections of the normal onto the shell's reference surface. Simulation of a 30×30 cm fabric draped over a 12×12 cm table was carried out. The material characteristics used were Young's modulus in the warp and weft directions, shear modulus and Poisson's ratio. In a number of simulations they varied the values of these quantities and observed the differences in the draped shapes. They concluded that the shear modulus has the greatest influence on draping behavior and Poisson's ratio the least.

Gan and Ly[11] employed a model and a computational approach similar to Chen and Govindaraj's to study fabric deformation. They addressed three issues: (i) proper calculation of shell normals at the finite element nodes, (ii) elimination of shear and membrane locking during element evaluation, and (iii) the definition of an accurate stress–strain relationship for the material. The tensile, bending and shear rigidities are used for the mechanical properties of fabrics in the simulation. The constitutive relation of fabrics is determined mainly on their bending and shear properties. Comparison between the produced results of 2D bending and 3D draping and the corresponding real objects confirms that by using this constitutive relation, the finite element method can give satisfactory results to problems in which bending deformation dominates.

Eischen *et al.*[12] also modeled fabric using the geometrically exact shell theory proposed by Simo *et al.* A woven fabric is considered as an elastic isotropic material. The mechanical properties of fabrics used are Young's modulus, Poisson ratio and the Kawabata bending plots. An adaptive arc-length control algorithm is employed to account for fabric buckling. The non-linear bending response is derived from fifth-order polynomial curves

approximating to KES bend plots. A contact procedure based on a penalty method is used to simulate interactions with solid objects. They developed modeling techniques that allowed the simulation for not only the draping of fabric, but also the picking, placing, and folding of a piece of fabric. They produced several simulations and favorably compared them to photographs of actual fabric drapings and manipulations.

Hu and Chen,[13] and Hu, Chen and Teng[14] predicted the drape behavior of circular fabric sheets over circular pedestals using a geometrically non-linear finite-volume method. An initially flat circular fabric sheet is first subdivided into a number of structured finite volumes, each containing a grid node, by mesh lines along the warp and weft directions. The strains and curvatures and the out-of-plane bending and in-plane membrane strain energies of a typical volume can be evaluated using the global coordinates of its grid node and several neighbors surrounding it. The equilibrium equations of the fabric sheet are derived by employing the principle of stationary total potential energy. The full Newton–Raphson iteration method with line searches is used to solve the non-linear algebraic equations resulting from the formulation. The comparison between the predicted symmetrically deformed shapes and the experimental results is presented to demonstrate the validity and accuracy of the method. The perturbation force is also introduced to simulate the random disturbance in real experiment.

Dynamic continuum model

The previously mentioned finite element or volume approaches are mainly for static draping problems; only static equilibrium equations are involved. However, sometimes dynamic fabric deformation needs to be solved. Since cloth is the most visible object in our daily life, the computer graphics community has shown great interest in dynamic cloth modeling. The goal of their work is not to model any particular deformable material accurately; instead they are interested in creating physically-based models to produce cloth-like deformation for computer animation without expensive computation cost. Measured data of mechanical properties are rarely used in these simulations. Many dynamic finite element and finite difference approaches have been developed.[15–18]

Taking continuum mechanics and differential geometry as their starting point, Terzopoulos and Fleischer[16,19] and Terzopoulos *et al.*[15] developed a wide range of physically-based deformable models that becomes the basis of deformable surface models in the computer graphics area.[15,16,19] They presented a simplified set of equations based on elasticity theory that describe elastic and inelastic deformations, interactions with solid geometry, and fracture for flexible curves, surfaces and solids. For deformable surfaces, the deformation energy is:

$$\varepsilon(r) = \int_{\Omega} \|G - G^0\|^2_{w^1} + \|B - B^0\|^2_{w^2} \, \mathrm{d}a_1 \mathrm{d}a_2$$

Here, $r(a_1, a_2, t)$ denotes the material coordinate of a surface, G is the metric tensor, to measure the local distances and angles between nearby points in the deformable sheet, $\|\cdot\|_{w^1}$, $\|\cdot\|_{w^2}$ are weighted matrix norms, and B is the curvature tensor, defining the local curvature properties of the surface. Lagrange's equations of motion are used to obtain a motion equation for the elastic object.

$$\frac{\partial}{\partial t}\left(\mu \frac{\partial r}{\partial t}\right) + \gamma \frac{\partial r}{\partial t} + \frac{\delta \varepsilon(r)}{\delta r} = f(r, t)$$

Here $\varepsilon(r)$ denotes the deformation energy. To obtain the solutions, the equation has to be discretized by a finite-difference or finite-element method, resulting in a large system of simultaneous ordinary differential equations. By integrating the equations through time, the model simulates the dynamics at each time step. An implicit alternating-direction (ADI) method, which generates a series of tightly-banded linear systems rather than one large sparse system, was used for the large simulations. The produced simulations include a waving flag, a carpet over various objects, and a sequence in which a piece of cloth is torn apart.

A research group from MIRALab, University of Geneva, extended Terzopoulos' general model to cloth modeling.[17,20,21] They developed a cloth simulator for their clothing virtual actors system. The major extension is the way that the damping and collisions are handled. The damping of rigid body motion and the inappropriately springy behavior in collision response that may occur are avoided in Terzopoulos' model. The system uses the midpoint method to advance the simulation. They also developed the computational methods needed for cloth collision detection and producing animations of complete sets of clothing.

Fabric strongly resists stretching deformation while being comparatively permissive in allowing bending and shearing deformations. This results in a 'stiff' underlying differential equation of motion. Explicit methods are not a good choice to solve stiff equations because they require many small steps to stably advance the simulation forward in time. In cloth animation, the computational cost is a critical issue. Many approaches have been developed to increase the time step[22,23] and the most remarkable contribution was made by Baraff and Witkin.[18] They derived the internal cloth forces using a simple continuum formulation that supports modeling operations such as local anisotropic stretch or compression. A unified treatment of damping forces is also included. An implicit integration method (backward Euler method) is used to generate a large, unbanded sparse linear system at each time step, which is then solved using a modified conjugate gradient

method that simultaneously enforces particles' constraints. These techniques allow large time steps in cloth animation. They presented garments including shirts, pants and skirts exhibiting complex wrinkling and folding behavior on both key-framed and motion-captured characters.

5.3.2 Discrete models

Continuum models involve solving large systems of simultaneous ordinary differential equations, and the computational cost is often very expensive. Rather than consider a woven fabric as a whole, another approach is to discretize the fabric into a set of point masses (particles) which interact through energy constraints or forces, and thus model approximately the behavior of the material. The usual way to numerically simulate a mechanically-based particle system is to directly integrate Newton's second law for a mass particle over all particles:

$$F(t) = m\frac{\mathrm{d}^2 X}{\mathrm{d}t^2}$$

where X is the particle position, F is the sum of the forces acting on the particle and m is its mass. The forces exerted on each particle depend on the current state of the system, which is represented by the position and speed of all particles. These forces usually represent all the mechanical effects on the system, which include internal deformation forces, gravity and aerodynamic effects, and different kinds of other external constraints.

Mass–spring systems are the simplest way to design a volume model using a particle system. In this approach, each particle represents a point mass, which is linked to its neighbors by a 'spring' representing the elastic behavior of the material. The springs tend to keep the particles at their initial resting positions. In 1995, Provot[24] proposed a mass–spring system to model cloth. The mass particles, arranged in a rectilinear grid, are connected with three types of springs. The structural springs connect nearest-neighbor particles along thread lines; the shear springs connect nearest-neighbor particles along diagonals; and the flexion springs connect a particle with its second neighbor along thread lines. Provot calculated the dynamic behavior of the springs in order to simulate a cloth hanging from two points and a waving flag. A heuristic method is presented, which first takes a step in time based on the dynamics of the system, then adjusts the positions of the particles that have violated local distance constraints. The enforcement of distance constraints eliminates the unacceptable elongation generally found near fixed model points in elastic models. Removing the elongation makes these kinds of models less 'stretchy' and more cloth-like. Actually, this technique is most widely used in various cloth animations.

In computer graphics applications, curved surfaces are often represented by polygonal meshes. A convenient way to build a mass–spring system from this kind of description is to consider each vertex of the mesh as a particle and the edges or polygons as the interaction forces among several particles. Volino and Thalmann's[25,26] mass–spring model is a typical description of such approaches. They modeled the in-plane elasticity and out-of-plane curvature elasticity and calculated the in-plane deformation within each triangle. By introducing a parameter α ($|\alpha| < 1$), they controled the Poisson coefficient of the simulated fabric. The way to measure the bending curvature in an irregular mesh is to consider the angle θ formed by two triangles about the connecting edge. The resulting curvature force moment is then given by forces applied to the four vertices respectively.

Explicit integration methods are the simplest methods available for solving particle motion equations. The fourth-order Runge–Kutta method is most widely used in particle systems. Since explicit methods are ill-suited to solving stiff equations, various implicit integration methods are proposed to produce real-time cloth animation.[23,25] However, these approaches are mostly used in the computer graphics area, where fast and stable animation is the key issue. The simulated cloth is a 'cloth-like' deformable surface rather than any particular textile material. Parameters of mechanical properties are rarely used in the calculation.

Breen,[27] and Breen *et al.*[28,29] developed a non-continuum particle model for fabric drape that explicitly represents the micro-mechanical structure of a fabric, *via* a particle system. Their model is based on the observation that a fabric is best described as a mechanism of interacting mechanical parts rather than a continuous substance, and derives its macro-scale dynamic properties from the micro-mechanical interaction between threads.

The particle model represents a fabric sheet by particle meshes, where $X_{i,j}$ with three components $(x_{i,j},y_{i,j},z_{i,j})$ denotes the three-dimensional position of a particle. The mass of each particle is the mass of the particle's local regular area and its strain energy represents the aggregate of the strain energies in the local area. Nevertheless, the particle grid still preserves the underlying woven structure of the fabric, and the various inter-crossing strain energies are computed, based on simple geometric relationships among local particle neighbors. The energy functions account for the four basic mechanical interactions of yarn compression, stretching, out-of-plane bending and trellising. The total energy for particle i is given by:

$$U_i = U_{repel_i} + U_{stretch_i} + U_{bend_i} + U_{trellis_i} + U_{\text{gravity}_i}.$$

The energy function U_{repel_i}, prevents particles connected to particle i from approaching it, and the function $U_{stretch_i}$, capturing the energy of tensile

strain between each particle and its four-connected neighbors, are given by generated approximation functions; the energy functions U_{bend_i} and $U_{trellis_i}$ are derived from Kawabata bending and shearing tests.[30] This particle-based approach was first applied to the problem of computing static drape. The simulation was in two stages. In the first stage, particles are allowed to fall freely. Any collision with the object or the ground is determined during this step. The particle positions can be obtained using the equation

$$ma + cv = mg,$$

where a is the acceleration, v is the velocity, m is the mass, c is the air resistance, and g is the gravitational acceleration constant. The result is a rough shape of the draped fabric. In the second stage, an energy minimization process is applied to the inter-particle energy functions to generate fine detail in the shape of the fabric. The final equilibrium shape of the fabric occurs when there is minimum energy over the whole fabric. The simulated tablecloths showed obvious characteristics of materials and agreed with actual ones. However, it is quite slow to compute a drape and it cannot produce the dynamic response.

Several forward dynamics translations of the Breen–House model have been implemented that not only produce cloth motion, but actually compute the final drape more quickly than the original method. One of the most successful of these models was proposed by Eberhardt *et al.* in 1996.[31] They used a Lagrangian dynamics reformulation of the basic energy equations suggested in the Breen–House model, resulting in a system of ordinary differential equations from which dynamics could be calculated. In their energy function, the anisotropy and hysteresis of the fabric are also modeled. A Runge–Kutta method, with adaptive step-size control, was used to solve the differential equations. With their approach, Eberhardt *et al.* simulated a cloth draping over a table top, a sphere and a castle model utilizing significantly less computation time than previously published particle methods. However, there was no comparison with any actual objects reported.

House and Breen[32,33] also extended their model to include dynamics by a force-based formulation approach. Non-linear 'cloth springs' are imagined acting on the yarn segments between crossing-point particles. The magnitude of each spring force or torque is determined by differentiating the corresponding energy equation of the particle model and its direction is determined geometrically. There was no evidence that the measured tensile data was used.

Dias *et al.*[34] proposed a discretized cloth model in which the planar deformation is modeled as the plate under plane stress and the out-of-plane deformation is to model curvature interactions along the edges of neighboring

triangles. This model combines the continuum and discrete models and benefits from both of them. The fabric is described by a mesh of irregular triangles. Each irregular triangle corresponds physically to a set of three linked strain gauges, which are able to evaluate the extensional deformation of the underlying continuum along the angle that the gauge makes with the warp direction. The stress applied on each edge is calculated according to the laws of mechanics of materials. Out-of-plane deformation is the bending interaction between pairs of adjacent triangles along their common edges. The bending curvature was modeled by assuming a cantilever beam's bending, and the Kochaneck–Bartels spline interpolation is used to define the bending curve $\zeta(x)$. Then the curvature increases as the distance from the fixed point increases. Measured data of fabric mechanical properties are used in this model and the non-linearity is included by a piecewise linear approximation approach. Simulated fabrics in tensile, draping and buckling situations are presented but no comparisons with respective real objects are provided.

On the basis of the extended particle model of Breen and House, Dai *et al.*[35] developed a particle model by deriving general force/displacement relationships of various deformations according to fundamental elasticity mechanical laws. Then mechanical data resulting from various tests can be used in this model, and material non-linearity is also included by the piecewise linear approximation. Moreover, twisting, which occurs easily in flexural fabrics, is taken into account. The twist deformation often occurs in clothes such as flared skirts, in which a fabric is subjected to large bending along bias directions. Besides the separation, bending, and shearing springs, a twisting spring is assumed to be acting on each particle square. The twisting spring exerts a torque opposing twisting. As there are no methods to measure the twist rigidity; it is obtained indirectly from known fabric mechanical properties. The heart-loop test is carried out to validate simulation accuracy. The model is also applied to skirt simulation[36]. Fabric anisotropy is visualized by the different draped shapes formed by the skirts made of the patterns of the same shape but with different cutting directions. Various internal forces can also be visualized.

5.3.3 Sewing simulation

It is difficult to simulate the process that a human body is undertaking in a garment with a particular shape by means of a computer. Rather than doing so, to construct a 3D garment worn on a body, a common approach is to first place the 2D cloth patterns that will make up the garment properly around the body. Then to invoke a mechanical simulation to force the patterns to approach each other along the prescribed seam lines. As a result, the patterns are attached and sewn on the borders as specified and attain a shape influenced by the form of the body.

It is slightly difficult for a continuum model to realize the sewing process. Kang and Sung[37] introduced a virtual sewing method by creating new points at the middle of each pair of sewing points and reconstructing the boundary elements using those new points. And the strain reduction method is followed to reshape the elements, especially those in which large deformations are introduced by sewing. Okabe *et al.*[38] developed a 3D CAD system for dresses, in which the topological connections between seam lines on planer cloth patterns are constructed as an initial state for the dress and a succeeding iterative numerical analysis is followed to obtain the mechanical stable state of minimum potential energy.

It is much easier for a discrete model to realize the sewing process. The process often relies on a simplified simulation, where the seaming forces are pulling the matching pattern borders together. There are tasks in sewing simulation: (i) to bring two objects' attachment points progressively together; (ii) to maintain these points together. Volino and Thalmann[26] introduced 'elastics' to bring two extremities together, and then maintain the closest distance between them. 'Elastics' can be either mechanical forces or geometrical constraints. The mechanical approach is to use force-driven elastics directly integrated in the cloth model. An adaptive scheme would then modify the elastic strength force depending on the actual motion and deformation of the concerned objects. The constraint-based interaction is a general scheme that may be implemented in the particular case of collision response effects. The user should be given a very simple way to characterize the effect of the elastics and to describe its strength, using a few parameters, such as the time needed to bring the objects together and the damping of the motion.

Dai and Li[36] have also carried out skirt-sewing simulation by applying a seaming force inversely proportional to the distance between each pair of particles to be attached. After sewing, mechanical properties near seam lines were different from other parts and depended on sewing style and sewing threads. They considered a simple style and neglected the difference, and the sewn parts were regarded as a continuous whole. A seam force was employed to bring the pair of particles together. The direction of the force was along the line connecting the two particles; the magnitude of it only affects the seaming speed. Once two particles approached to a prescribed close distance, they were regarded as one and their neighbourhoods were added to those of each other. When the sewing finishes, all patterns become a continuous whole.

5.4 Conclusion

In this chapter, the characteristics of cloth deformation in garment construction and wear that need to be taken into account in clothing modeling

have been introduced. Drape, stretch and sewing were considered as three major elements in garment formation. The high-level cloth models to predict the whole aesthetic appearance of fabrics and garments were reviewed, including the continuum approach and the discrete approach. Sewing simulation techniques were also briefly considered.

5.5 Acknowledgement

We would like to thank Hong Kong Polytechnic University for funding this research through Projects A188 and G-YD31.

5.6 References

1. Postle, R. and Norton, A.H., Mechanics of Complex Fabric Deformation and Drape, in *Science and Technology of Fibres and Related Materials*, L. Rebenfeld, Editor. 1991, John Wiley & Sons: New York. p. 323–340.
2. Kilby, W.F., Planar Stress–Strain Relationships in Woven Fabrics. *Journal of the Textile Institute*, 1963. **54**: p. T9–T27.
3. Shanahan, W.J., Lloyd, D.W. and Hearle, J.W.S., Characterizing the Elastic Behavior of Textile Fabrics in Complex Deformation. *Textile Research Journal*, 1978. **48**(4): p. 495–505.
4. Lloyd, D.W., The Analysis of Complex Fabric Deformations, in *Mechanics of Flexible Fibre Assemblies*, J.W.S. Hearle, J.J. Thwaites, and J. Amirbayat (Editors.) 1980, Sijthoff & Noordhoff, Alphen aan den Rijn: The Netherlands. p. 311–342.
5. Imaoka, H. *et al.*, Analysis of Deformations in Textile Fabric. *SEN-I GAKKAISHI*, 1988. **44**(5): p. 217–228.
6. Imaoka, H. *et al.*, Prediction of Three-dimensional Shapes of Garments from Two-dimensional Paper Patterns. *SEN-I GAKKAISHI*, 1989. **45**(10): p. 420–426.
7. Collier, J.R. *et al.*, Drape Prediction by Means of Finite-element Analysis. *Journal of the Textile Institute*, 1991. **82**(1): p. 96–107.
8. Kang, T.J., Yu, W.R. and Chung, K., Drape Simulation of Woven Fabric Using the Finite-element Method. *Journal of the Textile Institute*, 1995. **86**(4): p. 635–648.
9. Chen, B. and Govindaraj, M., A Physically Based Model of Fabric Drape Using Flexible Shell Theory. *Textile Research Journal*, 1995. **65**(6): p. 324–330.
10. Chen, B. and Govindaraj, M., A Parametric Study of Fabric Drape. *Textile Research Journal*, 1996. **66**(1): p. 17–24.
11. Gan, L. and Ly, N.G., A Study of Fabric Deformation Using Nonlinear Finite Elements. *Textile Research Journal*, 1995. **65**(11): p. 660–668.
12. Eischen, J.W., Deng, S. and Clapp, T.G., Finite-element Modeling and Control of Flexible Fabric Parts. *IEEE, Computer Graphics and Applications*, 1996. **16**(5): p. 71–80.
13. Hu, J.L. and Chen, S.F., Numerical Drape Behavior of Circular Fabric Sheets over Circular Pedestals. *Textile Research Journal*, 2000. **70**(7): p. 593–603.

14. Chen, S.F., Hu, J.L. and Teng, J.G., A Finite-volume Method for Contact Drape Simulation of Woven Fabrics and Garments. *Finite Elements in Analysis and Design*, 2001. **37**: p. 513–531.
15. Terzopoulos, D. *et al.*, Elastically Deformable Models, in *SIGGRAPH*. 1987.
16. Terzopoulos, D. and Fleischer, K., Deformable Models. *The Visual Computer*, 1988. **4**: p. 306–331.
17. Volino, P., Courchesne, M. and Thalmann, N.M., Versatile and Efficient Techniques for Simulating Cloth and Other Deformable Objects, in *SIGGRAPH*. 1995.
18. Baraff, D. and Witkin, A., Large Steps in Cloth Simulation, in *SIGGRAPH*. 1998.
19. Terzopoulos, D. and Fleischer, K., Modeling Inelastic Deformation: Viscoelasticity, Plasticity, Fracture, in *SIGGRAPH*. 1988.
20. Carignan, M. *et al.*, Dressing Animated Synthetic Actors with Complex Deformable Clothes, in *ACM SIGGRAPH*. 1992. New York.
21. Volino, P. *et al.*, An Evolving System for Simulating Clothes on Virtual Actors. *IEEE, Computer Graphics and Applications*, 1996. **16**(5): p. 42–51.
22. Choi, K.J. and Ko, H.S., Stable but Responsible Cloth. *ACM Transactions on Graphics*, 2002. **21**(3): p. 604–611.
23. Kang, Y.M. *et al.*, Fast and Stable Animation of Cloth with an Approximated Implicit Method, in *Computer Graphics International* 2000. Geneva, Switzerland.
24. Provot, X., Deformation Constraints in a Mass–Spring Model to Describe Rigid Cloth Behavior, in *Graphics Interface*, 1995.
25. Volino, P. and Thalmann, N.M., Implementing Fast Cloth Simulation with Collision Response, in *Computer Graphics International*, 2000.
26. Volino, P. and Thalmann, N.M., Collision Response, in *Virtual Clothing: Theory and Practice*. 2000, Springer. p. 145–182.
27. Breen, D.E., A Particle-based Model for Simulating the Draping Behavior of Woven Cloth, in *Computer and Systems Engineering*. 1994, Rensselaer Polytechnic Institute: Troy, New York. p. 62–63.
28. Breen, D.E., House, D.H. and Getto, P.H., A Physically Based Particle Model of Woven Cloth. *The Visual Computer*, 1992. **8**(6): p. 264–277.
29. Breen, D.E., House, D.H. and Wozny, M.J., A Particle-based Model for Simulating the Draping Behavior of Woven Cloth. *Textile Research Journal*, 1994. **64**(11): p. 663–685.
30. Kawabata, S., The Standardization and Analysis of Hand Evaluation, The Textile Machinery Society of Japan, Japan. 1980.
31. Eberhardt, B., Weber, A. and Strasser, W., A Fast, Flexible, Particle-system Model for Cloth Draping. *IEEE, Computer Graphics and Applications*, 1996. **16**(5): p. 52–59.
32. House, D.H. and Breen, D.E., eds. Cloth Modeling and Animation. 2000, A. K. Paters Ltd: Natick, Massachusetts. p. 55–77.
33. House, D.H. and Breen, D.E., Representation of Woven Fabrics, in *Course Notes of SIGGRAPH'98*. 1998.
34. Dias, J.M.S., Gamito, M.N. and Rebordao, J.M., A Discretized Linear Elastic Model for Cloth Buckling and Drape. *Textile Research Journal*, 2000. **70**(4): p. 285–297.

35. Dai, X.Q., Li, Y. and Zhang, X., Simulation of Anisotropic Woven Fabric Deformation with an Improved Particle Model. *Textile Research Journal*, 2002.
36. Dai, X.Q. and Li, Y., Virtual Visualization of Draping, Fitting and Pressure in Apparel Design, in *International Conference of IFFTI 2002*. 2002. Hong Kong, China.
37. Kang, T.J. and Sung, M.K., Development of Three-dimensional Apparel CAD System, Part II: Prediction of Garment Drape Shape. *International Journal of Clothing Science and Technology*, 2000. **12**(1): p. 39–39.
38. Okabe, H. *et al.*, Transformation from Paper Pattern to Spatial Structure of Dress by Computer-simulation of Sewing and Dressing. *SEN-I GAKKAISHI*, 1988. **44**(3): p. 53–60.

6

The human body

A. LUXIMON[2] AND M. ZHANG[1]
[1]The Hong Kong Polytechnic University, China
[2]Milanezy (Excel Last) Co Ltd, China

6.1 Introduction

The study of the human body, or anatomy, is probably as old as the origin of the human itself.[1] Our earliest ancestors must have observed growth, development and motor behavior as well as the surface anatomy for aesthetic and pleasurable purposes.[2] They would have observed diseases together with their symptoms and they would have experimented by using different herbs. As techniques for making accurate observation evolved, knowledge of the human body increased rapidly. As the amount of knowledge increased and in order to communicate effectively, medical practitioners devised specific terms, many of them originated from Greek and Latin, to describe locations, body parts, and functions.[3]

It is impossible to address the complete anatomy and physiology of the human body in this chapter. Detailed anatomy and physiology can be found in medical books, which are widely available.[1,3–7] Instead, this chapter considers some aspects of human body biomechanics that are important for clothing design. These include anatomical landmarks,[8] skeletal and musculoskeletal system,[1] anthropometry,[9] range of motion,[10] and the human skin.[11] In order to have a complete understanding, an overview of the human systems is provided.[1] These topics are important for clothing design and without their knowledge, the beauty and aesthetic of fashion will be lost.

6.2 Definitions and anatomical landmarks

In order to communicate effectively, a set of terms have been defined to describe anatomical positions with precise meanings. Some of these terms are related to imaginary planes as shown in Fig. 6.1. There are three hypothetical reference planes.[12] The sagittal plane, also called the median plane, is a plane dividing the body into two equal right and left halves. The transverse plane, also called the horizontal plane, is a plane that cuts the body

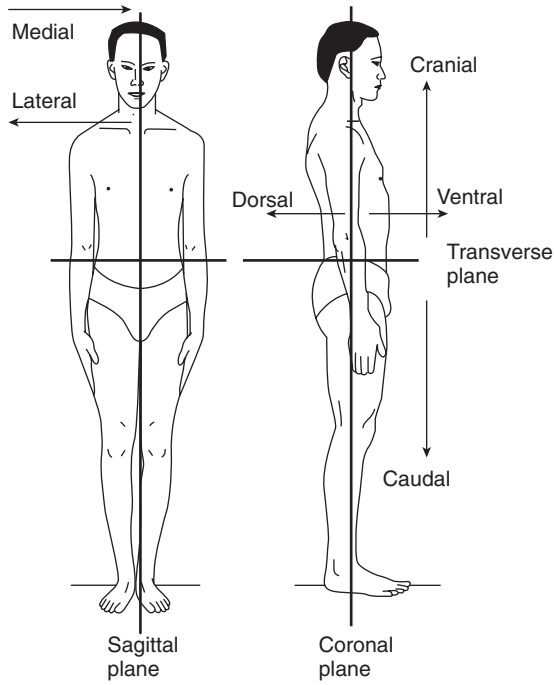

6.1 The planes of reference.

into a 'top' and 'bottom' section as shown in Fig. 6.1. The coronal plane, also called frontal plane, is a plane that divides the body into 'front' and 'back' (Fig. 6.1). Instead of using front, back, top, and bottom, specific terms, such as posterior, inferior, etc., are used to describe relative positions. These are described in Table 6.1.

Figure 6.2 provides the terms used to describe body regions.[8,13] The regions described in Fig. 6.2 are widely used in medical fields whereas the regions described in Fig. 6.3 are rarely used in medical fields but are of immense practical value. They are used by the NASA for anthropometric studies.[12] Knowledge of these terms enables us to understand most text and articles related to anatomy and physiology. Before discussing the skeletal system, some definitions are provided:

- *Cell* This is the basic unit of structure and function in an organism. Some organisms, such as virus and bacteria, are unicellular (one cell) organisms. The cells contains protoplasm (viscous translucent membrane), plasma membrane (cell external boundary), and nucleus (responsible for cell growth, metabolism, and reproduction). In humans, cells are grouped together to form tissues.[14]

Table 6.1 Relative positions

Term	Description
Superior (Cranial)	A body part above another part, or closer to the head.
Inferior (Caudal)	A body part below another body part, or toward the feet.
Anterior (Ventral)	Towards the front.
Posterior (Dorsal)	Towards the back.
Medial	Closer to the Sagittal* plane.
Lateral	Away from the Sagittal* plane.
Proximal	Section of the body part closer to the point of attachment.
Distal	Opposite of Proximal. Section of the body part away from the point of attachment.
Superficial	Situated near the surface.
Deep	Parts that are more internal.
Rostral	Toward the nose.
Bilateral	On both sides of the body or head.
Ipsilateral	On the same side of the body or head.
Contralateral	Opposite of Ipsilateral. On the opposite side of the body or head.

* see Fig. 6.1

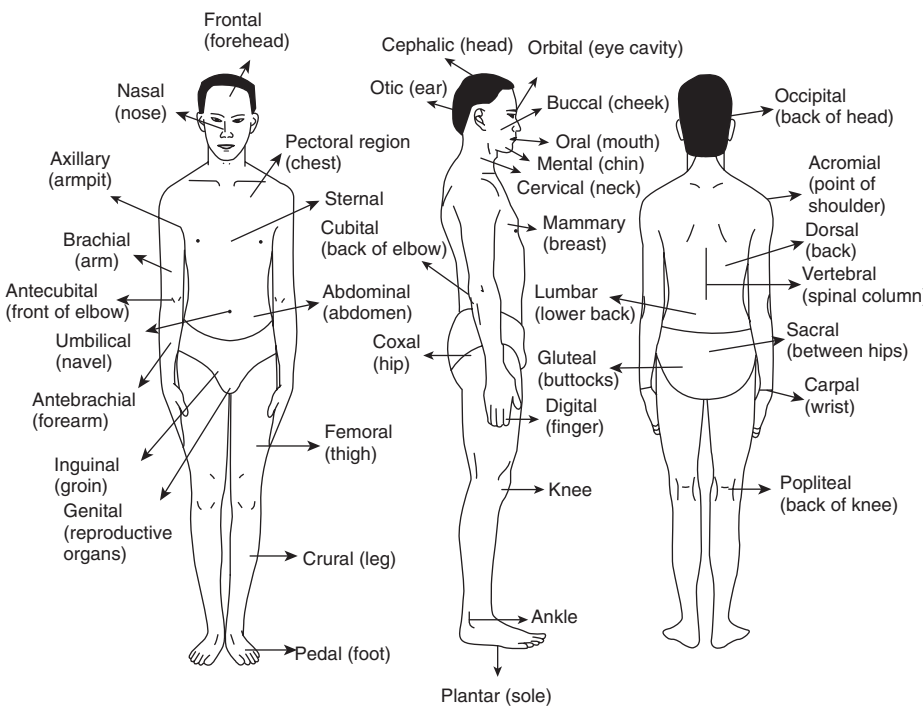

6.2 Body regions.

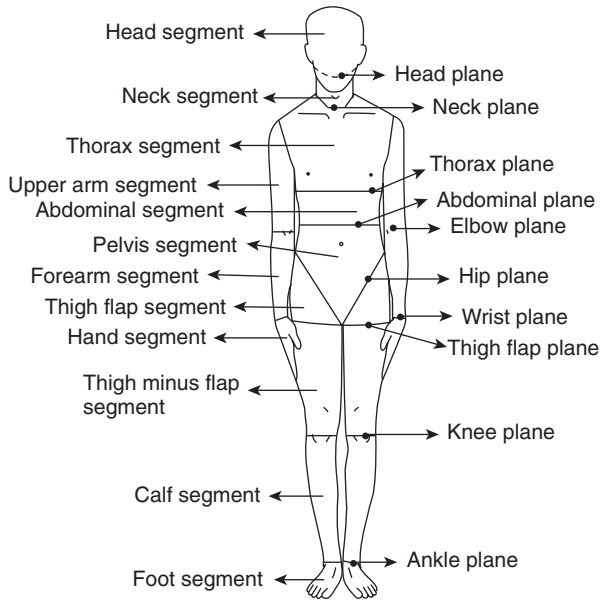

6.3 Body segments and planes of segmentation.

- *Tissue* Tissue is a group of similar cells. They have specialized structure and function. There are four main types of tissues: epithelial, connective, muscle and nervous tissues. Epithelial tissues cover organs, forming a lining. Generally they lack blood vessels. Connective tissue, with a good supply of blood vessels, provides support and protection, serves as a framework, stores fat, produces blood cells, protects against infection, and helps repair tissue damage. The muscle tissues with the help of muscle fibers can contract. This enables movement. Nervous tissues are found in the brain, spinal cord, and peripheral nerves. These tissues are specialized for transmission of nerve impulses.[5,14]
- *Organ* Different kinds of tissue working together in the same place may form an organ such as heart, lungs, eyes, or brain.[5]
- *Bone* Bones consist of bone tissue (connective tissue), blood vessels, bone marrow, and nervous tissue. Nonliving material (mineral salts) in the bone makes it appear inactive. The bones have projections called processes. These projections provide sites for ligament and tendon attachment.[15]
- *Muscle* There are three types of muscle: skeletal, smooth and cardiac. Skeletal muscles, together with the skeletal system, play a vital role in movement. Smooth muscles are somewhat similar to skeletal muscles. They are found in the irises of the eye, and the walls of the blood vessels,

the stomach and the intestines. They are slower to contract and relax compared with skeletal muscles; however, they can maintain contraction longer. Cardiac muscles are found only in the heart.[16]

- *Blood* Blood is used to transport substances throughout the body. It consists of red blood cells, white blood cells, and platelets in a fluid matrix called plasma.[5,14] The red blood cells transport oxygen to the tissues. The five types of white blood cells (neutrophils, eosinophils, basophils, monocytes, and lymphocytes) protect against foreign bodies.[14]
- *Cartilage* Cartilages are connective tissues. They are gel-like structures (look like white plastic) that provide support and protection. They are found at the end of bones in many joints, nose, and ribs.[17] There are three types of cartilage: hyaline, fibrous, and elastic. Hyaline cartilage, also known as articular cartilage, covers bone surfaces at joints. Fibrous cartilage, containing abundant amounts of fibrous material, is strong and rigid. It is used mainly at the intervertebral disks. Elastic cartilage is elastic and resilient. It is used at the auditory canal and external ear.
- *Ligament* Ligament is a dense fibrous connective tissue connecting bones to bones at joints.[17] The ligament can resist tensile forces without considerable elongation.
- *Tendon* Tendons are dense fibrous connective tissues connecting bones to muscles.[17] They are resistant to tension but flexible. They enable bones to move while muscles contract.

6.3 Skeletal system

The skeletal system[1] consists of bony and cartilaginous parts that support and protect the organs. In addition, it is also used for locomotion, together with the muscular system. The skeletal system includes the skull, vertebral column, thoracic cage, upper limbs, and lower limbs. The skull is composed of the cranium and facial bones. The cranium protects the brain, while the facial bones support the teeth and enable us to eat. The vertebral column consists of seven cervical vertebrae, twelve thoracic vertebrae, five lumbar vertebrae, scrum, and coccyx. The cervical vertebrae located at the neck (cervical) region support the head and enable head movement. The first cervical vertebra, the Atlas vertebra, supports the head. Together with the Atlas vertebra, the second vertebra (the Axis), enables head movements. The thoracic vertebrae, larger than the cervical vertebrae, have long transverse process (or projections) on the dorsal side. The two sides of the transverse process provide facets for attachment of rib bones, while the center spinous process is used for muscle attachment. The lumbar vertebrae

are larger, to support the body from above them. The Sacrum is formed of five fused vertebrae and is triangular in shape. The coccyx, composed of four fused vertebrae, is the lowest part of the vertebral column and is usually referred as the tailbone. It provides an attachment for muscles, and also serves as a shock absorber when sitting. The spinal cord, carrying nerve cells from the brain to the body, passes through the vertebral foramen (center hole) of all the vertebrae of the vertebral column except the coccyx.

The thoracic cage comprises the ribs, thoracic vertebrae, sternum, and coastal cartilages. The coastal cartilages connect the ribs to the sternum. The sternum, also referred to as the breast bone, is flat and elongated. It consists of three parts: manubrium, sternum body, and xiphoid process. The ribs form an enclosure to protect the important organs such as the lungs and the heart. Most people have twelve ribs, of which only seven superior ones are attached to the sternum. The next three are attached to the seven ribs via cartilage. Thus, they are indirectly attached to the sternum and are called false ribs. The final two (sometimes three) anterior ones are floating ribs, since they are not attached to the sternum directly or indirectly.

The upper limb (arm and hand) consists of the pectoral girdle, humerus, radius, ulna, and the hand bones. Sometimes the pectoral girdle is grouped in a separate set rather than with the upper limb. The pectoral girdle, also called the shoulder girdle, consists of one pair (left and right side) of clavicles and one pair of scapulae. The clavicles (collar bones) hold the scapula in place and provide attachments for muscles of the upper limb, chest and back. At the medial side, it is attached to the manubrium, while at the lateral side it is connected to the acromion process of the scapula. The scapulae (shoulder blades) are broad triangular bones located at the upper back. The glenoid cavity of the scapula articulates with the head of the humerus. The scapulae provide attachment for the upper limb and chest muscles. The humerus, connected at the proximal side to the scapula at the head, forms the main bone for the upper arm. At the inferior side, the lateral and the medial epicondyle articulates with the radius and ulna forearm bones, respectively. The radius is located at the thumb side of the forearm while the ulna is located toward the small finger side. The hand bones include eight small tarsals that form the wrist, five metatarsals that form the palm of the hand, and 14 phalanges that form the finger. The thumb has only two phalanges, while the other fingers have three phalanges.

The lower limb (leg and foot) consists of the pelvic girdle and the bone forming the thigh, leg, and foot. The pelvic girdle consists of two coxal bones articulated anteriorly to form the pelvis bone. The coxal bones articulate with the sacrum posteriorly. The coxal bones provide attachments for liga-

ments and muscles. The thigh contains the femur bone, the longest bone in the body. The femur articulates at the head with the coxal bone. At the distal end of the femur, the lateral and medial condyles articulate with the tibia bone of the leg. At the distal end, there is also the patella or knee cap that articulates with the femur on its distal anterior surface. The tibia, which is larger than the fibula, is located at the medial side. At the distal end, the tibia form the medial malleolus at the ankle. The long and slender fibula is located in the lateral side of the tibia. The fibula head articulates with the tibia just below the lateral condyle of the tibia. At the distal side, the fibula forms the lateral malleolus at the ankle. The foot consists of seven tarsals (calcaneus, talus, navicular, cuboid, lateral cuneiform, intermediate cuneiform, and medial cuneiform) which form the hind foot. The seven metatarsals of the foot form the mid foot, while the 14 phalanges form the forefoot.

6.4 Musculoskeletal system

Skeletal muscles provide a variety of body movements together with the skeletal system.[4] Each movement depends upon the joint and the degree of freedom at the joint.[18] The joints can be classified, based on function, as synarthrosis (immovable), amphiarthrosis (slightly movable), and diarthrosis (freely movable). There are synarthrosis joints on the skull. Diarthrosis joints are also called synovial joints based on their structure. In a cartilaginous joint, cartilage connects the bones and allows slight movement. Cartilaginous joints can therefore be included with the amphiarthrosis group. The knee and the shoulder are synovial joints, while the joints between vertebrae are cartilaginous joints. The knee can be mechanically modeled as a hinge joint, while the shoulder can be modeled as a ball and socket joint. The cartilaginous joints of the spine (between vertebrae) enable rotation, slight shear, and some compression and extension.

At the synovial joints, in general one end of the muscle is connected to a bone that is movable and other end of the muscle at the other side of the joint to a relatively fixed bone. The immovable end of the muscle is called the origin and the movable end is called the insertion. Muscles can have more than one origin and insertion point. When the muscle contracts (shortens), it pulls the movable bone, thus causing the desired movement. Several muscles work together to generate the desired effect. For a particular movement, one muscle provides the main force and is referred to as the prime mover. Muscles usually work in pairs, so when one muscle contracts the other one relaxes and *vice versa*. The muscle that contracts to generate the prime move is called the agonist or synergist muscle, while the relaxing muscle is called the antagonist. When the antagonist muscle

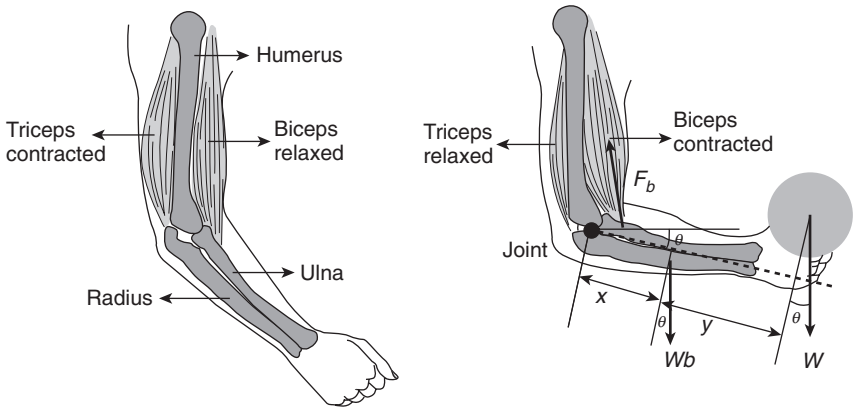

6.4 Simplified musculoskeletal system at the elbow joint.

contracts, motion opposite to the prime movement takes place. Figure 6.4 shows a simplified musculoskeletal system at the elbow joint. The insertion point of the biceps is at the radial tuberosity on the radius bone. The biceps has two origins: coracoid process and tubercle above glenoid cavity of scapula. The insertion point of triceps is at the olecranon process of ulna. The triceps has three origins: tubercle below glenoid cavity, lateral, and medial surfaces of humerus. When the biceps contracts, the triceps relaxes, moving the forearm toward the arm. When the triceps contracts, the biceps relaxes, moving the forearm away from the arm. A simple biomechanical model of the elbow joint can easily be constructed to estimate joint and muscle forces using the distances x (perpendicular distance of center of gravity of forearm from the elbow joint) and y (perpendicular distance of center of gravity of the object from the elbow joint), the angle θ (angle of forearm respective to a given axis system), and the forces W_b (weight of forearm), W (weight of the object lifted), and F_b (force of the bicep muscle).

6.5 Overview of other systems

Several organs can work together in a system. The eleven systems in the human body are the circulatory system, digestive system, endocrine system, immune system, muscular system, lymphatic system, nervous system, reproductive system, respiratory system, skeletal system, and urinary system.[3,5,7,14] The skeletal system has already been discussed sufficiently. It is impossible to describe in detail all the systems in this chapter; however, a brief overview is essential.

The *circulatory system*, the body's transport system, is made up of a group of organs that transport blood throughout the body. The heart pumps

the blood and oxygen-rich blood leaves the left side of the heart and enters the biggest artery, the aorta. The aorta branches into smaller arteries which branch into even smaller vessels called arterioles that travel all over the body. The smallest blood vessels (capillaries), found in body tissue, provide nutrients and oxygen to the cells and take in carbon dioxide, water, and waste. Veins are the opposite of arteries. The capillaries form the venules (small veins) and then veins. The oxygen and nutrient depleted blood goes back to the heart through veins. The veins join together from different branches to form larger veins until they reach the right side of the heart at the vena cava. Blood is pumped from the heart at high pressure, so the arteries have thicker walls than the veins. In addition, veins have valves to assist the transportation of blood back to the heart. These are essential especially when blood has to move 'uphill' from the lower limbs. The oxygen-depleted blood arriving at the right side of the heart is pumped to the lungs, via the pulmonary artery. At the lungs, the blood is oxygenated and arrives to the left side of the heart via the pulmonary vein. The heart beats continuously supplying nutrients and oxygen to all parts of the body.

The *digestive system* is made up of organs that break down macromolecular food particles (protein, carbohydrates, and fats) into simpler molecules (amino acids, glucose, and fatty acids) that can be absorbed by the body. The simpler molecules are 'burned' at the cells to release energy and to facilitate growth and repair. In addition, the digestive system enables the absorption of minerals (calcium, potassium, sodium and others) and vitamins (A, B, C, etc.). After food is chewed in the mouth and swallowed, it goes down the esophagus and enters the stomach. At the stomach, it is broken down by powerful stomach acids. From the stomach, the food travels into the small intestine, where the food is further broken down into nutrients that can enter the blood stream. The excess food that the body does not need or cannot digest is turned into waste and is eliminated from the body via the anus.

The *endocrine system* is a group of glands that produce hormones. Hormones are chemicals that control body functions such as metabolism, growth, and sexual development. The glands (pituitary gland, thyroid gland, parathyroid glands, adrenal glands, thymus gland, pineal body, pancreas, ovaries (in females), and testes (in males)) release hormones directly into the bloodstream, which transports them to organs and tissues throughout the body.

The *immune system* is our body's defense system against infections and diseases. There are three types of response systems in the immune system: the anatomic response, the inflammatory response, and the immune response. The anatomic response physically prevents threatening substances from entering the body. Examples of the anatomic system include the

mucous membranes and the skin. If substances do get by, the inflammatory response goes on the attack. The inflammatory system works by excreting the invaders from the body. Sneezing, running noses, and fever are examples of the inflammatory system at work. When the inflammatory response fails, the immune response goes to work. This is the central part of the immune system and consists of white blood cells, which fight infection by swallowing up antigens. About a quarter of white blood cells, called the lymphocytes, migrate to the lymph nodes, and produce antibodies, which fight disease.

The *muscular system* is made up of tissues that work with the skeletal system to control movement of the body. Some muscles, such as those in the arms and legs, are voluntary, meaning that one decides when to move them. Other muscles, such as the ones in the stomach, heart, intestines and other organs, are involuntary. This means that they are controlled automatically by the nervous system and hormones. The body is made up of three types of muscle tissue: skeletal, smooth and cardiac. Further details may be found in Section 6.4.

The *lymphatic system* is also a defense system for the body. It filters out organisms that cause disease, produces white blood cells, and generates disease-fighting antibodies. It also distributes fluids and nutrients in the body and drains excess fluids and protein so that tissues do not swell. The lymphatic system consists of a network of vessels that help to circulate body fluids. These vessels carry excess fluid away from the spaces between tissues and organs and return it to the bloodstream.

The *nervous system* is made up of the brain, the spinal cord, and nerves. One of the most important systems in the body, the nervous system is the body's control system. It sends, receives, and processes nerve impulses throughout the body. These nerve impulses tell muscles and organs what to do and how to respond to the environment. There are three parts of the nervous system that work together: the central nervous system, the peripheral nervous system, and the autonomic nervous system. The central nervous system consists of the brain and spinal cord. It sends out nerve impulses and analyzes information from the sense organs, which tell the brain about things one sees, hears, smells, tastes and feels. The peripheral nervous system includes the craniospinal nerves that branch off from the brain and the spinal cord. It carries the nerve impulses from the central nervous system to the muscles and glands. The autonomic nervous system regulates involuntary actions, such as heart beat and digestion.

The *reproductive* system allows humans to produce children. Sperm from the male fertilizes the female's egg, or ovum, in the fallopian tube. The fertilized egg travels from the fallopian tube to the uterus, where the fetus develops over a period of nine months.

The *respiratory system* brings air into the body and removes carbon dioxide. It includes the nose, trachea, and lungs. On breathing in, air enters the nose or mouth and goes down a long tube called the trachea. The trachea branches into two bronchial tubes, or primary bronchi, which go to the lungs. The primary bronchi branch off into even smaller bronchial tubes, or bronchioles. The bronchioles end in the alveoli, or air sacs. Oxygen follows this path and passes through the walls of the air sacs and blood vessels before entering the blood stream. At the same time, carbon dioxide passes into the lungs and is exhaled.

The *urinary system* eliminates waste from the body, in the form of urine. The kidneys remove waste from the blood. The waste combines with water to form urine. From the kidneys, urine travels down two thin tubes called ureters to the bladder. When the bladder is full, urine is discharged through the urethra.

6.6 Anthropometry

Anthropometry is a method of assessing the size, proportions, and composition of the human body using simple equipment.[9] It is universally applicable, inexpensive and non-invasive. The anthropometric percentage values are used to compare different populations. Anthropometric measures have been widely used for equipment and workplace design, growth and nutrition evaluation, and for clothing design and sizing.[19–21] Tables 6.2 and 6.3 show anthropometric values for Japanese young males and females collected by Kouchi and Mochimaru.[22] Figure 6.5 shows the location of the measurements. Most of the measurements were taken using anthropometers and tape. In addition, Fig. 6.6 shows the mass and volume of the 12 body segments according to the NASA.[12] This can be used for development of biomechanical models.

6.7 Range of motion

In Section 6.4, the musculoskeletal system was discussed. The amount of movement that occurs at a joint is the range of motion (ROM). Medical practitioners and physiotherapists use ROM to determine abnormality or injury in patients.[10,18] For clothing design, ROM is important for developing items that will be appealing but at the same time do not restrict movement.

6.8 Human skin and temperature regulation

The skin is the largest organ responsible for protecting us against the harsh environment.[11] It is also an element of beauty[2] and racial conflict.[23] Additionally and importantly, it regulates the body's temperature.[24–28] Since

Table 6.2 Anthropometric values for young Japanese males

		Male (N = 109)						
		mean	SD.	Min.	Max.	5th percentile	50th percentile	95th percentile
1	Age	20.5	1.6	19.1	27.1	19.2	19.9	24.7
2	Body mass	59.6	6.9	44.2	82.2	48.2	59.4	68.9
3	Stature	1706.1	53.8	1578.0	1839.0	1619.0	1700.0	1800.4
4	Suprasternal height	1375.7	46.8	1272.0	1504.0	1305.4	1374.0	1460.0
5	Waist height	1030.4	42.0	939.0	1148.0	964.2	1028.0	1110.0
6	Cristal height	995.9	39.1	913.0	1102.0	926.0	999.0	1065.8
7	Iliac spine height, standing	921.6	39.7	821.0	1038.0	860.2	921.0	987.0
8	Trochanterion height	865.0	35.8	788.0	962.0	803.2	865.0	928.2
9	Symphyseal height	851.1	38.5	758.0	959.0	786.4	850.0	914.0
10	Epicondyle height (lateral)	467.3	20.4	418.0	532.0	435.4	467.0	500.4
11	Upper limb length	726.7	29.2	656.0	811.0	683.8	727.0	774.6
12	Forearm length	241.2	11.7	218.0	275.0	223.4	241.0	260.2
13	Upper arm length	307.9	16.4	274.0	353.0	281.0	307.0	337.2
14	Total head height	239.0	7.6	218.0	261.0	225.4	239.0	249.6
15	Head breadth	161.9	5.2	149.0	176.0	154.0	162.0	171.0
16	Head length	189.3	6.3	175.0	206.0	180.0	190.0	200.0
17	Shoulder (biacromial) breadth	396.5	15.5	356.0	440.0	369.6	398.0	418.6
18	Waist breadth	257.1	18.3	213.0	313.0	228.4	258.0	284.2
19	Bicristal breadth	270.4	12.7	240.0	301.0	250.0	272.0	289.6
20	Bicondylar, humerus	64.6	2.8	59.0	72.0	60.4	65.0	69.6
21	Bicondylar, femur	94.6	4.3	84.0	106.0	88.4	94.0	102.0

22	Chest circumference	841.8	44.2	747.0	967.0	777.0	843.0	918.2
23	Waist circumference	730.7	51.9	600.0	884.0	628.6	701.0	780.0
24	Hip circumference	888.6	42.3	799.0	1018.0	814.6	887.0	952.6
25	Upper arm circumference	261.2	19.6	214.0	313.0	230.0	259.0	291.6
26	Upper arm circumference, flexed	273.7	19.0	225.0	330.0	242.0	272.0	305.6
27	Forearm circumference	246.8	11.9	217.0	277.0	229.4	246.0	268.2
28	Thigh circumference	515.1	36.0	441.0	618.0	457.4	515.0	567.4
29	Calf circumference	356.1	23.7	305.0	420.0	318.0	357.0	393.2
30	Foot length	253.2	10.8	226.5	274.0	234.4	254.0	270.3
31	Instep length	182.0	8.1	164.5	201.0	169.5	182.0	194.3
32	Fibular instep length	160.8	7.9	144.5	183.0	148.2	160.0	175.7
33	Ball breadth	99.3	4.4	89.0	108.5	91.9	99.0	106.0
34	Foot breadth	101.6	4.6	90.5	114.0	94.2	101.5	108.5
35	Heel breadth	64.6	3.2	55.0	73.5	60.2	65.0	69.8
36	Foot circumference	250.8	10.2	225.0	269.0	235.0	251.0	266.0
37	Ball angle	78.2	3.1	68.0	86.0	73.2	78.0	83.0
38	Toe I angle	8.7	3.5	–2.0	18.5	2.7	9.0	14.0
39	Toe V angle	11.5	4.8	1.0	23.5	2.2	11.5	19.5
40	Medial malleolus height	82.8	5.1	67.0	98.0	75.0	83.0	91.0
41	Lateral malleolus height	69.7	5.0	57.0	84.0	62.0	69.0	79.0
42	Hand length from crease	180.6	7.2	162.0	198.0	169.4	180.0	190.6
43	Hand length from stylion	189.2	7.8	169.0	212.0	177.8	189.0	202.6
44	Hand breadth	81.8	3.3	74.0	89.0	76.0	82.0	86.6
45	Hand thickness	28.8	1.9	25.0	36.0	26.4	29.0	32.0
46	Subscapular skinfold thickness	11.8	3.6	6.4	27.4	7.6	11.0	18.6
47	Suprailiac skinfold thickness	10.3	5.5	3.6	27.4	4.5	9.0	22.1
48	Triceps skinfold thickness	9.2	3.8	4.2	24.0	5.0	8.2	17.2
49	Calf skinfold thickness	7.5	2.6	3.2	17.8	4.3	7.0	12.2

Table 6.3 Anthropometric values for young Japanese females

		Female (N = 98)						
		mean	SD.	Min.	Max.	5th percentile	50th percentile	95th percentile
1	Age	20.2	1.1	19.2	26.0	19.3	19.9	22.2
2	Body mass	53.1	7.1	37.2	76.4	41.6	52.1	65.0
3	Stature	1583.4	50.6	1440.0	1688.0	1511.0	1578.0	1665.2
4	Suprasternal height	1278.6	44.3	1143.0	1380.0	1216.1	1277.5	1346.3
5	Waist height	991.4	38.7	882.0	1064.0	929.3	992.5	1053.2
6	Cristal height	941.4	39.7	815.0	1022.0	885.6	939.5	1005.0
7	Iliac spine height, standing	848.4	36.0	730.0	919.0	792.4	847.0	908.3
8	Trochanterion height	799.3	35.5	709.0	876.0	740.6	799.0	855.2
9	Symphyseal height	787.1	34.3	685.0	862.0	733.7	787.0	839.4
10	Lateral epicondyle height	428.0	19.1	372.0	479.0	398.7	429.5	459.0
11	Upper limb length	667.4	29.1	605.0	729.0	622.7	668.0	718.2
12	Forearm length	218.1	11.9	185.0	248.0	199.7	218.0	239.2
13	Upper arm length	282.6	14.3	252.0	312.0	256.9	282.0	305.0
14	Total head height	230.7	6.5	215.0	247.0	220.9	232.0	240.2
15	Head breadth	155.8	5.1	144.0	169.0	148.9	156.0	164.0
16	Head length	181.1	6.1	168.0	194.0	171.0	181.0	190.2
17	Shoulder (biacromial) breadth	360.2	16.7	304.0	399.0	331.9	361.0	384.0
18	Waist breadth	237.5	21.1	195.0	348.0	205.0	236.5	268.0
19	Bicristal breadth	276.3	13.6	246.0	323.0	256.9	275.0	300.0
20	Bicondylar, humerus	56.9	3.0	50.0	63.0	52.0	57.0	62.0
21	Bicondylar, femur	89.3	5.1	80.0	101.0	81.9	89.0	97.2
22	Chest circumference	828.3	61.0	678.0	1075.0	735.8	825.0	927.9

23	Waist circumference	657.1	57.7	543.0	937.0	581.5	651.5	744.1
24	Hip circumference	913.5	49.9	777.0	1053.0	834.3	915.0	986.0
25	Upper arm circumference	252.3	24.7	203.0	343.0	215.4	250.0	293.3
26	Upper arm circumference, flexed	257.5	23.6	213.0	338.0	221.9	255.0	297.2
27	Forearm circumference	227.7	13.3	200.0	266.0	210.0	227.0	250.8
28	Thigh circumference	540.9	38.7	458.0	636.0	477.9	544.0	609.1
29	Calf circumference	349.8	24.9	305.0	413.0	314.7	347.0	389.9
30	Foot length	233.3	10.1	209.5	257.0	218.0	233.3	247.2
31	Instep length	168.2	7.9	151.5	187.0	154.9	168.8	180.5
32	Fibular instep length	148.1	7.7	132.0	167.0	137.4	148.3	162.2
33	Ball breadth	91.1	4.0	81.5	103.0	84.9	91.5	97.5
34	Foot breadth	93.2	4.1	85.0	106.0	86.9	93.5	100.1
35	Heel breadth	60.3	3.1	54.0	68.5	56.0	60.0	65.6
36	Foot circumference	231.2	9.3	210.0	256.0	217.0	231.0	245.0
37	Ball angle	77.8	2.5	72.0	84.0	73.4	78.0	81.6
38	Toe I angle	10.9	4.5	1.5	26.0	3.9	11.0	18.0
39	Toe V angle	8.5	5.2	−6.0	21.5	−1.6	9.8	14.0
40	Medial malleolus height	75.5	4.5	66.0	86.0	69.0	76.0	83.3
41	Lateral malleolus height	62.8	4.2	55.0	74.0	57.0	62.5	70.0
42	Hand length from crease	167.3	7.7	146.0	186.0	155.0	167.5	178.0
43	Hand length from stylion	176.6	8.3	154.0	194.0	164.7	177.0	189.0
44	Hand breadth	73.6	3.0	66.0	81.0	69.0	74.0	79.2
45	Hand thickness	25.7	1.4	23.0	29.0	23.9	26.0	28.0
46	Subscapular skinfold thickness	19.8	6.3	8.0	37.8	10.7	18.8	31.5
47	Suprailiac skinfold thickness	24.8	7.5	11.0	38.4	13.0	25.4	37.2
48	Triceps skinfold thickness	18.2	5.2	7.2	34.4	10.3	17.8	26.2
49	Calf skinfold thickness	15.3	4.6	5.8	30.0	8.4	15.2	22.3

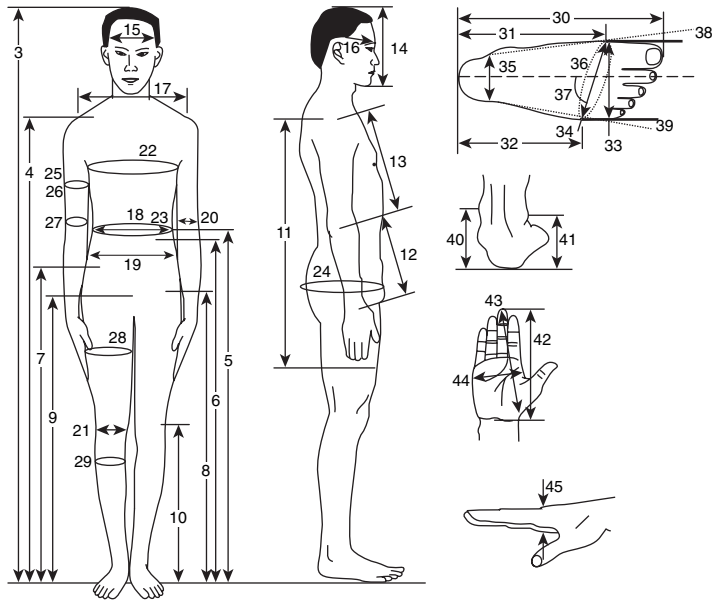

6.5 Anthropometric measures.

Segment	Mass (g)			Volume (cm^3)		
	5th percentile	50th percentile	95th percentile	5th percentile	50th percentile	95th percentile
1 Head	4280	4560	4560	4260	4440	4550
2 Neck	860	1140	1140	930	1100	1270
3 Thorax	20520	26220	31720	20420	26110	31760
4 Abdomen	2000	2570	2850	2030	2500	2960
5 Pelvis	9410	12260	15110	9420	12300	15150
6 Upper arm	1710	2000	2570	1600	2500	2500
7 Forearm	1140	1430	1710	1180	1450	1720
8 Hand	570	570	570	460	530	610
9 Hip flap	2850	3710	4280	2890	3640	4380
10 Thigh	5420	6840	7980	5480	6700	7920
11 Calf	3420	3990	4850	3320	4040	4760
12 Foot	860	1140	1140	840	1010	1180

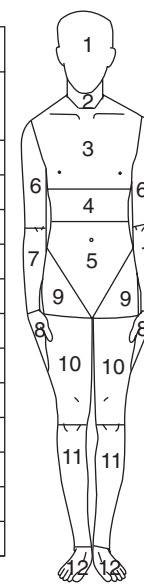

6.6 Mass and volume for different segments.

clothing can influence the temperature of the body, it is essential to know the skin and its properties. The skin has three layers: epidermis, dermis and subcutaneous layer.[11]

The *epidermis* (outer layer), also called cuticle or scarf skin, is non-vascular (does not have blood vessels), and consists of stratified epithelium. However, the deepest epidermal layer (stratum basale), close to dermis, is nourished by blood vessels. The more superficial layers of cells, called the stratum corneum, may be regarded separately from a deeper stratum (stratum mucosum). The epidermis varies in thickness. For example, in the palms of the hands and soles of the feet, it is thick, hard, and horny in texture. Moving from the deep to the outer layer of the epidermis, the nutrient decreases. At the surface, the cells are dead and provide protection against mechanical injury as they can be rubbed away. The epidermis provides protection against water loss, chemicals, and injury. Specialized cells (melanocytes) in the epidermis produce melanin, a dark pigment that absorbs the sun's ultraviolet rays. The amount of melanin in the skin is responsible for the skin color. More melanin causes darker skin. The amount of melanin depends upon genetics, and environmental and physiological factors.

The epidermis is non-vascular whereas the *dermis*, just below the epidermis, is well supplied with blood vessels. The blood vessels provide nutrients to all the skin cells and at the same time are responsible for temperature regulation. The dermis also has nerve ending and specialized nerve cells responsible for detecting mechanical, temperature, pressure, and vibration effects. In hairy skin, the 'root' of the hair (hair follicle) is situated in the dermal layer. The hair inclination can be changed using the arrector pili muscle. The eccrine sweat gland produces sweat which travels along the sweat gland duct and emerges at the pore on the epidermal surface. The sebaceous gland on the other hand secrets an oily liquid (sebum) through small ducts into the hair follicles. This oily liquid keeps the hair and skin soft.

The *subcutaneous layer* consists of loose connective and adipose tissue. There is no sharp boundary between dermis and the subcutaneous layer and, in many cases, the subcutaneous layer is considered part of the dermis. The adipose tissue stores fat and is used for insulation and energy storage.

As previously mentioned, the skin is used for temperature regulation[28] and clothing has much influence in the skin's function.[29] Being warm blooded, the temperature of human deep body parts is kept at 37 °C. Only slight changes of this disrupt the normal body functions, so when the body temperature changes, prompt action is taken. The body can lose heat by three mechanisms: conduction, convection and radiation. When the temperature of the body increases, nerve impulses from the brain (in the

hypothalamus region) cause the blood vessels to dilate.[28] This results in more blood flowing in the dermis. Heat is lost from the skin surface through radiation (more heat is lost from darker skin). At the same time, nerve signals stimulate the eccrine gland to produce sweat. When the sweat evaporates, the skin is cooled further (by convection). In a windy environment, we feel cooler; however, high humidity hinders heat evaporation. Heat is also lost via conduction if the skin is in direct contact with a colder material, especially a heat conducting material. However, when the temperature of the body decreases, nerve signal causes the blood vessels to contract. This decreases blood flow and thus heat loss through the skin is reduced. The sweat glands are inactive and the hair can be erect to create an insulation layer of air on top of the skin. Further reduction in temperature causes shivering, as nerve signals causes the contraction of muscles to produce heat. Thermal regulation is very important for clothing design.[25,26,29]

6.9 Conclusion

Since clothes are designed for humans, it is essential to know the anatomy and physiology of the human body. Only then will we be able to merge the knowledge of clothing mechanics with those of human biomechanics in order to predict the effect of clothing on the human body. This chapter has provided a basic understanding of the human body. First, some terms were defined to enable the user to better understand the human body. Then, the skeletal and musculoskeletal systems were discussed, since it forms the main system for movement and support. Anthropometry and range of motion, together with an understanding of the musculoskeletal system provide the fundamental knowledge for clothing sizing, biomechanical analysis, and fashion design. In addition, the human skin was discussed. The skin not only protects the body but also regulates the body's temperature. Since clothing can influence the skin's function, it is essential to understand the anatomy and physiology of the skin. Sensors in the skin influence the perception of comfort and fit and, as a result, knowledge of the skin enables the design of comfortable clothing for any temperature. In order to make the study of the body complete, an overview of all the human systems (circulatory, digestive, endocrine, immune, lymphatic, muscular, nervous, reproductive, respiratory, skeletal, and urinary) have been provided.

6.10 References

1. Agur, A. M. R. and Grant, J. C. B. (2005). *Grant's Atlas of Anatomy*. Philadelphia: Lippincott Williams & Wilkins.

2. Constance, D. (1993). *An Introduction to Drawing the Nude: Anatomy, Proportion, Balance, Movement, Light, Composition*. London: Apple Press.
3. Gray, H., Williams, P. L. and Bannister, L. H. (1999). *Gray's Anatomy: The Anatomical Basis of Medicine and Surgery*. New York: Churchill Livingstone.
4. Palastanga, N., Field, D. and Soames, R. (1998). *Anatomy and Human Movement: Structure and Function*. Oxford: Butterworth-Heinemann.
5. Sheir, D., Butler, J. and Lewis, R. (1998). *Essentials of Human Anatomy and Physiology*. New York: McGraw Hill.
6. Mader, S. S. and Galliart, P. (2005). *Understanding Human Anatomy and Physiology*. New York: McGraw-Hill Higher Education.
7. Saladin, K. S. (2005). *Human Anatomy*. New York: McGraw-Hill.
8. Tixa, S. (1999). *Atlas of Palpatory Anatomy of the Lower Extremities: A Manual Inspection of the Surface*. New York: McGraw-Hill, Health Professions Division.
9. Pheasant, S. (1994). *Bodyspace.* London: Taylor and Francis.
10. Soames, R. (2003). *Joint Motion: Clinical Measurement and Evaluation*. Edinburgh: Churchill Livingstone.
11. Forslind, B., Lindberg, M. and Norlen, L. (2004). *Skin, Hair, and Nails: Structure and Function*. New York: M. Dekker.
12. NASA (1995). Man-systems integration standards (revision b). USA, NASA Johnson Space Center: (http://msis.jsc.nasa.gov/).
13. Field, D. (2001). *Anatomy: Palpation and Surface Markings*. Oxford: Butterworth Heinemann.
14. Springhouse (2001). *Anatomy & Physiology Made Incredibly Easy!* Pennsylvania: Springhouse Corporation.
15. Behiri, J. and Vashishth, D. (2000). Biomechanics of bone. *Clinical Biomechanics*. Z. Dvir (ed). New York: Churchill Livingstone: 65–82.
16. Dvir, Z. (2000). Biomechanics of muscle. *Clinical Biomechanics*. Z. Dvir (ed). New York: Churchill Livingstone: 83–102.
17. Bader, D. L. and Bouten, C. (2000). Biomechanics of soft tissue. *Clinical Biomechanics*. Z. Dvir (ed). New York: Churchill Livingstone: 35–64.
18. An, K.-N., Chao, E. Y. S. and Kaufman, K. R. (1997). Analysis of muscle and joint loads. *Basic Orthopaedic Biomechanics*. V. C. Mow and W. C. Hayes (eds). Philadelphia: Lippincott-Raven: 1–36.
19. Laing, R. M., Holland, E. J., Wilson, C. A. and Niven, B. E. (1999). Development of sizing systems for protective clothing for the adult male. *Ergonomics*, **42**, (10): 1249–1257.
20. Meunier, P. and Yin, S. (2000). Performance of a 2D image-based anthropometric measurement and clothing sizing system. *Applied Ergonomics*, **31**, (5): 445–451.
21. Luximon, A. (2001). Foot shape evaluation for footwear fitting. *Industrial Engineering and Engineering Management*. Hong Kong: Hong Kong University of Science and Technology.
22. Kouchi, M. and Mochimaru, M. (2002). *Japanese body dimensions data 1997–1998.* Tokyo, Japan: Digital Human Research Center, National Institute of Advanced Industrial Science and Technology.
23. Lappbe, M. (1996). *The Body's Edge: Our Cultural Obsession with Skin*. New York: H. Holt.

24. Kim, H. E., Tokura, H., Nagashima, R. H. S. and Nishizawa, K. (1995). Do cooled women select soft or hard clothing? *Journal of Thermal Biology*, **20**, (4): 327–332.
25. Kraning, K. K. and Gonzalez, R. R. (1997). A mechanistic computer simulation of human work in heat that accounts for physical and physiological effects of clothing, aerobic fitness, and progressive dehydration. *Journal of Thermal Biology*, **22**, (4–5): 331–342.
26. Li, X. and Tokura, H. (1997). Lower critical temperature under the influences of seasonal cold acclimatization due to the two types of clothing. *Journal of Thermal Biology*, **22**, (4–5): 357–363.
27. Noakes, T. D. (2000). Exercise and the cold. *Ergonomics*, **43**, (10): 1461–1479.
28. Clancy, J. and McVicar, A. J. (2002). *Physiology & Anatomy: A Homeostatic Approach*. London: Arnold.
29. Malcolm, S., Armstrong, R., Michaliades, M. and Green, R. (2000). A thermal assessment of army wet weather jackets. *International Journal of Industrial Ergonomics*, **26**, (3): 417–424.

7

Mechanics of the human skin and underlying soft tissues

J.T. CHEUNG AND M. ZHANG
The Hong Kong Polytechnic University, China

7.1 Introduction

Tissues of the human body are often grouped into hard tissues and soft tissues. The hard tissues, i.e. bone and tooth, have been quantitatively characterized at either macro- or micro-levels in many studies. Their mechanical behaviors and properties can be found in many references.[1] Soft tissues refer to a large family of tissues, such as connective tissues, muscle and internal organs. Connective tissues, such as cartilage, ligament, tendon and skin, perform mainly a mechanical function. Their specific functional roles determine the differences in mechanical properties as a result of their diverse combinations of composition and micro-structure.

The human skin directly interacts with external environments, especially with clothes or garments. An understanding of the biomechanical properties of skin and its underlying tissues has considerable impact in the textile and clothing field. This chapter will focus on the biomechanical and structural characteristics of the human skin and underlying tissues. The mechanical behaviors of human skin and underlying tissues, such as its inhomogeneous, anisotropic, nonlinear and viscoelastic properties, and the mathematical models for representing the skin material properties, will be discussed.

7.2 Mechanical behavior of human skin

Soft tissues consist of a network of intertwining fibers with ground substance (matrix of connective tissue) immersed in fluid. The extracellular matrix of fibers contributes mainly to the mechanical properties, which may vary with species, age, hydration, obesity and biological difference between individuals. For the same individual, the properties vary with site and orientation and may be altered by irradiation, drugs, and chemicals.

The human skin possesses complex mechanical behaviors because of its multi-component material constituents, namely collagen fiber, elastin fiber

and ground substance with fluid. It exhibits non-homogeneous, anisotropic, nonlinear, and time-dependent viscoelastic properties. Collagen is a main structural component of connective tissues and accounts for about 70–80% of the dry weight of the skin, depending on age, gender and location.[2] Collagen fibers form a three-dimensional, disordered network of wavy coiled structures, with some preferential orientation. The collagen fibers near the epidermis are finer and randomly oriented, while at the mid zone they are coarser and densely packed.[3] In the deep zone, they are coarse again but are loosely packed. Collagen fibers have high tensile strength, up to 350 MPa, and are stiff with a Young's modulus of approximately 1 GPa.[3]

Elastin accounts for only about 1–2% of the dry weight of skin but is important for the maintenance of skin elasticity and resilience.[2] The elastin fibers are thought to be the first to be stretched when the tissue is strained;[3] they dominate the skin response at very low strain levels when the collagen fibers are still buckled. Elastin fibers appear as fine fibers that intertwine around the thicker collagen fibers in the deep layers of the dermis, but are rather straight close to the epidermis.[3] They are coarser in the dermis layer than close to the epidermis. Elastin is considerably less stiff than collagen and can be reversibly stretched to more than 100%.

The ground substance accounts for about 70–90% of the skin volume.[2] It is gelatinous and imparts viscoelastic behavior. The fluid-like ground substance exudes from the interfiber space while the fibers become reoriented and densely packed upon stretching.[3] This flow of ground substance is associated with the viscosity of the skin, governing the toe region of the nonlinear portion of the stress–strain curve, in which the collagen fibers are not yet fully aligned and stretched. The ground substance shows significant effects on compression, due to the water affinity of the matrix of glycosaminoglycans.[3]

7.2.1 Subject dependent mechanical behavior

Biological variability often dominates the results of mechanical testing. The mechanical properties vary with age, gender, activity levels and healthy conditions.

7.2.2 Site dependent (inhomogeneous) mechanical behavior

The mechanical properties of soft tissue are site-dependent or inhomogeneous. Because the functions of different locations may vary, the skin tissue exhibits inhomogeneous responses to mechanical loading.

7.2.3 Anisotropic mechanical behavior

Skin is an anisotropic material and its characteristics can be described by the directional pattern of pre-stress lines or the so-called Langer's lines (Fig. 7.1). These are related to the visible crease and wrinkle lines of the skin, corresponding to the directions of preferred disposition of collagen fibers.[4] The elastin and collagen fibers along Langer's lines are more stretched than those across the line, so that the extensibility of skin is lower in the directions of these lines and its stiffness is higher in these directions.

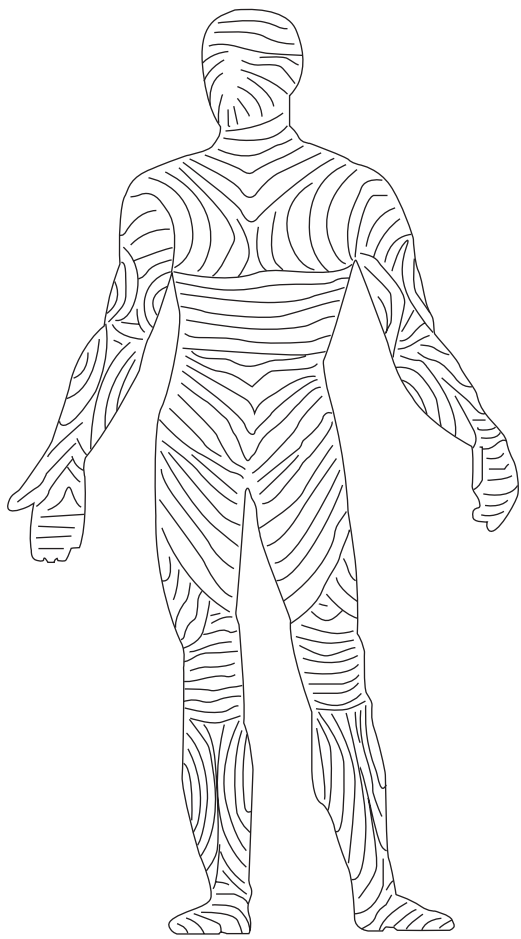

7.1 Langer's lines.

7.2.4 Nonlinear mechanical behavior

Although individual collagen and elastin fibers can be approximated as linearly elastic, non-uniformity of these structures results in nonlinear stress–strain relationships of the skin tissue. This nonlinearity is the result of gradual straightening of the collagen fibers. Figure 7.2 describes a typical stress–strain curve of the skin under tension. At range OA, with very low strains in the skin, the elastin fibers are primarily stretched and the collagen fibers are still coiled, resulting in a very low stiffness and an approximately linear stress–strain relationship. With increasing strains to range AB, a gradual straightening of the originally buckled collagen fibers contributes to the increasing stiffness of the skin tissue. The range OB is often called the toe region. At higher strains to range BC, the collagen fibers are all straightened and the stress–strain relationship becomes linear. Beyond the linear region, skin fibers begin to partially break, until complete tissue rupture occurs. As the skin response exhibits significant nonlinearity, its mechanical behavior depends highly on its state of tension.

7.2.5 Plastic behavior

If the magnitude of deformations is small enough, skin can be reversibly stretched. However, when it is stretched frequently or to a relatively large strain for a long period, permanent deformation occurs, which appears as permanent wrinkles or sutured wounds. The residual deformation after the

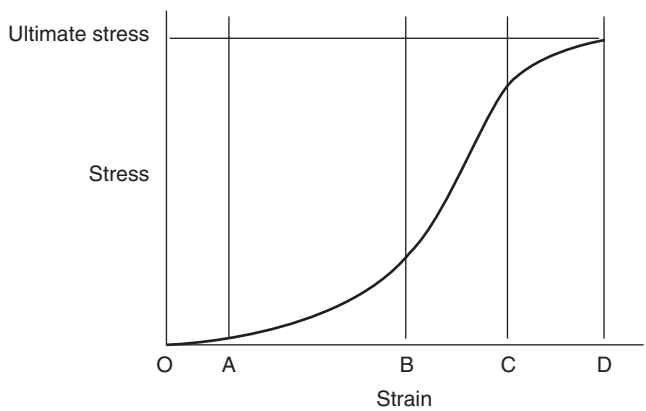

7.2 A typical stress–strain curve of skin tissue under uniaxial tension. From the toe region (O to B), the load increases linearly under initial tension and exponentially with increasing elongation. From the linear region (B to C), the relationship is approximately linear. Going into the plastic region (C to D), the relationship is nonlinear and the tissue will rupture after it has reached its ultimate stress (D).

release of the external loading corresponds to the plasticity of the skin tissue.

7.2.6 Viscoelastic behavior

Viscoelasticity describes time-dependent mechanical properties. Soft tissues consist of both solid and fluid, and behave as viscoelastic material. The mechanical properties are strain-rate-dependent. With increasing strain rate, the material becomes stiffer and stronger. It is necessary to consider and specify the strain rate or load rate when conducting tests and reporting the results. Skin tissues show stress relaxation under constant strain and creep under constant stress. When a tissue is stretched to a certain strain level and kept constant, the stress gradually decreases with time (Fig. 7.3a). This phenomenon is called stress relaxation. Alternatively, when the tissue is stretched to a certain stress level and then kept constant, its strain increases with time (Fig. 7.3b). This phenomenon is called creep. Soft tissues also exhibit considerable hysteresis under a cyclic load, i.e. the stress–strain curve shows two distinct paths during the loading and unloading cycle (Fig. 7.3c). Because of its viscoelastic nature, the stress response at any instant of time depends not only on the tissue strain at that time, but also on the history of the deformation.[4]

7.2.7 Preconditioning

When loading and unloading cycles are applied to the skin tissue successively up to the same stress level, the stress–strain curve is gradually shifted to the right (Fig. 7.3d). After a number of subsequent cycles, the mechanical response becomes reproducible from one cycle to the next. This phenomenon is called preconditioning, a steady state being reached. Preconditioning of the tissues prior to experimentation is important in order to obtain generalized, steady-state response of the materials. Recovery of preconditioning with both initial configuration and initial response will occur provided the specimen has not been damaged or undergone plastic deformation.

7.2.8 Compressibility

The degree of compressibility of skin is determined by the extent of its volume reduction under external pressure. Skin is difficult to compress because it contains a high proportion of chemically-bound water molecules with little free fluid inside. The change in skin tissue volume is extremely small for large changes in pressure; therefore, skin is often considered as incompressible.[4]

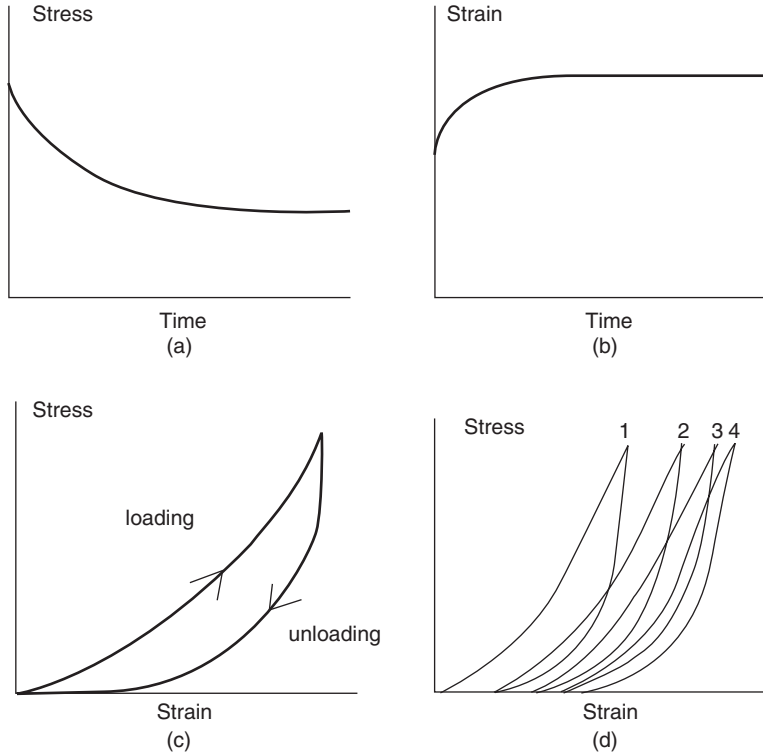

7.3 Typical stress–strain curves characterizing (a) stress relaxation, (b) creep, (c) hysteresis and (d) preconditioning of skin tissue.

7.3 Models of mechanical properties for soft tissues

A linear elastic model is often used for the description of skin mechanical properties. Young's modulus, shear modulus and Poisson's ratio are parameters to specify linear elastic properties. However, soft tissues behave in a more complicated way, such as highly nonlinear and time-dependent. Many more sophisticated models have been developed.

7.3.1 Strain–energy function of nonlinearity

One way to represent the nonlinear stress–strain relationship is the strain energy function method. Let W be the strain energy per unit mass of the tissue, and ρ_0 be the density in the unstressed state. Then $\rho_0 W$ is the strain energy per unit volume of the tissue in the unstressed state. The strain energy function W can be expressed in terms of nine strain components E_{ij} in symmetric forms.[5] The stress components S_{ij}, defined for a unit mass of tissue, can be obtained from the partial derivatives of $\rho_0 W$ with respect to E_{ij}:

$$S_{ij} = \partial\rho_0 W/\partial E_{ij} \quad (i,j = 1,2,3). \qquad [7.1]$$

The general form of the strain energy function W for a material has been given in terms of strain invariants and the extension ratios of the strain tensor as a polynomial or an exponential function.[4]

The commonly used Mooney–Rivlin model has a polynomial strain energy function of the form:

$$U = C_{10}\left(\overline{I}_1 - 3\right) + C_{01}\left(\overline{I}_2 - 3\right) + \frac{1}{D_1}(J_{el} - 1)^2 \qquad [7.2]$$

where U is the strain energy potential,
$\overline{I}_1$, $\overline{I}_2$ the first and second deviatoric strain invariants,
J_{el} the elastic volume ratio, and
C_{10}, C_{01} and D_1 the material parameters.
If D_1 is zero, the material is fully incompressible.

7.3.2 Models of linear viscoelasticity

Models developed to describe a viscoelastic material are a combination of a spring and a dashpot. The spring represents the elastic portion of the material, whereas the dashpot represents the viscous portion. Combinations of spring and dashpot can be used to represent different linear viscoelastic materials. The three most popular models of viscoelasticity are the Maxwell model, a spring in series with a dashpot (Fig. 7.4), the Voigt model, a spring and a dashpot in parallel, and the Kelvin model or the so-called standard linear solid, which is a combination of a spring in parallel with a Maxwell body.

A linear spring instantaneously produces a deformation proportional to the load $\sigma = E\varepsilon$, while a dashpot produces a velocity proportional to the load at any instant $\sigma = \eta\dot{\varepsilon}$. Spring coefficient E and viscous coefficient η are constants. The constitutive relations of the above viscoelastic models can be accordingly derived as follows:[6]

- For the Maxwell model having a series spring-dashpot arrangement, the associated stresses for both spring and dashpot are equal, while the associated strain is the sum of the strains in the two elements; then the constitutive equation is

$$\frac{\sigma}{\eta} + \frac{\dot{\sigma}}{E} = \dot{\varepsilon}. \qquad [7.3]$$

- In a similar manner, the constitutive relation for the Voigt model can be readily shown as

$$\sigma = E\varepsilon + \eta\dot{\varepsilon}. \qquad [7.4]$$

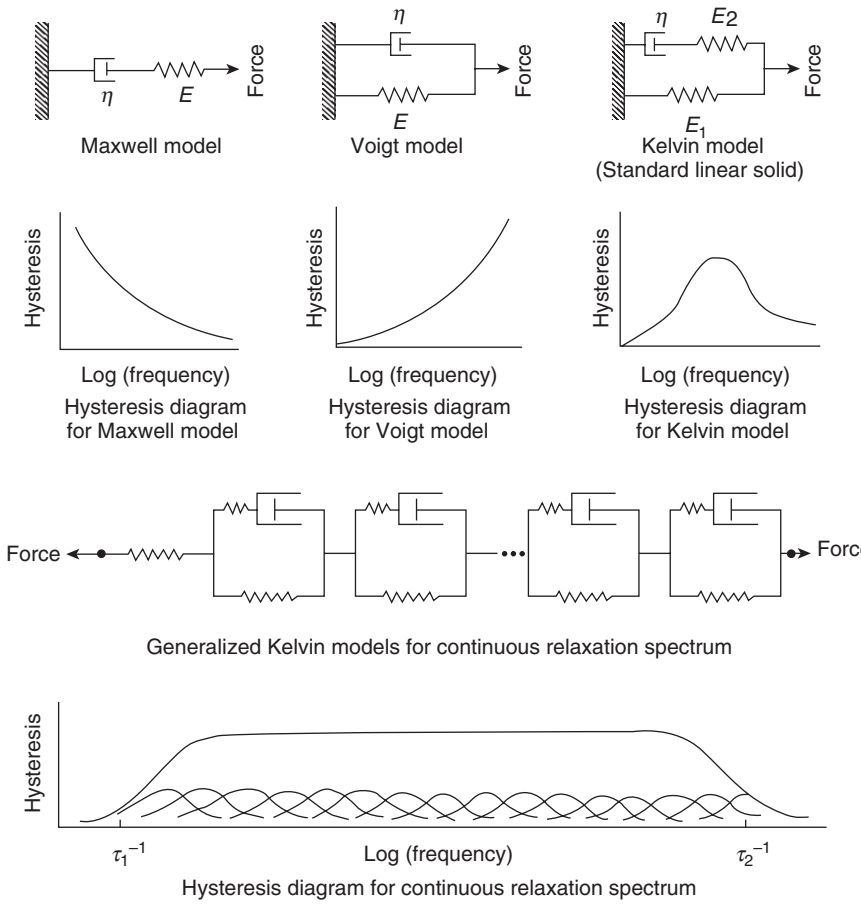

7.4 Viscoelastic models and associated hysteresis diagrams for discrete and continuous relaxation spectra (adapted from Fung, 1993, in Mechanical Properties of Living Tissues, 2nd edition, Springer-Verlag, New York).

- The constitutive relation for the Kelvin model or standard linear solid is

$$\left(1+\frac{E_1}{E_2}\right)\sigma+\left(\frac{\eta}{E_2}\right)\dot{\sigma}=E_1\varepsilon+\eta\dot{\varepsilon}. \qquad [7.5]$$

The above three models have been widely used to describe the viscoelasticity of materials. However, there are limitations for accurate representation of soft tissues.[4] For example, when a material represented by any one of these models is subjected to a cyclic load, the hysteresis will not be

insensitive to strain rate. As loading frequency increases, under the magnitude of load the damping effect exhibited by the dashpot in the Maxwell body decreases with frequency. However, the damping effect of the dashpot in the Voigt body increases with loading frequency. For the standard linear solid, there exists a characteristic loading frequency at which the damping is at a maximum. Therefore, none of these models can represent the nearly constant damping property of soft tissue, which is independent of loading frequency.[7] A model suitable for soft tissues should have more springs and dashpots. Fung[5] described the continuous relaxation spectrum of soft tissues by a generalized Kelvin model in which a large number of Kelvin units are combined in series (Fig. 7.4). The corresponding hysteresis diagram shows an infinite number of bell-shaped curves, which add up to a continuous curve of nearly constant height over a very wide range of frequencies (Fig. 7.4).

Experimental determination of linear viscoelastic properties

For the linear viscoelastic theory, there are different means of expressing the mechanical properties in which the stress–strain properties are given by relaxation and creep functions. Standard testing procedures, such as the relaxation and creep tests, provide the most direct means of obtaining the mechanical properties involved in the linear theory of viscoelasticity.[8] Such tests are usually applied to uniaxial deformation conditions whereby the appropriate constitutive relations are given by

$$\sigma(t) = \int_{-\infty}^{t} E(t-\tau)\frac{\partial \varepsilon}{\partial \tau}\,\mathrm{d}\tau \qquad [7.6]$$

$$\varepsilon(t) = \int_{-\infty}^{t} L(t-\tau)\frac{\partial \sigma(\tau)}{\partial \tau}\,\mathrm{d}\tau \qquad [7.7]$$

where $E(t)$ and $L(t)$ are the respective uniaxial relaxation function and creep function.[8]

In a stress relaxation test, the material specimen is subjected to a strain suddenly applied at time $t = 0$ and maintained constant thereafter. The measured load output can be converted into either true or nominal stress values. If $\sigma(t)$ is measured throughout the experiment, the stress-relaxation function, $E(t)$, is readily determined. In the creep test, the material specimen is subjected to a load which is applied as quickly as possible and is varied in such a manner as to keep the stress, σ_0, at a constant value after load application. With the resulting deformation or strain $\varepsilon(t)$, in the specimen being measured as a function of time elapsed since the load was first applied, the creep function, $L(t)$ can be determined.

7.3.3 Quasi-linear viscoelasticity

The theory of linear viscoelasticity is valid in the case of small deformation. For finite deformations, the nonlinear stress–strain characteristics of soft tissue have to be taken into account. The features of relaxation, creep and hysteresis can be condensed into a mathematical formulation called quasi-linear viscoelasticity theory.[7] In this theory, the instantaneous stress response to strain is nonlinear. The stress at any given time is related to the entire past history of the elastic stress with a linear relationship. The present stress is obtained by multiplying the past elastic stress increment with a relaxation function and integrating the product convolutionally from the beginning of the time to the present. The relaxation function has a continuous relaxation spectrum.

Considering a cylindrical specimen subjected to tensile load, if a step increase in elongation (from $\lambda = 1$ to λ) is imposed on the specimen, the stress developed will be a function of time as well as of the stretch λ. The history of the stress response, called the relaxation function, $K(\lambda,t)$, is assumed to be of the form

$$K(\lambda,t) = G(t) \quad T^{(e)}(\lambda), \quad G(0) = 1, \qquad [7.8]$$

where $G(t)$, a normalized function of time, is called the reduced relaxation function, and $T^{(e)}(\lambda)$, a function of λ alone, is called the elastic response. Assuming that the stress response to an infinitesimal change in stretch, $\delta\lambda(\tau)$ superposed on a specimen in a state of stretch λ at an instant of time τ, is, for $t > \tau$:

$$G(t-\tau)\frac{\partial T^{(e)}[\lambda(\tau)]}{\partial\lambda}\delta\lambda(\tau), \qquad [7.9]$$

and with superposition principles, the stress response is written as

$$T(t) = \int_{-\infty}^{t} G(t-\tau)\frac{\partial T^{(e)}[\lambda(\tau)]}{\partial\tau}\mathrm{d}\tau, \qquad [7.10]$$

where the tensile stress at time t is the sum of contributions of all the past changes, each governed by the same reduced relaxation function. From Eq. 7.10, the stress response is described by a linear law relating the stress T with the elastic response $T^{(e)}$. The function $T^{(e)}(\lambda)$ plays the role assumed by the strain ε in the conventional theory of viscoelasticity.

The inverse of Eq. 7.10 may be written as

$$\varepsilon(T,t) = \int_{-\infty}^{t} J(t-\tau)\frac{\mathrm{d}\varepsilon^{(e)}[T(\tau)]}{\mathrm{d}\tau}\mathrm{d}\tau, \qquad [7.11]$$

which defines the reduced creep function $J(t)$.

The elastic response, $T^{(e)}(\lambda)$.

Assuming $T = \varepsilon = 0$ for $t < 0$ and from Eq. 7.10:

$$T(t) = T^{(e)}[\lambda(t)] + \int_0^t T^{(e)}[\lambda(t-\tau)]\frac{\partial G(\tau)}{\partial \tau}\mathrm{d}\tau. \qquad [7.12]$$

Observing that the steady-state stress–strain behavior of soft tissue is not sensitive to strain rate, its elastic response $T^{(e)}(\lambda)$ may be described using elasticity theory, which can be approximated by its tensile stress response in a loading experiment.[7] By definition, $T^{(e)}(\lambda)$ is the tensile stress instantaneously generated in the tissue when a step function of stretching λ is imposed on it. Strict laboratory measurement of $T^{(e)}(\lambda)$ according to this definition is difficult because, at a sudden application of loading, transient stress waves will be induced in the specimen and a recording of the stress response will be confused by these elastic waves. However, if the relaxation function $G(t)$ is assumed as a continuous function, then $T^{(e)}(\lambda)$ may be approximated by the tensile stress response in a loading experiment with a sufficiently high rate of loading. Besides, the repeatable loading and unloading tensile curves upon preconditioning may be characterized separately using the elasticity theory.

The elastic response function $T^{(e)}(\lambda)$ can be of different forms. A linear stress–strain relationship can be assumed for strains up to about 30% while an exponential or a parabolic form is recommended for larger strains.[4]

The reduced relaxation function, $G(t)$.

With the feature of strain rate independency, a reduced relaxation function of the form:[7]

$$G(t) = \alpha \ln(t) + \beta \qquad [7.13]$$

with $\alpha = -\dfrac{c}{1 + c\ln\left(\dfrac{\tau_2}{\tau_1}\right)}$ and $\beta = -\dfrac{1 - c\gamma + c\ln(\tau_2)}{1 + c\ln\left(\dfrac{\tau_2}{\tau_1}\right)}$

where c, γ, τ_1 and τ_2 are constants with, $\tau_1 \le t \le \tau_2$, has been commonly employed in the quasi-linear viscoelastic theory to incorporate the continuous relaxation spectrum of hysteresis (Fig. 7.4). The two ends of the spectrum, marked by frequencies τ_1^{-1} and τ_2^{-1} define two characteristic times τ_1 and τ_2 which can be determined from experimental data. The quasi-linear viscoelastic theory has been widely applied to characterize the viscoelastic behavior of various soft tissues, including the muscle, ligament and tendon structures.[4]

7.3.4 The poroelastic model of soft tissues

The phenomenon of viscoelasticity can be classified as flow-dependent or flow-independent. Flow-dependent viscoelasticity is the result of the

interaction between the solid matrix of the tissue and the interstitial fluid, whereas the flow-independent viscoelasticity is the result of the intrinsic viscoelastic tissue behavior. The characteristic of flow-dependent viscoelasticity of soft tissue can be described by a poroelastic or a biphasic model.

In the poroelastic model, the diffusive interaction between the solid matrix and the interstitial fluid is assumed to be the sole source of the viscoelastic phenomenon of the tissue in the so-called flow-dependent viscoelasticity. The development of the poroelastic model was based on a consolidation theory introduced by Biot[9] for analyzing the mechanical behaviour of soil structures. This consolidation theory, also known as the poroelastic theory, defined a structure as a porous media consisting of an elastic solid matrix with interconnected fluid saturated pores. A biphasic model for describing the mechanical behavior of soft tissue was introduced by Mow *et al.*,[10] which is based on theory of mixtures.[11] The biphasic theory assumes that tissue is a mixture of two distinct constituents, an incompressible fluid phase (interstitial water) and an incompressible porous solid phase (PG, collagen, and other minor protein molecules). The biphasic model has been recognized to simulate the role of the interstitial fluid in the mechanical behavior of articular cartilage. In the linear biphasic theory, it is assumed that the fluid phase is inviscid and that the solid phase is linearly elastic. The overall viscoelastic behavior of the tissue is mathematically modeled in terms of the diffusive momentum exchange between the fluid phase and the porous solid phase and is dependent on the permeability of the tissue matrix. All of the material parameters, such as the volume fraction of each constituent, permeability, and elastic moduli, are assumed to be constant and independent of tissue deformation. This biphasic theory used a similar approach to that of the poroelastic theory in analyzing the porous media. The poroelastic model of Biot[9] differs from the biphasic model[10] in that the latter does not take into account the compressibility of the individual constituents. The biphasic and poroelastic models are basically the same provided that the described porous media consisted of incompressible elastic solid matrices saturated with an incompressible Newtonian fluid.

A poroelastic model of skin subcutaneous tissue was built by Mak *et al.*[12] to study the effects of epidermal loadings on pressure sores. A layer of skin and subcutaneous tissue on a bony substratum was modeled as a homogeneous layer of biphasic material with uniform thickness. The epidermal surface and the bony interface were taken to be impervious. The cases for surface pressure loadings and displacement-controlled indentations were simulated and the transient tissue response of hydrostatic pressure and tissue compaction were analyzed. The model provided an overview on how various materials, and geometric and loading parameters can affect the transient biomechanical responses of a layer of skin and subcutaneous tissue on a bony substratum; in particular, the hydrostatic pressure build-up

within the tissue and the subsequent tissue compaction as the fluid gradually moves away from the loaded area.

The biphasic model has been extended to include nonlinear behaviors such as strain-dependent permeability and finite deformation.[13–16] Identifying the intrinsic viscoelastic effect on the dynamic behaviour of articular cartilage, Mak[17,18] introduced the poroviscoelastic theory, which took into account the intrinsic viscoelasticity of the solid matrix based on the biphasic theory. Lai *et al.*[19] presented an extended version of the theory, called the triphasic model, to include the dissolved solute concentration, which is known to be responsible for the osmotic pressure and swelling effect of soft tissue.

7.4 References

1. Black, J. and Hastings, G. (1998). *Handbook of Biomaterial Properties*, Chapman & Hall.
2. Elsner, P. (2002). *Bioengineering of the Skin: Skin Biomechanics*, Boca Raton, Fla.: CRC Press.
3. Lanir, Y. (1987). Skin mechanics. In: *Handbook of Bioengineering*, Chapter 11, New York: McGraw-Hill,.
4. Maurel, W. (1998). *Biomechanical Models for Soft Tissue Simulation*, Berlin; New York: Springer-Verlag.
5. Fung, Y.C. (1993). *Mechanical Properties of Living Tissues*. 2nd Edition, New York: Springer-Verlag.
6. Lockett, F.J. (1972). *Nonlinear Viscoelastic Solids*, London, New York: Academic Press.
7. Fung, Y.C., Perrone, N. and Anliker, M. (1972). *Biomechanics: Its Foundations and Objectives*. Englewood Cliffs, N.J: Prentice-Hall.
8. Christensen, R.M. (1971). *Theory of Viscoelasticity; an Introduction*, New York: Academic Press.
9. Biot, M.A. (1941). General theory of three-dimensional consolidation. *J Applied Physics*, **12**, 155–64.
10. Mow, V.C., Kuei, S.C., Lai, W.M. and Armstrong, C.G. (1980). Biphasic creep and stress relaxation of articular cartilage in compression: Theory and experiments. *J Biomech Eng,* **102**, 73–84.
11. Truesdell, C. and Toupin, R. (1960) *The Classical Field Theories, Handbuch der Physik III/I*, Berlin: Springer-Verlag.
12. Mak, A.F., Huang, L. and Wang, Q. (1994). A biphasic poroelastic analysis of the flow dependent subcutaneous tissue pressure and compaction due to epidermal loadings: issues in pressure sore. *J Biomech Eng* **116**, 421–9.
13. Holmes, M.H. (1986). Finite deformation of soft tissue: analysis of a mixture model in uni-axial compression. *J Biomech Eng*, **108**, 372–81.
14. Holmes, M.H. and Mow, V.C. (1990). The nonlinear characteristics of soft gels and hydrated connective tissues in ultrafiltration. *J Biomech*, **23**, 1145–56.
15. Kwan, M.K., Lai, W.M. and Mow, V.C. (1990). A finite deformation theory for cartilage and other soft hydrated connective tissues – I. Equilibrium results. *J Biomech*, **23**, 145–55.

16. Lai, W.M., Mow, V.C. and Roth, V. (1981). Effects of nonlinear strain-dependent permeability and rate of compression on the stress behaviour of articular cartilage. *J Biomech Eng*, **130**, 61–6.
17. Mak, A.F. (1986). The apparent viscoelastic behaviour of articular cartilage – the contributions from the intrinsic matrix viscoelasticity and interstitial fluid flows. *J Biomech Eng*, **108,** 123–30.
18. Mak, A.F. (1986). Unconfined compression of hydrated viscoelastic tissues: a biphasic poroviscoelastic analysis. *Biorheology*, **23**, 371–83.
19. Lai, W.M., Hou, J.S. and Mow, V.C. (1991). A triphasic theory for the swelling and deformation behaviours of articular cartilage. *J Biomech Eng*, **113**, 245–58.

8

Contact mechanics in wearing garments

X-Q. DAI[1,2], Y. LI[1] AND X. ZHANG[3]
[1]The Hong Kong Polytechnic University, China
[2]Soochow University, China
[3]Xian University of Engineering Science & Technology, China

8.1 Introduction

The biomechanical functional performance of garments and devices is determined by the mechanical interactions between clothes and the human body during wear in static and/or dynamic situations. Therefore, how to treat the contact mechanics at the cloth–skin interfaces is critical for establishing scientific understanding and knowledge for the purpose of biomechanical engineering. In this chapter, the techniques and processes developed in the area of contact mechanics in relation to biomechanical engineering are introduced and discussed.

8.2 Contact problems involved in garments

When a garment is worn on a human body, it takes the body shape and follows body movements. During the wearing, cloth deformation is mostly caused by its contact with the body. However, since cloth is a kind of soft and flexible material, it can easily bend and fold to contact itself, especially in free draping. Such self-collision is also an important aspect of the cloth contact problem.

While self-contact is a major determinant of the garment aesthetic appearance, the contact between cloth and the organic human body will have deep influence on the human body. The interaction between fabric and human skin will stimulate various sensory receptors in the skin and may cause uncomfortable feelings, such as tickle, prickle and abrasion of the skin. The pressures exerted on the body will not only affect the person's compression comfort feelings, they will influence physiological performance, such as blood circulation. So it is very important to simulate the geometric and mechanical interaction of cloth contact accurately in biomechanical engineering garment design.

In most garment simulation, the human body is modeled as a shell rather than a solid body. The contact between the body and cloth is usually

considered as a non-penetration geometric constraint rather than a mechanical interaction. A generalized approach is introduced to deal with the contact problem and to generate realistic contact response. In computer simulation, shell or solid objects are often described as polygonal or polyhedral meshes. However, these virtual objects do not occupy any real volume in space, and there is nothing preventing them from occupying the same volume in virtual space, so some collision management is necessary to enable objects to interact, preventing geometrical interference.

8.3 Contact mechanics

When two objects contact, the reaction forces oppose geometrical interpenetration while the friction forces prevent relative sliding. Therefore, dealing with contact involves two types of problems:

(i) collision detection: to find out the locations of geometrical contacts between objects;
(ii) collision response: to integrate the resulting reaction and friction effects in the mechanical simulation.

The two problems are different in nature: the former is essentially a geometrical processing whereas the latter is relevant to the mechanical modeling. They are addressed respectively in the following two sections.

8.3.1 Contact kinematics

Assume two elastic bodies, β^i, i = 1, 2, each occupying the bounded domain $\Omega^i \subset R^3$. The two bodies initially separate from each other. When they come into contact, both of them get deformed and contact at a boundary due to the contact response. Within the contact boundary, the point x^1 in β^1 comes in contact with the point x^2 in β^2, and n^1 denotes the normal of the contact surface at point x^1. In the contact area, constraint equations or the approach function for normal contact have to be formulated, as well as the kinematical relations for the tangential contact.[1]

Normal contact of 3D bodies

As the two bodies come into contact, there are two cases for the contact condition: non-penetration, and a small penetration allowed. Once the point x^1 in contact with x^2 is known, an inequality constraint for the first case can be defined:

$$g_N = (x_2 - x_1) \cdot n^1 \geq 0;$$

or a penetration function for the second case:

$$g_N = \begin{cases} (x^2 - x^1) \cdot n^1 & \text{if } (x^2 - x^1) \cdot n^1 < 0 \\ 0 & \text{otherwise} \end{cases}.$$

Two main techniques can be followed to impose contact conditions in the normal direction. One is the formulation of the non-penetration as a purely geometrical constraint; the normal contact stresses then follow from the constraint equation. And another is the development of an elastic or elasto-plastic constitutive law for the micromechanical approach within the contact area, which yields a response function for the normal contact stresses.

The purely geometrical constraint for the non-penetration can be stated as:

$$g_N \geq 0,\ p_N \geq 0,\ p_N g_N \geq 0.$$

Here, p_N, contact pressure, is the force acting on both surfaces in the normal direction, which obeys the action–reaction principle. For contact, there is $g_N = 0$, and $p_N < 0$. If there is a gap between the bodies, then the relation becomes $g_N > 0$, and $p_N = 0$.

The micromechanical approach takes account of the roughness of the body surface. The mechanical behavior depends in general upon material parameters, such as hardness, and on geometrical parameters, such as surface roughness. Then, the contact pressure can be formulated as:

$$p_N = f(d),$$

where, f is a nonlinear function of the current mean plane distance d. The distance d is related to the geometrical approach g_N, via the relation: $g_N = \zeta - d$ as illustrated in Fig. 8.1.

Tangential contact of 3D bodies

In the tangential direction of the contact interface, there are generally two cases needing to be distinguished: the first is the 'stick state', in which a point that is in contact is not allowed to move in a tangential direction; the second is 'sliding', which means that a point moves in a tangential direction

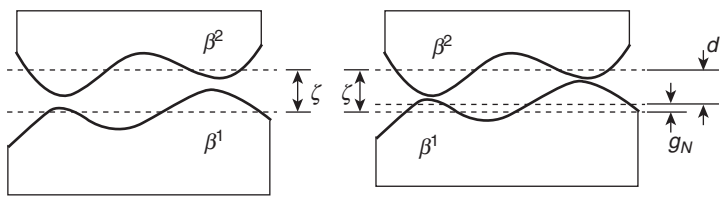

8.1 Physical approach of two bodies.

in the contact interface. The constraint for the 'stick state' can be formulated as: $g_T = 0$, where g_T denotes the relative displacement in a tangential direction. Once the tangential forces are above a certain limit, then the contacting surfaces no longer stick to each other, but move relative to each other. The 'sliding' is usually described by the law of Coulomb:

$$t_T = -\mu |p_N| \frac{g_T}{\|g_T\|}, \quad \text{if} \quad \|t_T\| > \mu |p_N|,$$

where μ is the sliding friction coefficient. The coefficient is a constant in the classical Coulomb law, depending on the material pairing of the solids in contact.

Formulation of contact constraints

The Lagrange multiplier method and the Penalty method are mostly often used to formulate the contact constraints. The Lagrange multiplier method is usually used for the non-penetration contact interface. If contact is active at the surface Γ_c, it adds a contact contribution to the weak form of the system as:

$$\Pi_C^{LM} = \int_{\Gamma_C} (\lambda_N g_N + \lambda_T \cdot g_T) \mathrm{d}A,$$

where λ_N and λ_T are the Lagrange multipliers and λ_N can be identified as the contact pressure P_N. The Penalty method is often used for the contact condition where penetration is allowed. A penalty term due to the penetration is added to the weak form of the system:

$$\Pi_C^P = \frac{1}{2} \int_{\Gamma_C} \left(e_N (g_N)^2 + e_T g_T \cdot g_T \right) \mathrm{d}A, e_N, e_T > 0.$$

Here, e_N and e_T represent the penalty parameters. There are several other variants for the formulation of the normal contact constraint detailed in reference 1.

8.4 Contact detection

Contact takes place between the surfaces of objects. In computer terms, a surface is usually described by polygonal meshes. So the contact detection is carried out between polygonal meshes that may have thousands of polygons. The main problem is to master the computational complexity due to the discretization. Testing each pair of polygons for potential collisions is tremendous work and it is inefficient. Some complexity reduction techniques are necessary in collision detection. There are many different solutions that have been proposed, relying on the geometrical context and situation considered.

Another problem involved in collision detection is that the exact contact locations on the objects are necessary for simulating realistic collision response, which includes preventing geometric interpenetration and generating mechanical interaction. So, to characterize contact geometrically is also an important part in collision detection. It is often a more complicated geometric process compared to just detecting whether two objects are colliding.

8.4.1 Various collision detection techniques

Bounding volumes

As a basic idea for complexity reduction, preliminary collision tests can be performed between simplified bounding volumes containing the complex objects to be tested. A bound volume is a geometric primitive that may contains a group of objects, a complex object, a group of primitives, or just a single polygon. Its construction should be simple and straightforward. Various bounding volumes can be considered, each of them having its own merits and weaknesses. Among them, the most common are bounding boxes, usually axis-oriented, and bounding spheres.

An axis-oriented bounding box is characterized by six parameters describing the minimal and maximal coordinates of the contained objects, as illustrated in Fig. 8.2. They are easy to build, merge, and detect collision with; only linear geometrical calculation is involved. A bounding sphere is described by four parameters: the center coordinates and the radius. They are difficult to build and merge since complex, non-linear geometrical calculations are needed to find the optimal position of the center, but their description is very compact and collision detection is very easy to carry out.

Prior to performing collision detection with the objects contained by the volume, simple and fast collision detection is performed between the volumes. Further detection is carried out only if the volumes intersect. Usually, the

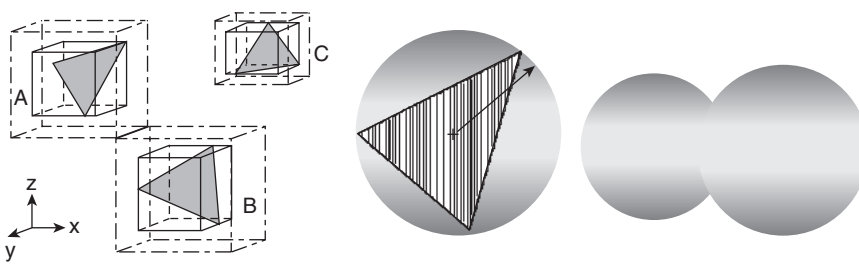

(a) Bounding box (b) Bounding sphere

8.2 Bounding volume.

volume collision detection is integrated to a hierarchical technique. Volume collision detection is performed among bounding volumes of higher level, and further detection among bounding volumes of lower level is carried out only if intersection is detected. Other more complicated bounding volumes aim to optimize the filling efficiency, i.e. to reduce the empty space so that the volume collision may be more representative of the collisions of the contained objects, and be able to describe more complicated shapes.

Axis projection methods

If objects are geometrically colliding, their projections are intersecting. This consideration allows us to carry out quick collision detection in spaces of reduced dimensions. As illustrated in Fig. 8.3, objects are usually projected onto the coordinates. Each object is represented by the intervals on the three axes. Two objects are likely to collide if all three intervals collide with each other, respectively. Here, only a simple interval interference algorithm is needed. Efficient sorting methods can also be implemented for ordering and sorting the intervals along the axes, and detecting the potential for colliding quickly. The technique becomes particularly efficient when integrated with the axis-oriented bounding box technique. Cohen *et al*. used this technique in their collision detection system.[2]

Space subdivision methods

Space subdivision methods are based on a consideration that objects geometrically close to each other are likely to collide. It divides the space into regions and maintains a group of objects contained in each region. Then, the collision detection is performed only between the objects sharing a common region. There are two major methods to divide the space: grid subdivision and hierarchical subdivision.

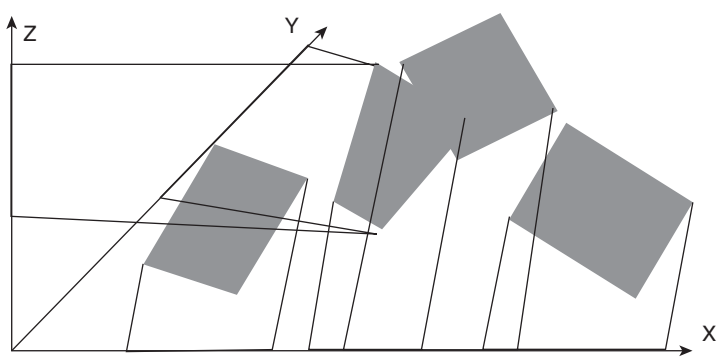

8.3 Projecting objects onto axes.

Grid subdivision divides the space into a regular array of boxes, called voxels, as illustrated in Fig. 8.4a. How to choose the voxel size is the main issue of the method. If the voxel is too large, too many objects may be contained in a same voxel; if it is too small, there will be too many voxels to realize efficient collision detection. The optimal discretization depends on the choice of the collision detection algorithm, the number of objects, and their size and motion. More complicated techniques can be progressive or dynamic grids.

Regular grid subdivision lacks the adaptability to the shapes and geometrical characteristics of objects. The common way to improve the subdivision is to implement a local refinement adapted to the objects' geometrical features, to obtain a hierarchical subdivision. Hierarchical is also the best algorithm technique for improving algorithm efficiency. Octree is the usual hierarchical scheme for space subdivision. As illustrated in Fig. 8.4b, each space box is divided into eight equal sub-boxes by using the three axis-aligned planes at the center of the box. An octree can describe any volume contained in the space at a given resolution represented by the maximal depth of the octree structure. The nodes in an octree structure have three states: *full*, if the corresponding space is contained in the object; *empty* if there is no intersection between the corresponding space volume and the object; *partial* if there is partial intersection. Among the three cases, only in the third one and only if the volume size is bigger than the given resolution, is the space further subdivided in the next step.

The overlap detection between the octree structures is quite simple. Starting from the whole scene, if there is *full–full* or *full–partial* overlap, collision is detected and the test stops; if *partial–partial* overlap occurs, potential collision is detected and further tests on the deeper level are necessary; if there is no overlap, no collision is detected and the test can stop at this level. Meager[3] and Chen and Huang[4] have good descriptions of octree construction.

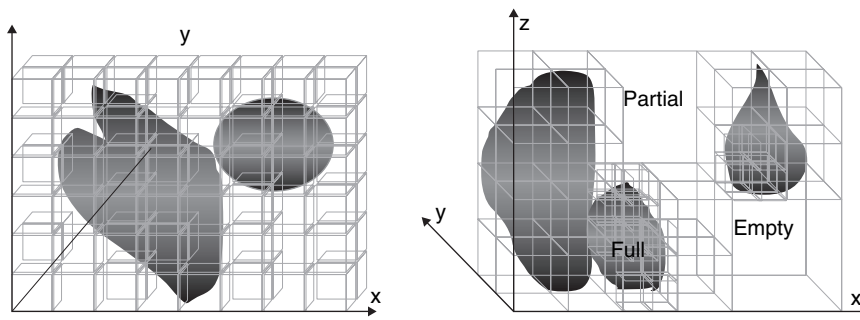

(a) Grid subdivision (b) Hierarchical subdivision

8.4 Space subdivision.

Object subdivision methods

A big problem of the hierarchical space subdivision algorithm is the difficulty of updating the structure efficiently as the objects move. To overcome this problem, one approach is to build the hierarchical structure on the objects themselves rather than based on the time-dependent space. Thus, the hierarchies can be very simply updated as objects move. This approach is only suitable for objects with constant topological structures. Fortunately, both the human body and clothing (deformable surfaces) meet this requirement.

The most common implementation of the object hierarchy technique groups several objects and performs successive tests using the bounding boxes containing the considered groups. If one group collides, collision detection will be performed for the children groups. This process is continued, progressively, until 'no collision' or 'sure collision' is announced for each bounding box. In references 5 and 6 bounding box hierarchy trees are constructed on the objects and dynamically updated as the objects move. Bounding sphere hierarchies are considered in references 7 and 8 for collision detection in animation.

To build an object hierarchy tree efficiently is quite difficult. An efficient tree should have minimum depth, while each tree node of it should correspond to a group of objects being as close as possible to each other in order that the bounding box test will be relevant. As objects move, it may be necessary to change the hierarchy organization using some incremental tree-manipulation techniques to reflect the vicinity changes among objects.

Proximity tracking techniques

An intuitive way for optimized collision detection is to detect collisions only among objects being close to each other. A 'vicinity map' can be built for the whole objects and be updated as objects move, using some computational geometrical techniques. Voronoi domain can be a good choice for this purpose. Figure 8.5 shows a 2D Voronoi domain. A Voronoi domain associated to an object consists of the space points that are closer to it than other objects. Voronoi domain for a group of objects can also be built using some specific techniques. For simplification, bounding spheres can be used instead of the objects themselves in the Voronoi domain calculation. Collision detection is only carried out between objects in neighbored domains. The major difficulty of this algorithm is to update the domains and their neighboring connectivity as objects move around.

A simple variation of the proximity tracking approach is to track the closest distance between bounding spheres containing grouped objects. The

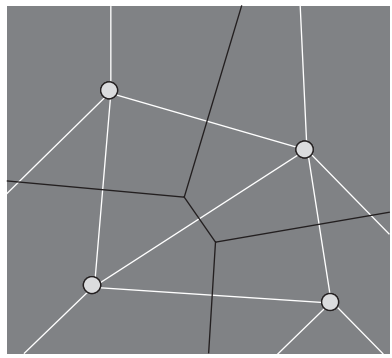

8.5 2D Voronoi domain.

neighborhood can also be roughly determined based on the hierarchical structures. To track the contact efficiently, many Finite Element Analysis software packages use hierarchical global/local search algorithms. For example, in the Finite Element (FE) package ABAQUS (Hibbitt, Karlsson & Sorensen, Inc., USA), a global search determines the globally nearest surface facet for each slave node in a given contact pair. A bucket sorting algorithm is used to minimize the computational expense of this search. A local contact search tracks the motion of a slave node along the nearest facets on the master surface.[9]

Collision detection on polygonal meshes

Both cloth and human body surfaces involved in clothing simulation are usually described in terms of polygonal meshes. By considering each polygon element as an individual primitive, the previously introduced techniques can be applied to the collision detection on polygonal meshes. Actually, the relatively fixed topology of a polygonal mesh is helpful for building a hierarchical tree for a surface. Then the collision detection is to find all the pairs of polygons in contact. For collision between a human body surface and a cloth surface, a 'pair' refers to a polygon on the body surface and a polygon on the cloth surface. However, there will be a big difference for the case of cloth self-collision.

Generally, there is no essential difference between a collision detection between two different objects and that within a single object since, in both cases, groups of elements have to be tested for collisions. Cloth self-collision detection can be performed in a similar way to the body–cloth collision detection. However, some specific algorithm to remove any relevant collisions such as an element colliding with itself is necessary. Collision detection on polygonal meshes has to find all the pairs of polygons in contact. Since

each polygon is naturally adjacent to a certain set of neighbor polygons on a polygonal mesh, these polygons will be detected as collision. Collision detection should not be triggered by these adjacencies and collision should only be tested between polygons that are not topologically in contact in the mesh structure.

Volino *et al*. developed a collision detection algorithm based on a hierarchical bounding-box scheme for polygonal meshes.[10] A hierarchy tree consisting of successive subdivisions of the entire surface is built, taking advantage of the structural continuity of the polygonal description. A node of the hierarchical tree represents a surface region containing a certain number of polygonal elements. Starting from the root of the hierarchy representing the entire surface, the children nodes are recursively built by successively subdividing the surface region of a parent node. Finally, the leaf nodes of the tree are the individual polygons of the surface. A bounding box hierarchical structure is built associated with the tree nodes. Collision detection is performed by testing the bounding box contact between two nodes. If there is a contact, the test is continued by recursively testing the children nodes. The algorithm yields pairs of polygon elements whose bounding boxes are colliding.

This algorithm is optimized for self-collision detection by using the surface curvature evaluation within surface regions defined by the hierarchy tree. As illustrated in Fig. 8.6, the self-collision in (a) can be detected by a standard intersecting test between two bounding boxes, while the collision in (b) within a bounding box cannot be detected in the same way. Further self-collision within a bounding box seems necessary. However, it is not necessary to perform a self-collision test for each leaf bounding box.

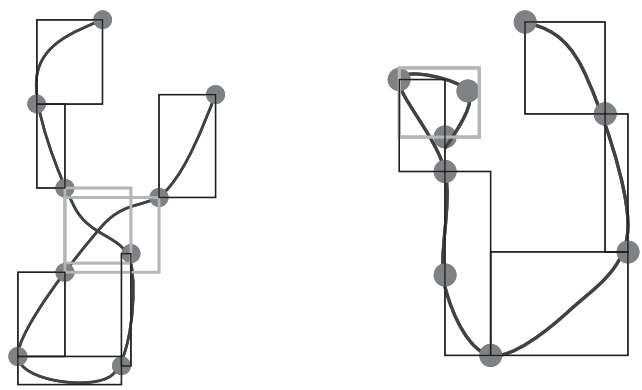

(a) Standard intersecting test (b) Within a bounding box test

8.6 Self-collision detection.

A flat surface cannot have self-collisions. Only if a surface folds is it likely to collide with itself. The curvature of the small piece of surface contained in the bounding box can be the key for achieving efficient self-collision detection. If proper curvature criteria can be set, then self-collision detection within a bounding box is performed only if the corresponding curvature is smaller than the criteria.

A detailed overview of collision detection techniques has been given by Volino and Thalmann in reference 10.

8.4.2 Characterizing collision geometrically

Most of the collision detection algorithms return a bunch of polygon couples that are geometrically close enough to be considered contact. Some further specific process is needed to judge if the pair of polygons are really in contact. If yes, the clear geometrical state of the contact is calculated and is then integrated into collision response. Depending on the application and the response type, two major kinds of contact are often considered:

(i) Penetrations: Objects are penetrating each other. In the case of surfaces, the two colliding surfaces are crossing each other.
(ii) Proximities: Objects are considered colliding when their closest distance becomes less than a given threshold.

Penetration judgment

For polygonal meshes, penetration detection is performed between polygon and polygon. However, it is often simplified as penetration between vertex and polygon. For two objects separated initially, it seems enough to avoid penetration. However, there are some exceptions that cannot be covered by vertex/polygon, as shown in Fig. 8.7, where $P_{a1}(t)$ and $P_{a2}(t)$ denote the positions at time t of two vertices of an edge on object A; $P_{a1}(t + \Delta t)$ and $P_{a2}(t + \Delta t)$ denote the respective predicted positions after a time interval of Δt. In these cases, the two vertices have not penetrated any polygons, but the two objects A and B do cross each other. It can be considered that the edges a_1a_2 and b_1b_2 penetrate each other. To address such problems, penetration detection between edge and edge should be performed in additional to vertex/polygon penetration.

Vertex/triangle has been taken as an example to describe the processing of vertex/polygon penetration detection. Figure 8.8 illustrates the penetration between a vertex on object A and a triangle on object B, where $P_a(t)$ denotes the position of the vertex of A at time t, $P_a(t + \Delta t)$ denotes its predicted position after a time interval of Δt, and $P_{b0}(t)P_{b1}(t)P_{b2}(t)$ represents the position of the triangle at time t. If the line $P_a(t)P_a(t + \Delta t)$ intersects the

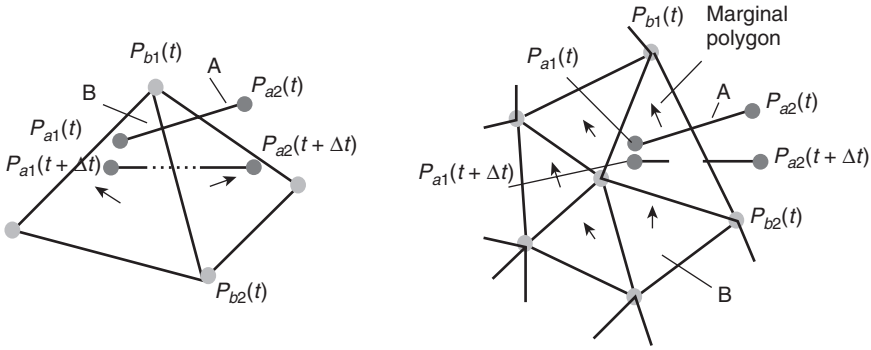

(a) Convex edge (b) Boundary edge

8.7 Edge/edge penetration.

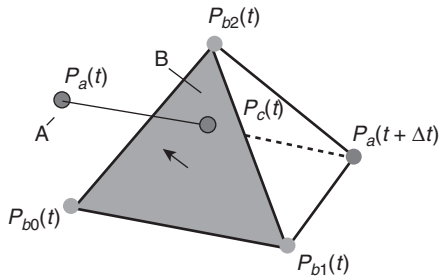

8.8 Vertex/triangle penetration.

triangle, then the vertex of object A is determined to be colliding with the triangle. Whether a line intersects a triangle or not can be judged by using a Euclid 4×4 determinant defined as the following equation:

$$S_{a(t)012} = \begin{vmatrix} x_{a(t)} & y_{a(t)} & z_{a(t)} & 1 \\ x_0 & y_0 & z_0 & 1 \\ x_1 & y_1 & z_1 & 1 \\ x_2 & y_2 & z_2 & 1 \end{vmatrix}.$$

Here, $x_a(t)$, $y_a(t)$, $z_a(t)$ and so on denote the coordinates of the vertex of A at time t and the vertices of the triangle, and $S_{a(t)012}$ is actually the volume of the polyhedron formed by these four vertices. If the vertex locates at the right side of the triangle, $S_{a(t)012}$ is positive and if the vertex locates at the back side of the triangle, $S_{a(t)012}$ is negative. And if the four vertices locate on the same plane, $S_{a(t)012}$ equals zero. Using these characteristics of the equation, it can be judged whether a line intersects a triangle. If either of the following two sets of equations is satisfied, the vertex intersects the triangle.[11]

$$S_{a(t)012}S_{a(t+\Delta t)012} \le 0 \cap S_{a(t)012} \ge 0 \cap S_{a(t)a(t+\Delta t)01} \ge 0 \cap S_{a(t)a(t+\Delta t)01} \ge 0 \cap S_{a(t)a(t+\Delta t)12} \ge 0 \cap S_{a(t)a(t+\Delta t)20} \ge 0,$$

$$S_{a(t)012}S_{a(t+\Delta t)012} \le 0 \cap S_{a(t)012} \le 0 \cap S_{a(t)a(t+\Delta t)01} \le 0 \cap S_{a(t)a(t+\Delta t)01} \le 0 \cap S_{a(t)a(t+\Delta t)12} \le 0 \cap S_{a(t)a(t+\Delta t)20} \le 0.$$

Furthermore, the position of the contact point on the triangle can be calculated as:

$$P_c(t) = P_a(t) + \frac{S_{a(t)012}}{S_{a(t)012} - S_{a(t+\Delta t)012}} \times (P_a(t+\Delta t) - P_a(t))$$

Edge/edge penetration detection can be converted to a line and triangle intersecting problem. In Fig. 8.7, whether the edge $P_{a1}(t)P_{a2}(t)$ is colliding with the edge $P_{b1}(t)P_{b2}(t)$ depends upon whether the edge $P_{a1}(t + \Delta t)P_{a2}(t + \Delta t)$ intersects the two triangles for the case in Fig. 8.7a or the one triangle for the case in Fig. 8.7b connecting to the edge $P_{b1}(t)P_{b2}(t)$. Then the above mentioned approach can be applied.

Proximity judgment

Proximities are represented by the two 'closest distance' points on the elements of the two objects, which can be vertices, edges or polygons. Figure 8.9 illustrates the proximity domains for vertex, edge and polygon. Among the combinations of possible elements involved in the proximities, a collision is set up if both contact points are inside the respective proximity regions, and collision response processing is followed. The possible collision combinations include vertex/vertex, vertex/edge, edge/edge, vertex/polygon, and edge/polygon. Full proximity detection on all the element combinations generates a very dense collision network that can be appreciable for an accurate response simulation. The computational cost is extremely high.

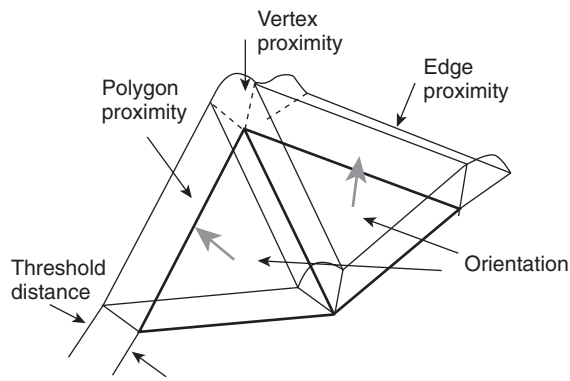

8.9 Proximity domain for vertex, edge and polygon.

However, it is not necessary to carry out all these types of collision detections. The geometrical characteristics of the polygonal meshes can be used to avoid extra processing. A vertex or an edge can be classified as convex or concave as illustrated in Fig 8.10. In cloth simulation, proximities for polygons are always considered. The detection of proximities for concave vertices and edges are covered by the polygon proximities, so they can be omitted. Therefore, edge/edge proximity detection, only for the convex edges, together with the polygon proximity detection, yielding a lighter collision network, is suitable for rapid processing.

In many Finite Element Method (FEM) software packages, the contact is often defined between a 'master' surface and a 'slave' surface, and the penetration detection is then performed between a slave node and a master polygon. A clearance is set; if the distance between the node and the polygon is smaller than the clearance, the two elements are considered in contact.

8.5 Contact response

Once two objects are detected to be interacting, 'feedback' should be performed on their behavior. Collision response aims to visualize the interaction in an accurate way: to avoid interpenetration of the objects and to simulate the bouncing and effects.

8.5.1 Collision on polygonal meshes

In a polygonal mesh, a collision means an interaction between two elements; and each element can be a vertex, an edge, or a polygon. The collision

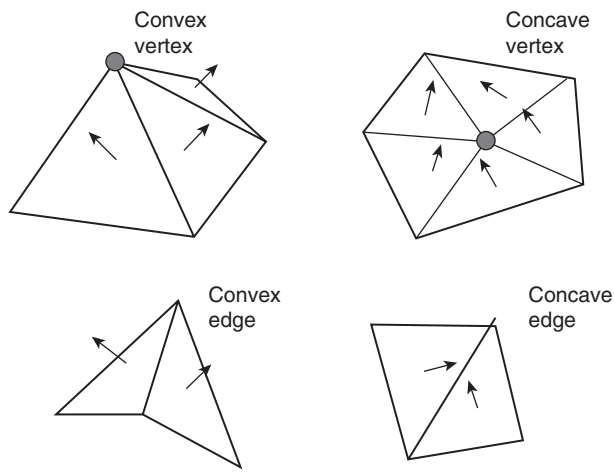

8.10 Characteristics of vertex and edge on polygonal meshes.

itself is applied on specific geometrical locations of the two elements; a pair of contact points. Then a collision is usually identified by both the contact points and a collision distance separating them. A contact point, which may often not be a vertex, can be described by its mass coordinate from the vertices defining the polygon element to which it belongs. Once the position of the contacted point is detected, its area coordinate can be computed using simple geometry. In Fig. 8.11, the area coordinates of the point P_a can be calculated using the following equations:

$$r_{a0} = S_{\Delta P_a P_{a1} P_{a2}} / S_{\Delta P_{a0} P_{a1} P_{a2}},\ r_{a1} = S_{\Delta P_a P_{a2} P_{a0}} / S_{\Delta P_{a0} P_{a1} P_{a2}},\ r_{a2} = S_{\Delta P_a P_{a0} P_{a1}} / S_{\Delta P_{a0} P_{a1} P_{a2}}.$$

As the mesh vertices carry the state of the object position, velocity and acceleration, collision effects need to be distributed on the vertices supporting the colliding elements. Again the area coordinates are used to obtain a linear interpolation.

As for any mechanical interaction, collision interaction obeys some mechanical conservation laws. The major law is the action–reaction equality, which states that the pair of forces exerted on the two objects are exactly opposite. To translate a mechanical response into a geometric effect, it will go through the division by the object mass, where Newton's second law is obeyed. To take the friction effect during contact into account, the Coulombian friction model, which considers a friction force proportional to the normal reaction force and with the direction opposed to the relative sliding speed, is often used.

There are two main approaches for handling collision response:

(i) mechanical reaction: the collision response is simulated by forces or by force adjustments that reproduce the contact effect;
(ii) geometrical reaction: the collision response is simulated by direct corrections on the positions and velocities of the objects.

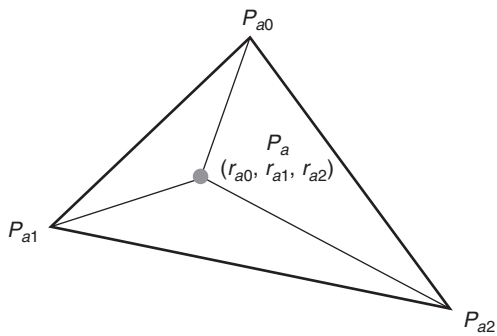

8.11 Area coordinate representation of a point within a triangle.

8.5.2 Mechanical response

The mechanical approach is the most formal way of handling collision response. The forces or energetic contributions generated from the response can be directly integrated into the mechanical model of cloth, and simulated. Collision penalty force or impulse is often employed to simulate the collision behavior. The function for the penalty force is usually designed as a continuous function of collision distance or as a piecewise function using simple linear or polynomial intervals. The penalty force, which acts on the contact point, needs to be distributed to the vertices of the polygon element. A suitable way to perform this response repartition is to use a linear interpolation. The penalty force approach is mostly used in the continuum cloth model, especially in many FEM software packages.

Baraff[12] introduced a non-penetration constraints approach based on rigid body motion to compute the contact forces between contacting bodies.[13] Although neither the cloth nor the human body is rigid, at the colliding moment the elements involved in the collision, which are of small size compared to the dimension of the whole piece of cloth, can be handled as a rigid body. This approach is adaptable for discrete cloth models.

Figure 8.12 shows a particle of object A colliding with a triangle of object B. A particle is imagined existing on the triangle at the contact point B for collision response calculation. The relative velocity between the particles A and B can be obtained as: $v_{rel}^{-} = \hat{n}(t) \cdot (\dot{P}_a^{-}(t) - \dot{P}_b^{-}(t))$. Here, $\hat{n}(t)$ denotes the normal of the triangle, the superior '·' denotes the first order derivative, and we use the superiors '–' and '+' to identify the states of pre-colliding and post-colliding. Depending on this velocity, the contact can be classified as: separating ($v_{rel}^{-} > 0$), resting ($v_{rel}^{-} = 0$), and colliding ($v_{rel}^{-} < 0$). Here the colliding contact is focused on and the impulse is calculated.

To avoid inter-penetration in a colliding contact, a vector quantity J, called an impulse and having the units of momentum, is postulated. To

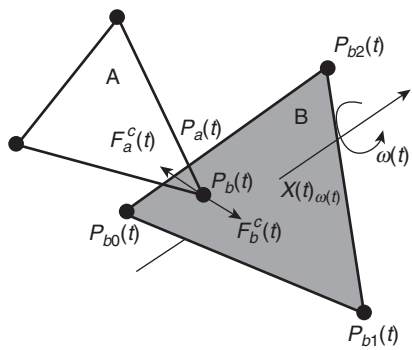

8.12 Vertex/triangle collision.

determine the effect of J, a large force $F_a^C(t)$ is imagined to act on the vertex of A for a small time interval Δt. For frictionless collision, the direction of J will be in the direction of $\hat{n}(t)$, and J can then be described as: $J = F_a^C(t) \cdot \Delta t = j\hat{n}(t)$, where j is the magnitude of J, to be computed. The impulse will change the velocities of the two objects as described in the following equations:

$$\begin{cases} \dot{P}_a^+(t) = \dot{P}_a^-(t) + j\hat{n}(t)/M_a \\ \dot{P}_b^+(t) = \dot{P}_b^-(t) - j\hat{n}(t)/M_b \end{cases}.$$

Here, M_a and M_b denote the mass of particles A and B. The relative velocity between the two colliding particles in the normal direction of the triangle can be described as: $v_{rel}^+ = \hat{n}(t) \cdot \dot{P}_a^+(t) - \dot{P}_b^+(t)$. According to the empirical law for frictionless collision, there are: $v_{rel}^+ = -ev_{rel}$. Here e, called the coefficient of restitution, must satisfy $0 \le e \le 1$. It is usually determined empirically depending on the materials of the colliding objects. Consequently, j can be obtained from the above equations as: $j = \dfrac{-(1+e)v_{rel}^-}{1/M_a + 1/M_b}$.

This impulse acts at the point B, which may often not be the mass center of the triangle, $X(t)$, and will produce an impulsive torque: $\tau_{impulse} = (P_b(t) - X(t) \times J)$. The impulsive torque gives a change in the angular momentum of the triangle ($\Delta L = \tau_{impulse}$), producing a change in angular velocity: $I^{-1}(t)\tau_{impulse}$. Here, $I(t)$ is the inertia tensor, describing how the mass in a body is distributed relative to the element's center of mass. It depends on the orientation of a body, and can be calculated as: $I(t) = R(t)I_{element}R(t)^T$. Here, $R(t)$ is the orientation matrix of the element at time t; and $I_{element} = \sum_{i=0}^{2} m_{bi}(r_{0i}^T r_{0i} I - r_{0i} r_{0i}^T)$ is a constant for a triangular element; r_{0i} denotes a vector from the mass center pointing to a vertex B_i in the triangle at the initial moment.

Since all the effects are taken into account in the same computation step, the resulting simulation by mechanical response approach produces an animation where collision and other mechanical forces add their effects in a compatible way. However, this approach may cause a calculation instability problem. Defining a very small 'response interval' in a small collision region implies the use of very strong and discontinuous reaction forces, which are difficult to simulate numerically. The mechanical response approach is also widely used in the continuum cloth model, especially in many FEM software packages.

8.5.3 Geometric collision response

The geometrical approach is to reproduce directly the effects of collision response on the geometrical state of the objects without making use of

mechanical forces. As mentioned previously, in polygonal meshes, collision often takes place between two elements, A and B, which can be vertices, edges, or polygons; the exact collision positions may locate at specific points, the contact points P_a and P_b. These points can be described by their linear/mass coordinates (r_{ai} and r_{bi}) from the vertices of the respective elements, P_{ai} and P_{bi} as follows:

$$P_a = \sum_i r_{ai} P_{ai}\,,\; P_b = \sum_i r_{bi} P_{bi}\,.$$

The other geometrical quantities for the contact points can be obtained in the same way. Generally, the geometrical collision response is considered to be the difference between the response of the two contact points, a geometrical quantity that can be distance, velocity or acceleration, $Q_{ab} = Q_a - Q_b$. Since it is a geometric value, the conservation laws have to consider the mass of the colliding objects, so the response distribution becomes more complicated. Here, the concept of inverse mass is often introduced. It will allow us to represent fixed and constrained objects as having a null inverse mass rather than an infinite mass. Given the mass M_{ai} for each vertex in the colliding polygon, then the inverse mass of the element A, M_a^{-1}, can be calculated as follows: $M_a^{-1} = \sum_i r_{ai}^{\,2} M_{ai}^{-1}$. Also, it is the same for the other element in contact B, $M_b^{-1} = \sum_i r_{bi}^{\,2} M_{bi}^{-1}$. Then according to conservation laws, the distribution of collision response between the two elements is as follows:

$$\Delta Q_a = \frac{-M_a^{-1}}{M_a^{-1} + M_b^{-1}} Q_{ab},\; \Delta Q_b = \frac{-M_b^{-1}}{M_a^{-1} + M_b^{-1}} Q_{ab}.$$

The response ΔQ_a is further distributed to each vertex of element A as: $\Delta Q_{ai} = \dfrac{-M_{ai}^{-1} r_{ai}}{M_a^{-1}} Q_{ab}$. And the same for ΔQ_b.

Geometrical constraints are directly enforced by a geometrical algorithm, and the simulation process is relieved from high intensity and high discontinuous forces or other mechanical parameters. This makes the simulation faster and more efficient. However, as the collision response changes the geometrical state of the objects separately from the mechanical process, nothing ensures the compatibility of this deformation to be a correct variation of the resultant mechanical state. Therefore, the resulting collision effects may be incompatible with mechanics. These issues have to be addressed for obtaining a collision model with acceptable and steady response.

Volino *et al.* developed an acceleration-based approach for collision response modeling. It performs corrections on position, speed and acceleration simultaneously, ensuring the response is more accurate.[14] Since

the reaction and friction are respectively modeled as a normal and tangent effect along the collision surface, the collision distance, speed and acceleration are decomposed into normal and tangent components as follows:

$$P_{ab}^{N} = P_b - P_a = P_{ab},\ P_{ab}^{T} = 0;$$

$$P_{ab}'^{N} = P_b' - P_a' = \frac{P_{ab}' \cdot P_{ab}}{P_{ab}},\ P_{ab}'^{T} = P_{ab}' - P_{ab}'^{N};$$

$$P_{ab}''^{N} = P_b'' - P_a'' = \frac{P_{ab}'' \cdot P_{ab}}{P_{ab}},\ P_{ab}''^{T} = P_{ab}'' - P_{ab}''^{N}.$$

Position correction is to alter the position of the colliding vertices so that the collision distance is maintained at a given contact distance P_0. The correction is: $P_{0\,ab}^{N} = P_0$.

Speed correction is to alter the speed P' of colliding vertices, ensuring that they will not continue moving toward each other, and further to control the bouncing effect of collision as well as friction effects. To reach the position of the given collision distance P_0 at the next frame, the speed correction should be: $P_{0ab}'^{N} = \frac{P_0 - P_{ab}^{N}}{\mathrm{d}t}$.

Acceleration correction is to alter the acceleration P'' of the colliding vertices so that the desired speeds can be maintained along with time. Given the desired position P and speed P' at the second next frame, the acceleration correction should be:

$$P_0''^{N}(t) = \frac{P_0 - P_{ab}^{N}}{\mathrm{d}t^2} - \frac{0.5P_0' + 1.5P_{ab}'^{N}}{\mathrm{d}t}.$$

The tangential speed and acceleration:

$$P_{0ab}'^{T} = \max\left(1 - \mu\frac{|P_{0ab}'^{N} - P_{ab}'^{N}|}{|P_{ab}'^{T}|}\right)P_{ab}'^{T}.$$

Then, the normal and tangential components are recombined as:

$$P_{0ab} = P_{0ab}^{N} + P_{0ab}^{T},$$

$$P_{0ab}' = P_{0ab}'^{N} + P_{0ab}'^{T},$$

$$P_{0ab}'' = P_{0\,ab}''^{N} + P_{0\,ab}''^{T}.$$

Finally, the corrections to be performed on the current geometrical values are as follows:

$$\Delta P_{ab} = P_{0ab} - P_{ab},$$

$$\Delta P_{ab}' = P_{0ab}' - P_{ab}',$$

$$\Delta P_{ab}'' = P_{0ab}'' - P_{ab}''.$$

8.6 Conclusion

In this chapter, the contact problems involved in simulation of garment construction and wearing have been introduced, including contact between the human body and garment, cloth self-collision, and the mechanical interaction between objects in contact. Various contact detection techniques were briefly reviewed, and also the approaches to characterize collision geometrically. Two major approaches (geometrical and mechanical) to enforce collision response were introduced.

8.7 Acknowledgement

We would like to thank Hong Kong Polytechnic University for funding this research through Projects A188 and G-YD31.

8.8 References

1. Wriggers, P., *Computational Contact Mechanics*. 2002: John Wiley & Sons, 45–91.
2. Cohen, J.D. *et al*., An Interactive and Exact Collision Detection System for Large-scale Environments. in Symposium of Interactive 3D Graphic Process, *ACM SIGGRAPH*. 1995.
3. Meager, D., Geometric Modeling Using Octree Encoding. *Computer Graphics and Image Processing*, 1982. **19**(2): p. 129–147.
4. Chen, H.H. and Huang, T.S., A Survey of Construction and Manipulation of Octrees. *Computer Vision, Graphics and Image Processing*, 1988. **43**(2): p. 409–431.
5. Webb, R.C. and Gigante, M.A., Using Dynamic Bounding Volume Hierarchies to Improve Efficiency of Rigid Body Simulations, in *Communicating with Virtual Worlds, CGI'92 Proceedings*. 1992.
6. Webb, R.C. and Gigante, M.A., Distributed, Multi-person, Physically-based Interaction in Virtual Worlds, in *Visual Computing, CGI'93 Proceedings*. 1993.
7. Hubbard, P.M., Approximating Polyhedra with Spheres for Time-Critical Collision Detection. *ACM Transaction on Graphics*, 1996. **15**(3): p. 179–210.
8. Palmer, I.J. and Grisdale, R.L., Collision Detection for Animation Using Sphere-trees. *Computer Graphics Forum*, 1995. **14**: p. 105–116.
9. Abaqus, V., Chapter 21 Defining Contact Interactions, in *Analysis User's Manual*. 2003, ABAQUS Inc., Pawtucket, RI, USA.
10. Volino, P. and Thalmann, N.M., Collision Detection, in *Virtual Clothing: Theory and Practice*. 2000, Springer. p. 103–144.
11. Yamagutsi, F., *Graphics and Forms Process Technique According to 4-dimensional Theory*. 1995. Nikkan Kougyou Shinbunsya, Japan. p. 301–328.
12. Baraff, D., Rigid Body Simulation, in Course Notes of *SIGGRAPH'98*. 1998.
13. Baraff, D., Rigid Body Simulation, in Course Notes of *SIGGRAPH'98*. 1998. p. D1–D68.
14. Volino, P. and Thalmann, N.M., Collision Response, in *Virtual Clothing: Theory and Practice*. 2000, Springer. p. 145–182.

9

Clothing comfort and compression therapy

Y. LI[1] AND X-Q. DAI[1,2]
[1]The Hong Kong Polytechnic University, China
[2]Soochow University, China

9.1 Clothing comfort

In the past, clothing was something that was kept going for as long as possible. Today, the main consumer purchasing considerations are good appearance and comfort. Comfort is being reinforced as a key parameter in clothing. However, comfort is a complex and nebulous subject that is very difficult to define. The Oxford English Dictionary defines comfort as 'freedom from pain, wellbeing'. Slater[1] defined comfort as 'a pleasant state of physiological, psychological and physical harmony between a human being and the environment'. Therefore, clothing comfort is a neutral sensation, when we are physiologically and psychologically unaware of the clothing we are wearing. There are physiologically and psychologically positive comfort sensations but these tend to be more individualistic and less frequently noticed when we are wearing a garment than discomfort sensations are. Discomfort, which occurs when we are unpleasantly conscious of the garments we are wearing, can be much more easily described in such terms as prickle, hot, and tight. Therefore, a widely accepted definition for comfort is 'freedom from pain and from discomfort as a neutral state'.[2]

Smith[3] pointed out that there are two major types of discomfort sensation: psychological discomfort, when the clothing we are wearing is inappropriate for us personally or for an occasion; and physiological discomfort, when the body feels uncomfortable, as for example when we feel too cold, feel itchy, or the garment is too tight. The psychological comfort depends on the aesthetic appearance of the garment. Psychological factors affecting comfort include color, flattering garment style, proper fit, fashion, suitability for an occasion, and prejudice. A consumer looks at a garment to see if it is the right style, if it is fashionable or traditional, and whether it will be flattering. Decisions are being made on whether the fabric color or print design is acceptable. A garment that is the latest fashion or is in some other way aesthetically appealing, may give the wearer the mental comfort of looking at his or her best. The status of the wearer is also

enhanced by a well-fitting and luxurious garment. An elegant designer gown, a new fur coat, or even the latest brand of jeans, can all confer status on the wearer and thus increase the satisfaction, hence mental comfort, of someone fortunate enough to own such a desirable object. Past experience of fabrics and garment styles also influences the wearer's feeling about the garment.

Physiological discomfort results from thermo-physiological and sensorial aspects. Thermo-physiological reactions include feelings from the temperature of the environment, and the effect of transport of perspiration. Humans must maintain an internal body temperature close to 99.6 °F (37 °C). A rise or fall in this 'core' temperature of up to 9 °F (5 °C) is usually fatal. The body constantly generates heat from the metabolism of food and muscle activity and loses this heat to the environment. A balance must be maintained between the rates of heat production and heat loss. The body is in a state of comfort when the skin temperature is 33–35 °C. The body maintains its comfort state by evaporating moisture to cause cooling when the external temperature or activity increases. A primary function of a garment is to act as a buffer against these environmental changes and to allow the skin to remain free of liquid water. Hatch has given a detailed description about the thermo–moisture interaction between the human body and the environment.[2]

The sensorial discomfort domain includes the feeling of the fabric next to the skin, allergic reaction, abrasion of the skin, tickle, prickle, wet fabric clinginess, and initial cold feel of fabric. Most of the work on clothing discomfort up until now has concentrated on thermo-physiological comfort, of which a researchable level of understanding and background information has been obtained. However, the amount of research work that has been carried out on 'sensorial' discomfort of clothing is very small, although the type of skin sensations produced by next-to-skin apparel are a major factor in determining the overall comfort of a garment. Pressure exerted on the body from garments is also a critical factor causing uncomfortable feelings. In biomechanical engineering design, sensory evaluation of clothing is based on next-to-skin sensorial comfort and pressure comfort.

9.1.1 Sensorial and pressure comfort

Sensory perceptions

As clothing is in direct contact with the human body, it interacts with the body continuously and dynamically during wear and this stimulates mechanical and thermal sensations. Sensorial discomfort, what the fabric/garment feels like when it is worn next to the skin, has been a neglected area. It is

unquestionably a very difficult quantity to assess and define scientifically. The human body is separated from the external environment by the skin, which has a very complex structure. The skin has two layers: the epidermis and the dermis. The epidermis is the outer layer, consisting of several layers of dead cells on top of a single living cell. The dermis is the inner layer, containing most of the nerve endings in the skin. Under the dermis are layers of connective tissue and fat cells.

The various sensations that result from the interaction of skin with fabric are triggered by sensory receptors in the skin. There are three types of sensory receptors, thermo-receptors, mechanoreceptors and nociceptors, and these cover all sensations: the pain group, the touch group of pressure and vibration, and the thermal group of warmth and coolness.

The two types of thermo-receptors are cold receptors and warm receptors. These can respond to both constant and fluctuating skin temperatures. The cold receptors have a peak sensitivity at around 25–30 °C, and the warm receptors have a peak sensitivity at around 39–40 °C.[4] When a fabric is placed on the skin surface, there is a momentary sensation of warmness or coolness due to the apparent difference between the temperature of the fiber and the temperature of the skin. In this case, the thermo-receptors are triggered.

There are two groups of mechanoreceptors: encapsulated receptors, including Pacinian corpuscles, Meissner corpuscles, Krause endings and Ruffini endings, which are all innervated by fast-conducting myelinated fibers; and receptors having an organized and distinctive morphology such as the hair follicle receptors and Merkle discs.[5] Each mechanoreceptor has a distinctive range of properties that enable it to receive and respond to a particular parameter of a mechanical stimulus.

Nociceptors respond to noxious stimuli such as heating the skin, strong pressure, or contact with sharp or damaging objects. These receptors have relatively high thresholds, functioning as warnings of potential damage.

Recent researches in conscious humans by recording directly from single nerve fibers in peripheral nerves have confirmed that isolated activation of an individual sensory receptor can result in distinct sensory perceptions. For instance, Meissner corpuscles cause touch sensation, Merkle receptors generate pressure, and nociceptors evoke pain. The encoding of specific sensory information is begun by these sensory receptors in the skin, and is further passed through neural pathways to the brain to formulate sensation.

Perception of sensations due to mechanical stimuli

Touch and pressure: Any point on our body's surface can evoke the sensation of touch, and our sensitivity of touch varies greatly from one region of

the body to another. Even within a relatively small area of the skin, say the leg, dramatic variations of thresholds are observed. For example, in the lower limb, the highest pressure threshold is at the hallux, and going upward, the threshold decreases. Some researchers have found that even at the same level, for example, the calf, the pressure threshold at the front is higher than that at the back.[6]

Due to the mechanical interaction between fabric and skin during wear, clothing exerts pressure and dynamic mechanical stimulation to the skin that will, in turn, trigger various mechanoreceptors and generate a variety of touch sensations. It further induces subjective perceptions and relevant pressure discomfort, or more serious pain sensations. At times, such discomfort may lead to life-changing consequences. Continuous high pressure may put a person at high risk of the development of various tissue lesions, such as pressure sores and ulcers.[7]

Prickle, itch, and inflammation: Prickle is a sensation caused by coarse and stiff fibers protruding from the fabric surface. It results from the stimulation of the pain group of sensory receptors. The degree of discomfort caused by prickle varies person-to-person and with the wear situation. Itch is a sensation that has been shown to result from the activation of some superficial skin pain receptors. The pain receptors responsible for itch may be of a different type from those responsible for the prickling sensation. Inflammation occurs in a small proportion of the population as a consequence of prickle and itch, resulting in mechanical stimulation of skin pain receptors, most likely through a mechanism termed axon reflex.

Roughness and scratchiness: The sensations of roughness and scratchiness are related to surface geometry, and are perceived when a fabric moves across the skin. During wear, a fabric moves across the underlying skin and friction resisting that movement forces the skin to displace. The skin displacement stimulates the touch group of sensory receptors. As more of the skin is displaced under the fabric moving across it, the perception of fabric roughness becomes greater. The frictional force is related to the roughness of the fabric. High friction makes skin abrasion more likely.

9.1.2 Factors affecting tactile-pressure comfort

The mechanical interaction between clothing and the body consists of two aspects: the local feel of the fabric against skin and the global feeling about the garment. The local feel, also regarded as ‘tactile comfort’, includes prickliness, itchiness, and roughness. The global feeling, relating more to ‘pressure comfort’, includes heaviness and tightness.

Fabric prickliness, itchiness, and roughness

Prickliness: Fabric-evoked prickle has been identified as one of the most irritating discomfort sensations for garments worn next-to-skin. Individual protruding fiber ends from a fabric are responsible for triggering the pain nerve endings when contacting the skin. Summation of responses from a group of pain nerves seems necessary for the perception of prickle sensations. Garnsworthy *et al*.[8] found that the intensity of fabric prickle perception is a function of the density of high load-bearing fiber ends at the fabric surface and the area of contact between the fabric and skin, indicating that both fiber mechanical properties and fabric surface features are important factors determining fabric-evoked sensations. Matsudaira *et al*.[9] compared three techniques for objective measurement of fabric prickle: low-pressure compression testing, laser-counting of protruding fibers, and a modified audio-pickup method. Through the comparison, they found that the third technique was the most effective and the measured mean force per contact correlated well with the subjective perception of fabric prickle. The two classic models, a load cantilever and an Euler column, were used to calculate the pointing force and the critical buckling load of the protruding fiber, which have been identified as the stimuli responsible for triggering the pain receptors. Buckling load can be expressed as: $P_E = \pi^2(EI/4l^2)$, where E is the Young's modulus of the fiber; I is the moment of inertia; and l is the length of the protruding fiber ends. The equation clearly shows that the Young's modulus, diameter, and length of the fiber are the key factors determining fabric prickliness.

Veitch and Naylor[10] also studied the mechanics of fiber buckling in the fabric prickling process, and concluded that the short fiber protruding ends obey Euler's simple buckling theory.

In their investigation into the influence of fabric mechanical properties on the discomfort sensations in wear, Li and Keighley[11] found that fabric prickle sensation was positively correlated with fiber diameter, fabric thickness at low loading, and fabric surface roughness.

Itchiness: Both prickliness and itchiness have been classified as tactile sensory factors. In a number of psychological wear trials, it was found that the perception of itchiness in clothing was highly correlated with the perception of prickliness. Therefore, it could be expected that the factors influencing fabric prickle would affect fabric itchiness as well. Comparing the subjective ratings of itchiness obtained from wear trials with the mechanical properties measured objectively, Li[12] found that the perception of itchiness correlated with fiber diameter, fabric thickness at low and high pressures, and fabric surface roughness.

Roughness: Behmann[13] reported a study on the perception of roughness and textile construction parameters. Roughness was defined as the irregularities in the surface that can be described geometrically by size or mechanically by friction coefficients, and a roughness model was built. A series of subjective perception trials were conducted using single nylon filament woven and knitted fabrics. The author concluded that the perception of roughness was determined by the roughness spacing.

Through comparison between the subjective sensory responses from wear trials with objective measured mechanical properties, Li[12] found that the perception of roughness correlated with fabric surface roughness (mean surface roughness coefficient, and deviation of surface roughness coefficient), compression properties (fabric thickness at high and low pressures, and energy of the compression-thickness curve), fiber diameter and fiber tensile properties (breaking load and elongation), and fabric tensile properties (maximum tensile elongation, elongation recovery load).

Hu and Newton[14] reported that fabric smoothness is related to fabric thickness at low pressure, geometric roughness, bending rigidity, linearity of the compression thickness curve, energy in extending the fabric to 5 N/cm, area density, hysteresis of bending moment, and energy in compressing the fabric under a pressure of 5 kPa.

In summarizing the findings from the literature, Bishop[15] showed that perception of fabric roughness is associated with a number of physical properties objectively measured, such as roughness, friction, prickle, shear and bend stiffness, thickness, and area density.

Garment weight, size and fit

Garment weight is a factor affecting our overall feeling about the garment. If it is too heavy, we can be aware of it as a burden. Since the area of the body supporting the garment is usually small, the pressure generated by the weight on the skin may be above the comfort level. The discomfort can become serious after a period of wearing, especially during walking or sports activity. However, if a garment is too light, it may be easily moved by the wind while walking. The fluttering is not always a pleasant feeling.

Denton[16] pointed out that there is a large difference between the weight of the clothes worn by women and those worn by men; even making an allowance for differences in average body dimensions, men wear heavier clothes than do women. Garment weight depends on the amount of fiber in the garment. In the past, clothes were necessarily heavy, particularly in winter. However, they have now benefited from the advance of the lightweight warmth technique. Sheer weight of outdoor clothing nowadays need not be an important comfort factor.

Slater pointed out that an important aspect of comfort, which is not strictly a textile problem but rather a clothing one, is that of size and fit.[17] When we first put on a garment, before being aware of the feel against skin, we certainly realize if it is too tight or too loose. Thus, no matter how well a fabric is engineered to have optimum values of heat–moisture transfer and feel against skin, any garment made from it cannot be regarded as comfortable if it does not fit properly. There are two distinct factors evident in a determination of whether the fit is good or not. The first one is a subjective one, depending on whether the wearer achieves psychological satisfaction from the garment. Another factor is a physical or physiological one, concerning the conditions of mechanical contact between garment and body. A badly fitting garment can result in high contact pressure concentrating on some regions of body surface, which can restrict cardiovascular flow, cause skin abrasion, cause pressure sores, induce irritation and so on. To achieve correct size selection and hence good fit, proper correspondence between an accurate anthropometric system and a good garment-sizing system needs to be established. Some research has been carried out.[18]

Another aspect affecting fit comfort can be construction factors. The principles of ergonomics are taken into account in clothing design[17] for various specific occupational uses, as well as for handicapped people. For many types of garment items, such as underwear, tights, and socks, variations of construction are designed to improve garment fit.[17] Dimensional change such as shrinkage also needs be taken into account in size selection.

Fabric stretch and body movement

People must be able to move around in the apparel items they wear. Discomfort may result when a fabric restrains movement, or exerts pressure on the body. Denton[16] pointed out that ease of movement is largely dependent on garment design and the relative size between body and clothing. Loose fitting allows freedom of movement but may not be desirable in many situations. Tight fitting may be suitable for certain end-uses, but can exert pressure on localized areas of the body surface and cause discomfort.

When people move, their skin, as a highly elastic material, stretches – it elongates and recovers. As the skin loses elasticity with age, it wrinkles and sags. The critical strain areas of the body are the knee, the seat, the back, and the elbows.[2] Kirk and Ibrahim's[19] study showed that the skin has a high level of two-way stretch and that differences in the percentages of skin stretch are small between men and women. Fabric placed close to the skin surface, especially in tight-fit garments, must

elongate to accommodate body movement and then recover. As elasticity is lost in a fabric, it bags and sags. Kirk and Ibrahim[19] examined the relationship between fabric extensibility and anthropometric requirements of garments. In analyzing the anthropometric kinematics, the authors identified three essential components to meet the skin strain requirements: garment fit, garment slip, and fabric stretch. Garment fit provides the space allowance for skin strain, which is determined by the ratio of garment size and the construction of garment design. Garment slip, influenced mainly by the coefficient of friction between skin and fabric, and between different layers of garments, is another mechanism for a garment to accommodate skin strain. Fabric stretch is the ability of a fabric to extend when a pulling force is applied and then to recover relatively quickly and fully to its original dimensions when the pulling force is removed.

Whether a garment slips or stretches is dependent on the balance of the tensile forces in the fabric and the frictional forces between skin and fabric. If the fabric has a low resistance to stretch and high friction against the skin or fabric, it tends to stretch rather than slip. The opposite is true if the fabric has low friction and high tensile resistance. If the fabric has both high friction resistance and stretch resistance, high clothing pressure is likely to be exerted on the body, which will result in discomfort sensations.

Fabric stretch is an important factor for pressure comfort. If a fabric exhibits more than 15% elongation, it is referred to as a stretch fabric. Use of stretch fabrics that can expand and contract without bucking or wrinkling is another way to fit the body shape. Fabrics exhibiting 15–30% elongation, which meets the requirements of many garments of various end-uses, are referred to as comfort stretch fabrics. These fabrics provide closer-fitting garments by reducing resistance to body movements, particularly around the elbows, knees, back, and seat. Power stretch fabrics have greater extensibility (30–200%) than comfort stretch fabrics, plus the ability to firm and shape body flesh. Body shaping results from compressive pressure of the fabric on the skin, which is useful in swimwear, foundation garments, stretch ski-pants, and active sportswear.

Kirk and Ibrahim[19] investigated the relationship between the pressure exerted on the body and fabric stretch level. The pressure, P, was calculated according to the following equation:

$$P = T_H/R_H + T_V/R_V,$$

where T is the tensile stress measured on an Instron tensile machine at the same level of the strain in the garment, and R is the radius of curvature of the relevant body part; the subscripts H and V indicate horizontal and vertical directions, respectively.

9.1.3 Assessment of sensorial comfort

There is only one accurate method of assessing fabric or garment comfort – wearer-trials. However, wearer-trials are an expensive and time-consuming method of testing a product. The most practical method of textile product assessment, therefore, is to use physical tests that are specially designed to measure a certain property of the fabric or garment that is known to influence a discomfort sensation. In many cases, more than one physical property contributes to producing the sensation, so a weighting factor to indicate the significance of each property has to be applied to the final analysis of results.

In an attempt to establish the relationship between subjective comfort perceptions and fabric properties, Li carried out a series of wear-trials in which three fundamental sensory factors were identified as thermal–wet, tactile, and pressure comfort.[12] Using canonical correlation analysis, Li studied the predictability between ten physical factors, including five transport properties and five mechanical properties, and three psychological factors. It was found that the sensory factors were significantly related to the corresponding dimensions of the physical properties of the fabrics. The tactile comfort factor was mainly related to fabric roughness and fullness, fabric stiffness and wettability; the pressure comfort factor was closely correlated to fabric stiffness, fabric permeability, and fiber tensile stiffness; the thermal–wet comfort factor was related to fabric wettability, fabric roughness and fullness, and fabric water evaporation propensity.

Some researchers aimed to establish relationships between objective measurement and subjective evaluation of fabric sensorial properties.[15] Among them, evaluation of fabric hand (the quality of a fabric or yarn assessed by the reaction obtained from the sense of touch[20]) through fabric objective measurement, which has been developed on the basis of the work of Kawabata and his co-workers, has been recognized and used around the world. The primary measurements use particular expressions, including KOSHI (stiffness), NUMERI (smoothness), FUKURAMI (fullness), SHARI (crispness), HARI (anti-drape stiffness), SOFOTOSA (softness), KISHIMI (scroop), SHINAYAKASA (flexibility), and TEKASA (crepe-like). They developed the KES-F system, consisting of four instruments, to measure fabric tensile, shear, bending, compression, and friction and roughness. Kawabata used a piecewise linear regression procedure to develop his equation between subjective perception and the objective measurements for predicting primary hand values (HVs) in the form of linear and mixed linear–log functions.

Besides the physical tests on fabrics, physiological tests, not directly involving textiles, can also be carried out. They include evaluations of

lung function or efficiency, blood pressure, body mechanical efficiency, and so on.

9.2 Compression therapy

9.2.1 Pressure garments

Pressure treatment for wound care

Normal skin is made up of connective tissues in the dermis that form a three-dimensional mesh, or collagen fibers aligned parallel to the skin's surface. The skin applies pressure against its underlying layers. Under normal circumstances, the pressure that the skin puts upon the body ensures that injured skin is replaced in its original state without scarring. When burns destroy the skin and the papillary dermis, normal pressure by these layers no longer exists. Without this pressure, hypertrophic scars will form irregularly causing possible deformities. Scar tissue consists of young, actively growing cells, which readily respond to changes in stress and external pressure. Various external pressure techniques are used in the treatment of burn scars and contraction. A pressure garment is one of the conventional devices most commonly used by occupational therapists. Instead of skin, pressure garments prevent and control the formation of hypertrophic scars by applying counter pressure to the wounded area, hence reducing scarring and deformities.[21]

It is important that burn patients begin wearing pressure garments while the scar is active and immature. Scar tissue is highly responsive in the early stages so an early application of a pressure garment is imperative. As soon as the wound has healed, wearing of the pressure garment may commence. They are worn continuously, night and day, except for short periods of personal hygiene, until the scar is mature. The length of time required for wearing the garment varies from several weeks up to more than two years, depending on the severity of the injury. The continuous wearing of pressure garments prevents the thickening, buckling, and nodular formations seen in hypertrophic scars. The external pressure applied by the garment decreases inflammatory response and the amount of blood in the scar, reducing itching and preventing collagen from synthesizing. Additionally, pressure garments provide protection against further injury.

Classification and functional requirements of pressure garments

According to the materials, pressure garments are classified into two types: garments made from firm elastic fabric containing Spandex (mainly warp knit powernet or sleeknit) and garments made in 'Tubigrip', a weft knit cotton elastic material containing horizontal rubber yarn, manufactured in

tubular lengths of different diameters.[22] Many doctors and therapists have found that the Spandex garments offer firmer pressure and last longer, whereas 'Tubigrip' garments have greater stretch tolerance and require fewer measurements for proper fitting, which makes them more suitable for the initial stages of treatment.[22]

Pressure garments are either made available as ready-to-wear garments, or manufactured according to the individual measurements of the patient. Ready-to-wear garments are made both in Spandex materials and in Tubigrip. They are generally used for preliminary treatment before custom-made garments can be available. Made-to-measure garments are constructed from Spandex materials in the main. They provide each individual patient with the correct continuous pressure over the scar area, regardless of size or shape and are thus advantageous in conforming precisely and comfortably to the contours of the patient's body, providing maximum benefit.

Early research work revealed that the assessment of the hypertrophic scar relative to the fitting of the pressure garment is subjective, since there is no widely available objective method for measurement of the pressure at the garment–scar interface.[22] The pressure exerted by pressure garments depends on three aspects: shape of the body parts; type and age of the fabric used; and design and fit of the garment.[21] The shape of the underlying body contours is an important influence because the greater the degree of curvature, the greater the pressure exerted. This indicates that it is easier to apply pressure to certain body parts, such as the limbs, rather than to less rounded areas such as the chest wall, pectoral and facial areas. Pressure garments made of different types of fabrics result in pressures of various values on body. The constant stretching and re-stretching of the fabric will eventually wear down the elasticity of the pressure garment and cause it to lose its ability to exert the correct pressure. Even though a pressure garment should be tightly fitted for medical treatment purposes, it should be designed in such a way that it is not too difficult for the patient to put on or take off.

Requirements of pressure garments are based on two aspects: clinical effectiveness and comfort in wear. For clinical effectiveness, a tightly fitting garment made of compressive elastic fabric is necessary to produce the required pressure over the scarred area, and the pressure should be capable of being maintained over a prolonged period of time. However, the acceptability to patients depends on patient mobility, contact and pressure comfort, and ease of wear. Patients are not willing to put on something that will restrict their movements and affect their daily activities. If the pressure values are higher than the patients' pressure pain thresholds, they cannot accept the garments. All these factors are related to the garment materials and design. From the view of mechanical properties,

there are the following requirements for the fabric material. The fabric should be soft and elastic, causing no irritation to the skin, and should fit the body contours like a second skin. It should also be smooth and cause no abrasion to the skin, especially during body movement. It should be easy-care and washable, and its properties should be maintained after multiple washings. With the reference to the manufacturing process, the fabric should be easy to tailor and sew. Both the fabric and the sewing method selected should be strong enough to resist the daily wear and tear.

9.2.2 Compression bandages and stockings

Compression therapy for venous and lymphatic disorders

For over 150 years, external compression therapy (CT) has been used as a treatment for venous and lymphatic disorders, such as deep vein thrombosis (DVT) and superficial phlebitis, as well as in chronic conditions such as chronic venous insufficiency (CVI), gravitational dermatitis, lipodermatosclerosis, leg ulcers and lymph-edema.[23,24] Further indications include thromboembolic prevention and edema prevention in pregnancy, long and microgravity flights, and softening of burns scars. Compression may be achieved by different modalities such as various bandages, wrapped dressings, legging orthosis, and compression stockings. Among them, compression stockings come into our daily life and a wide range of them is commercially available. The mechanism of action of compression therapy remains unclear and is probably multi-factorial. Many hypotheses have been advanced to explain the beneficial effect of compression by stockings, and these have been classified as follows:[24]

Venous: May achieve narrowing of veins, restoration of valvular competence, partial regression of parietal degenerative changes, reduction or suppression of superficial and deep venous reflux, diminution of venous pressure, acceleration of venous flow, improvement of venous pumping, diminution of venous pool, and blood shift into the central compartment.

Arterial: May reduce cutaneous arterial perfusion in a first step, then, paradoxally, improve arterial flow as a result of edema reduction.

Lymphatic: May improve lymphatic function and drainage.

Microcirculatory: May decrease edema, acceleration of capillary blood flow and inflammatory mediators.

Tissular: May increase intra-tissular pression and edema resorption, and decrease protein tissular concentration softening of lipodermetosclerosis.

Hematological: May enhance fibrinolysis.

Bio-functional requirement and classification

The two major compression modalities made of textile materials are bandages and compression stockings.

Compression bandages: There are two main types of bandages: inelastic or short-stretch bandages, and long-stretch elastic bandages. Inelastic bandages exert passive compression and are recommended in the treatment of edema, deep vein thrombosis, or trophic lesions of chronic venous insufficiency (CVI). Long-stretch elastic bandages are much easier to use. Their high resting pressure effectively compresses superficial veins after surgery, sclerotherapy, or thrombophlebitis. There are also some other bandages including four-layer bandages, adhesive dressings, zinc-coated bandages, and cohesive bandages.[24] Four-layer bandages consist of four superimposed layers: (1) padding with orthopaedic wool, absorbing exudates and protecting bony prominences; (2) cotton crepe bandage, holding the former in place; (3) long stretch elastic bandage; and (4) cohesive bandage, strengthening support and holding it all in place. The four-layer bandage provides permanent pressure to the leg in patients with CVI, in particular with leg ulcers.

Compression stockings: Compression stockings may be designed to apply graduated or uniform compression. Graduated compression refers to the application of varying degrees of constant compression to different segments of the leg, with pressure being greatest at the ankle and gradually decreasing proximally. Uniform compression aims to deliver a similar degree of pressure to the whole leg. Graduated compression has been the favoured option since Sigel *et al.*[25] demonstrated small but consistent increases in velocity of flow in the common femoral vein compared with that obtained from uniform compression. Graduated Compression Stockings (GCSs) can enhance venous return and reduce stasis by providing graded compression with the greater pressure applied more distally, as illustrated in Fig. 9.1.

Compression stockings can be further classified into two major types. One is leg-shaped, flat-knitted with a seam. The form of the stocking is achieved by changing the number of needles. This type of stocking can be made tailor-sized, and allows increase and decrease in the number of stitches for each row. Hence, the tension of the threads may not change while the circumference changes. The other type is round-knitted and is seamless. For this type of stocking, the only possibility to form the stocking is by varying the tightness of courses and the tension of the threads.

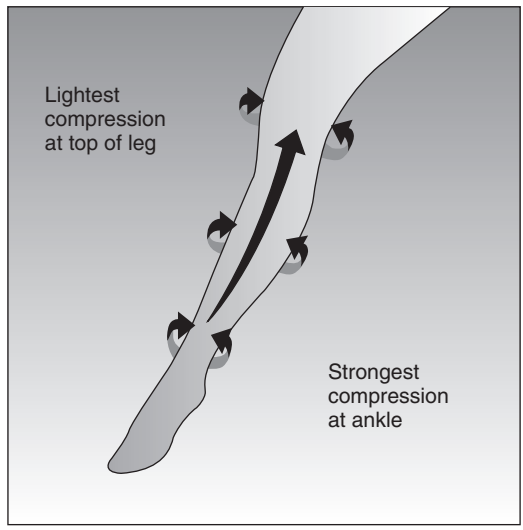

9.1 Graduated compression stocking (GCS).

9.3 Conclusion

In this chapter, the wearing comfort of clothing and compression therapy using textile devices has been discussed. For clothing comfort, the tactile-pressure comfort, which has been an ignored research area but is related directly to mechanical interaction between the human body and clothing, was focused upon. The main factors affecting tactile-pressure comfort include the surface properties of fabrics, garment fit and size, fabric stretch and body movement.

Pressure garments, and compression bandages and stockings, are the major clothing items used for wound care and various venous disorders. The functional requirements and classifications of these devices were also briefly introduced.

9.4 Acknowledgement

We would like to thank Hong Kong Polytechnic University for funding this research through the projects A188 and G-YD31.

9.5 References

1. Slater, K., *Human Comfort*, Thomas Springfield: USA.
2. Hatch, K.L., Chapter 3, Comfort, in *Textile Science*. 1993, West Publishing.
3. Smith, J.E., The Comfort of Clothing. Textiles, 1986. **15**(1): p. 23–27.
4. Iggo, A., Sensory Receptors, in *Sensory Systems II: Senses other than Vision*. 1988, Birkhauser: Boston, USA.

5. Coren, S., Ward, L.M. and Ward, E.J.T., Chapter 7, Taste, Smell, Touch, and Pain, in Sensation and Perception. 2004, John Wiley, p. 179–215.
6. Nakahashi, M. *et al.*, Effect of Clothing Pressure on Front and Back of Lower Leg on Compressive Feeling, in *Journal of the Japan Research Association for Textile End-Uses*. 1999. p. 661–668.
7. Phillips, P., Evans, A. and Popplewell, P., Diabetic Foot Ulcers, A Guide to Treatment. *American Journal of Clinical Dermatology*, 2000. **1**(2): p. 117–123.
8. Garnsworthy, R.K., Gully, R.L. *et al.*, Understanding the Causes of Prickle and Itch from the Skin Contact of Fabrics. *Australian Textiles*, 1988. **8**: p. 26–29.
9. Matsudaira, M., Watt, J.D. and Carnaby, G.A., Measurement of the Surface Prickle of Fabrics, Part I: The Evaluation of Potential Objective Methods. *The Journal of Textile Institute*, 1990. **81**: p. 288–299.
10. Veitch, C.J. and Naylor, G.R.S., The Mechanics of Fiber Buckling in Relation to Fabric-evoked Prickle. *Wool Technology, Sheep Breeding*, 1992. **40**: p. 31–34.
11. Li, Y. and Keighley, J., Relations Between Fiber, Yarn, Fabric Mechanical Properties, and Subjective Sensory Responses in Wear Trials, in *The 3rd International Conference on Ergonomics*. 1988. Helsinki, Finland.
12. Li, Y., *The Objective Assessment of Comfort of Knitted Sportwear in Relationship to Psycho-physiological Sensory Studies*, 1988 Dept. of Textile Industries. The University of Leeds: Leeds.
13. Behmann, F.W., Tests on the Roughness of Textile Surfaces. *Melliand Text.*, 1990. **71**: p. 438–440.
14. Hu, J.L. and Newton, A., A Psychophysical Model for Objective Hand Evaluation: An Application of Steven's Law. *Journal of the Textile Institute*, 1993. **84**: p. 354–363.
15. Bishop, D.P., Fabrics: Sensory and Mechanical Properties. *Textile Progress*, 1996. **26**(3): p. 5–26.
16. Denton, M.J., Fit, Stretch, and Comfort. *Textiles*, 1972. **1**(1): p. 12–17.
17. Slater, K., Comfort Properties of Textiles. *Textile Progress*, 1977. **9**.
18. Fan, J., Yu, W. and Hunfer, L., *Clothing Appearance and Fit*. 2004: Woodhead Publishing Ltd: Cambridge, UK.
19. Kirk, W.J. and Ibrahim, S.M., Fundamental Relationship of Fabric Extensibility to Anthropometric Requirements and Garment Performance. *Textile Research Journal*, 1966. **57**: p. 37–47.
20. McIntyre, J.E. and Damels, P.N., *Textile Terms and Definitions*. 1995, The Textile Institute: Manchester.
21. Pratt, J. and West, G., Chapter 1: Pressure Therapy: History and Rationale, in *Pressure Garments, A Manual on Their Design & Fabrication*. 1995, Butterworth-Heinemann Ltd: Oxford. p. 1–21.
22. Ng-Yip, F.S.F., Medical Clothing. *International Journal of Clothing Science and Technology*, 1993. **5**(1): p. 17–24.
23. Hamilton, O.A.G. and Baker, D., Graduated Compression Stockings in the Prevention of Venous Thromboembolism, in *British Journal of Surgery*. 1999. p. 922–1004.
24. Ramelet, A.A., Compression Therapy, *Dermatologic Surgery*. 2002. p. 6–10.
25. Sigel, B. *et al.*, Type of Compression for Reducing Venous Stasis, *Archives of Surgery*. 1975. p. 171–175.